Divalent metal nanoparticles

by

Gretchen Anne DeVries

B.S. Materials Science and Engineering
Stanford University, 2002

SUBMITTED TO THE DEPARTMENT OF MATERIALS SCIENCE AND ENGINEERING IN PARTIAL FULFILLMENT OF THE REQUIREMENTS FOR THE DEGREE OF

DOCTOR OF PHILOSOPHY IN MATERIALS SCIENCE AND ENGINEERING

at the
MASSACHUSETTS INSTITUTE OF TECHNOLOGY

February 2008

Signature of Author:_____
Department of Materials Science and Engineering
January 14, 2008

Certified by:_____
Francesco Stellacci
Associate Professor of Materials Science and Engineering
Thesis Supervisor

Accepted by:_____
Samuel M. Allen
POSCO Professor of Physical Metallurgy
Chair, Departmental Committee on Graduate Students

Divalent metal nanoparticles

by

Gretchen Anne DeVries

Submitted to the Department of Materials Science and Engineering on January 14, 2008 in partial fulfillment of requirements for the Degree of Doctor of Philosophy in Materials Science and Engineering

ABSTRACT

Metal nanoparticles hold promise for many scientific and technological applications, such as chemical and biological sensors, vehicles for drug delivery, and sub-diffraction limit waveguides. To fabricate such devices, a method to position particles in specific locations relative to each other is necessary. Nanoparticles tend to spontaneously aggregate into ordered two- and three-dimensional assemblies, but achieving one-dimensional structures is less straightforward. Because of their symmetry, nanoparticles lack the ability to bond along specific directions. Thus, the technological potential of nanoparticles would be greatly enhanced by the introduction of a method to break the interaction symmetry of nanoparticles, thus inducing valency and directional interparticle interactions.

When a nanoparticle is coated with a mixture of two different ligands, the ligands have been shown to phase-separate into ordered domains encircling or spiraling around the core. Topological constraints inherent in assembling two-dimensional vectors (e.g., ligands) onto a sphere (the core of the nanoparticle) dictate the necessary formation of two diametrically opposed defect points within the ligand shell. The molecules at these points are not optimally stabilized by intermolecular interactions and thus these sites are highly reactive. By functionalizing the polar singularities with a third type of molecule, we generate divalent nanoparticles with "chemical handles" that can be used to direct the assembly of the particles into chains. For example, taking inspiration from the well-known interfacial polymerization synthesis of nylon, we place carboxylic acid terminated molecules at the polar defect points and join the newly bifunctional nanoparticles into chains by reacting them with 1,6-diaminohexane through an interfacial reaction.

Furthermore, we perform a full kinetic and thermodynamic characterization of the molecularly defined polar defect points. We demonstrate that the rate of place-exchange at these points is significantly faster than it is elsewhere in the ligand shell. We also determine the equilibrium constant and standard free energy of the place-exchange reaction at the polar defect sites and demonstrate that the reaction is strongly affected by the molecular environment, i.e. the composition of the ligand shell.

Thesis supervisor: Francesco Stellacci
Title: Associate Professor of Materials Science and Engineering

Biographical Note

Gretchen DeVries received a Bachelor of Science with distinction from Stanford University in June, 2002. At MIT, she studied under Professor Francesco Stellacci. Her publications and conference presentations are listed below. She also served as a teaching assistant for the undergraduate classes 3.153, "Nanoscale Materials": and 3.014, "Materials Laboratory".

Publications

DeVries, G. A.; Talley, F. R.; Carney, R. P.; Stellacci, F., Thermodynamic Study of the Reactivity of the Two Topological Point Defects Present in Mixed Self-Assembled Monolayers on Gold Nanoparticles. *Advanced Materials* **2007** (accepted).

Carney, R. P.; DeVries, G. A.; Kim, H.; Kim, J. Y.; Dubois, C.; Singh, C.; Ghorai, P. K.; Tracy, J.; Murray, R. W.; Glotzer, S. C.; Stellacci, F., Size limitations for the formation of ordered striped nanoparticles. *Journal of the American Chemical Society* **2007** (in press).

DeVries, G. A.; Centrone, A.; Stellacci, F., Chains of divalent gold nanoparticles. *Proceedings of SPIE* **2007,** 6768.

DeVries, G. A.; Brunnbauer, M.; Hu, Y.; Jackson, A. M.; Long, B.; Neltner, B. T.; Uzun, O.; Wunsch, B. H.; Stellacci, F., Divalent metal nanoparticles. *Science* **2007,** 315, (5810), 358-361.

Jenkins, M.; DeVries, G.A.; Dauskardt, R.H.; Bravman, J.C., Studies of Silane Adhesion Promoters on Silica Filler Particles for use in Microelectronic Packagin. *MRS Symposium Proceedings, DD10.10* **2001,** 710.

Jenkins, M.; Snodgrass, J.; Chesterman, A.; DeVries, G.; Dauskardt, R.H.; Bravman, J.C. Adhesion Mechanisms of Silane Adhesion Promoters in Microelectronic Packaging. *MRS Symposium Proceedings, N6.4* **2001,** 682E.

Conference presentations

DeVries, G.A.; Talley, F.R.; Stellacci, F. Nano-polymers: Chains of gold nanoparticles. *Materials Research Society spring meeting* **2007**. Session DD11: Assembly, Pattering, and Collective Properties II.

DeVries, G.A.; Uzun, O.; Long, B.; Stellacci, F. Directed Assembly of Divalent Ligand-Coated Nanoparticles into One-Dimensional Chains. *Materials Research Society fall meeting* **2006**. Session QQ4: Porous and Nanostructured Materials.

DeVries, G.A.; Long, B.; Franchini, I.R.; Stellacci, F. Directed Assembly of Ligand-Coated Nanoparticles into Linear Chains of Controllable Composition. *Materials Research Society fall meeting* **2005**. Session CC1: Metal Nanoparticles – Electronic Properties.

DeVries, G.A.; Brunnbauer, M.; Franchini, I.R.; Stellacci, F. One-Dimensional Chains of Optically Interacting Gold Nanoparticles. *SPIE Optics & Photonics* **2005**. Session 1: Near-Field Imaging with Plasmonic Enhancement.

DeVries, G.A.; Li, K.; Stellacci, F. Tunable Electro-Optical Behavior of Monolayer Protected Metal Nanoparticles. *American Physical Society March meeting* **2004**. Session W36: Superlattices and Nanostructures: Electronic Properties.

DeVries, G.A.; Farinola, G.M.; Cioco, S.; Babudri, F.; Naso, F.; Stellacci, F. Localized Ligand Replacement on Gold Nanoparticle Monolayers: A Novel Method for the Generation of Supramolecular Wires. *Materials Research Society fall meeting* **2003**. Session M6: SPM-Based Lithography.

DeVries, G.A.; Stellacci, F. Localized Ligand Replacement on Gold Nanoparticle Monolayers: A Novel Method for the Generation of Supramolecular Wires. *American Chemical Society Northeast regional meeting* **2003**. Nanotechnology general session.

Acknowledgements

First and foremost, I would like to acknowledge Francesco Stellacci. Francesco is an excellent advisor and an excellent scientist, and it has been a pleasure to learn from him and work with him.

SuNMaG is a supportive and constructive research group. In particular, Markus Brunnbauer (now at Infineon in Germany) initiated the chain project and provided some valuable early results and interesting ideas. Frajovon R. Talley (Howard University) and Randy P. Carney (University of Arkansas) were undergraduate summer students who did substantial work characterizing the thermodynamics and kinetics of pole functionalization. Benjamin Wunsch was always available and happy to help with TEM imaging and nanoparticle synthesis. Alicia Jackson, Cedric Dubois, and Ying Hu provided valuable STM images of various nanoparticles. Oktay Uzun and Hyewon Kim both worked on chain synthesis and characterization. Brian Neltner, an undergraduate student from MIT (now a graduate student here) wrote the code that analyzed the chain population in TEM images. Outside of SuNMaG, Catherine Tweedie of the Van Vliet group performed extensive mechanical testing of the free-standing nanoparticle films, and Emily Watson provided simulations to help in understanding the results.

Finally, I thank my husband, Antonio Damato, for his love, encouragement, and support; and my parents for their ongoing support.

Contents Overview

Table of Contents

Chapter 1: Nanoparticles and self-assembled monolayers

1.1 Introduction

The field of nanoscience has attracted intense research efforts recently because of both the scientifically intriguing phenomena accessible at the nanoscale and the enormous technological potential offered by the development of nanoscale devices. Physical phenomena that previously were accessible only theoretically, such as quantum confinement effects, are commonplace at the nanoscale. Nanosized materials have already been introduced in some commercial applications such as stain-resistant trousers, anti-aging cosmetic creams, and stronger but lighter tennis rackets. Nanoparticles used as biological or chemical sensors, carbon nanotubes as components of integrated circuits, and nanowire arrays as high surface area electrodes are just a few examples of the many other potential applications predicted for nanotechnology.

Materials with at least one dimension less than 100 nm, and larger than approximately 1 nm, are typically considered to be nanomaterials. Above 100 nm, a material generally behaves with characteristics of the bulk; below 1 nm, such a small number of atoms is involved that the material behaves instead as a molecule or an artificial atom. Between these two limits, the surface-to-volume ratio is drastically increased over that of bulk materials, and surfaces play a significant role in determining the properties and behavior of the material as a whole. Additionally, the length scale of the electron wavefunction is of the same order of magnitude as the dimensions of nanosized materials, giving rise to confinement effects and other quantum mechanical phenomena not ordinarily observed in the bulk. The appearance of pure gold illustrates

the vastly varied properties a material can display in different size regimes. In bulk, gold is a lustrous yellow color; 20 nm diameter gold nanoparticles appear deep red; and 2 nm diameter particles have molecule-like behavior with discrete energy transitions between levels.

1.1.1 Nanoparticles

Nanoparticles (NPs) are zero-dimensional nanomaterials; they can be made of a variety of materials, including noble metals[1] such as gold and silver, semiconductors[1] such as cadmium selenide and zinc sulfide, and oxides such as silicon oxide[2] and titania.[3] NPs must be stabilized against aggregation into the thermodynamically preferable bulk state. This is often achieved by functionalization of the surface with molecules through electrostatic attraction[4] or covalent bonding.[5] The combination of core size and composition and the identity of the stabilizing shell imparts many unique properties to the NPs.

In this work we consider monolayer protected metal NPs, supramolecular assemblies consisting of a central metallic core of gold or silver stabilized by a self-assembled monolayer (SAM, see below) of thiol-terminated ligand molecules (Figure 1.1).[6] The metal core is generally a facetted single crystal or a twin.[7] A straightforward synthesis[5,6,8] allows for the selection of thiolated ligands with a wide variety of terminal functionalities, thus enabling the synthesis of NPs with a wide range of physiochemical properties.

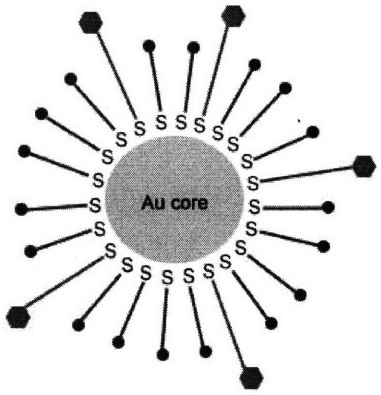

Figure 1.1
Cartoon of a gold nanoparticle coated with a self-assembled monolayer of thiolated ligands. The SAM can consist of multiple types of ligands; the end functionality of the ligands plays a significant role in determining the properties of the NP.

1.1.2 Properties of metal nanoparticles

Metal NPs have a variety of unique properties that arise from their small dimension. Here we briefly mention two notable examples: plasmon resonance and single electron charging.

Small metal NPs exhibit strong optical absorption at one particular frequency due to a collective oscillation of the free electron gas in the NP.[9] This frequency, known as the plasmon resonance frequency, is an effect of the small size of the NPs relative to the wavelength of the incident light. The resonance frequency can be tuned by varying the composition of the NP core[10] (Figure 1.2) and the dielectric constant of the surrounding material[11] (solvent and ligands). This sensitivity of the plasmon resonance to the environment has driven the use of NPs as biological and chemical sensors.[12,13] Furthermore, at resonance, the electric field surrounding the NPs is strongly enhanced,

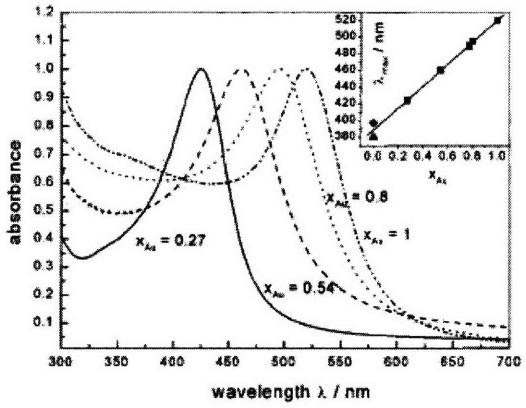

Figure 1.2
The absorption spectrum for Au-Ag alloy nanoparticles. A linear relationship is seen between the plasmon resonance wavelength and the composition of the core. (Reproduced from 10)

enabling inter-NP electromagnetic coupling and energy transfer between particles,[14] and inducing a red shift in the wavelength of the resonance (Figure 1.3).[15,16]

Individual metal NPs exhibit monoelectron conductivity due to their small capacitance (which scales as the inverse of the NP radius).[17] As a result, electron flux onto and off of a NP is quantized in one-electron increments, leading to Coulomb

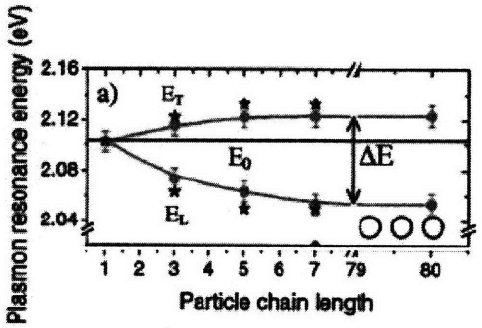

Figure 1.3
Plasmon resonance energies for arrays of Au nanoparticles of increasing length excited longitudinally (E_L) and transversely (E_T). Red circles were obtained via far-field spectroscopy and black stars were calculated with FDTD simulations. A shift in the plasmon resonance is observed due to interparticle coupling. (Reproduced from 15)

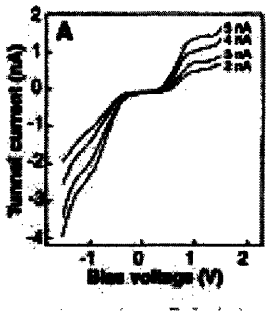

Figure 1.4
Plot of tunnel current as a function of bias voltage and tip height for a 1.8 nm Au cluster measured in Scanning Tunneling Microscopy. Coulomb staircase behavior is visible. (Reproduced from 18)

blockade and Coulomb staircase phenomena in which current through a NP increases in a stepwise manner. These behaviors are observable in the current-voltage response of individual NPs[18] (Figure 1.4) and in the electrochemical behavior of ensembles of NPs.[19] As with optical properties, the conductivity profile of metal NPs is affected by the dielectric environment.[20-22]

1.2 Self-assembled monolayers

Self-assembled monolayers (SAMs) are spontaneously formed ordered assemblies of molecules chemisorbed on a surface.[23-26] Molecules in a SAM consist of a headgroup that binds specifically to the substrate material and an endgroup that controls the surface properties of the SAM (Figure 1.5). In this work, we consider only SAMs of thiolated molecules (headgroup -SH) formed on noble metal surfaces such as Ag and Au, although there are a variety of other chemistries that also form SAMs. The endgroup can be virtually any chemical functionality that imparts desired properties to the surface; for example, the contact angle and thus the surface energy can be tuned by selecting an endgroup with a particular hydrophobic or hydrophilic character.[27] SAMs have been

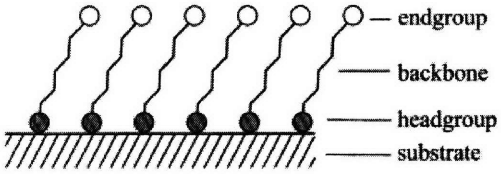

Figure 1.5
Schematic of a SAM. Shaded circles represent chemisorbed headgroups, which are thiol groups for assembly onto a gold surface; open circles are terminal endgroups, which can be a variety of chemical functionalities. (Reproduced from 24)

extensively studied for a wide range of applications in fields as disparate as organic electronics[28] and switchable drug releasing surfaces.[29] Here follows a general overview of the structure and selected properties of SAMs on both flat surfaces and nanoparticles.

1.2.1 Structure of self- assembled monolayers

SAMs of thiolated molecules on noble metal surfaces are highly ordered two-dimensional crystals in which the molecules arrange with a uniform tilt angle and direction relative to the surface normal (Figure 1.6) in order to maximize intermolecular

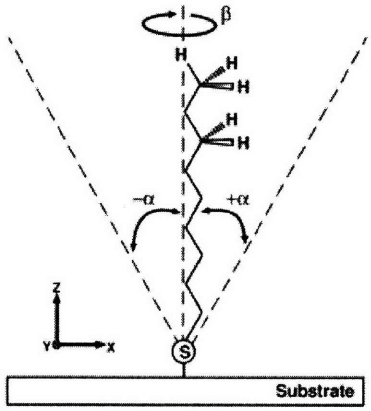

Figure 1.6
Schematic view of a single alkanethiolate molecule adsorbed to a surface, indicating the tilt angle (α) with respect to the surface normal and the twist angle (β) of the axis of the molecule. (Reproduced from 25)

van der Waals interactions.[30,31] On flat Au substrates, the tilt angle of alkanethiols is ~30°; for an alkanethiol SAM on Ag, the tilt angle of the molecules is roughly 10°.[24,25] Thus, the tilt angle is affected not only by the enthalpic driving force for interchain interactions, but also by the nature of the thiol-metal bond. At defects and domain boundaries in a SAM, molecules either do not conform to their standard tilt angle or cannot obtain maximal intermolecular interactions in all directions; molecules at such defects are less well stabilized than molecules in the ordered crystalline portion of the SAM.

1.2.2 Phase separation

On flat surfaces, SAMs composed of a mixture of two different thiolated molecules undergo phase-separation into randomly oriented and positioned nanometer-scale domains (Figure 1.7).[32-34] Phase-separation in SAMs is a generic phenomenon that has been observed with various combinations of molecular length and terminal functionality.

Further study of phase-separated SAMs reveals that they evolve to an equilibrium structure of nano-sized wormlike domains (Figure 1.8) in order to balance the enthalpic and entropic contributions to the free energy of the domain boundaries.[35] That is, phase separation into bulk (or macroscale) domains is favored by the enthalpic driving force for molecules to be next to similar molecules for optimal intermolecular interactions (for example, van der Waals forces for alkane chains or hydrogen bonding for molecules with hydrophilic end groups). However, random mixing is entropically preferred. For example,

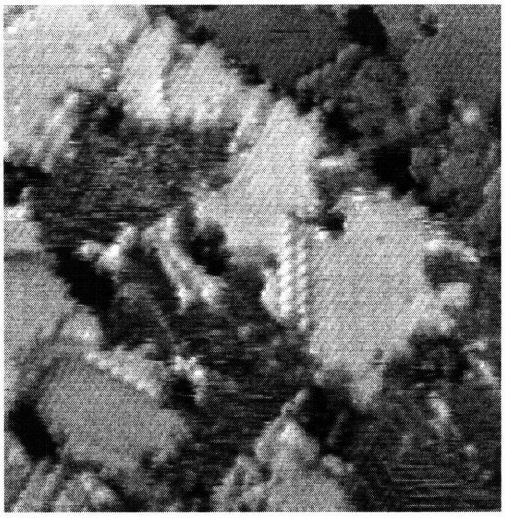

Figure 1.7
STM image of a phase-separated SAM consisting of *n*-decanethiol and an internally functionalized amide-containing thiol. The image is 300 Å x 300 Å in size. (Reproduced from 34)

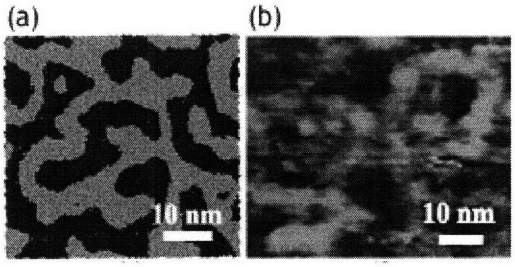

Figure 1.8
(a) Molecular dynamics simulation of a mixed SAM consisting of 1-butanethiol and 1-hexanethiol on a flat surface, showing the formation of stripe-like domains. Blue and yellow represent the head groups of the short and long molecule, respectively. (b) STM height image of a mixed SAM of the same composition showing stripe-like morphology. (Reproduced from 35)

considering two species of sufficiently different lengths, the configurational entropy is significantly increased when a long molecule has the additional space afforded it by shorter molecules surrounding it. This competition between enthalpically driven bulk phase separation and entropically favored random mixing results in nanoscale phase separation into wormlike domains.

1.2.3 SAMs on nanoparticles

Thiolated molecules also form SAMs on noble metal NPs; the SAM, known as the ligand monolayer, serves simultaneously to stabilize the NPs against aggregation and to influence the properties of the NPs through the nature of the molecule and the endgroup functionality.[36] For instance, the ligands affect NP properties ranging from solubility[37] to electronic[38] and optical[11] properties to the assembly of the NPs into complex structures.

The structure of SAMs on NPs is complicated by the fact that a two-dimensional crystal (the SAM) must be assembled onto a three-dimensional surface (the NP). Although SAMs on NPs retain all of the behavior of SAMs on flat surfaces, this additional complication gives rise to a unique situation of ordered nanoscale phase separation in mixed component SAMs.[35,37] The structure and related structure-determined properties of SAMs on NPs will be discussed in detail in Chapter 2.

1.2.4 Place-exchange on flat surfaces

Place-exchange is a process by which the composition of an existing SAM can be changed by exposing it to a solution of another kind of molecule.[26,39,40] For SAMs on gold surfaces, it is well-known that a dynamic equilibrium exists in which thiolated molecules reversibly adsorb to the surface and desorb to form disulfide molecules in solution.[41,42] As a result of this equilibrium, it is possible to immerse a SAM of a given composition into a solution of a second type of thiolated molecules and, after a period of time (hours to days), find that some of the second molecule has been incorporated into the SAM through place-exchange.[23,26,27,43] Place-exchange occurs faster at defect sites and pinholes in the SAM,[43-45] where molecules are less optimally stabilized by

intermolecular interactions. The process has a fast initial rate, as defect sites are populated; subsequent exchange is slower as terraces of crystallographically perfect SAM must be populated with the incoming molecules.

1.2.5 Place-exchange on nanoparticles

Place-exchange occurs on NPs as well as on flat surfaces, and a large body of work has characterized the kinetics of this reaction on Au NPs. The Murray group place-exchanged ω-ferrocenyloctanethiol (FcC_8SH) onto alkanethiol-protected NPs and used ^1H Nuclear Magnetic Resonance (NMR) to determine the number of FcC_8SH that had exchanged onto the NPs after a given amount of time.[46] NMR has also been used for various other ligand combinations.[47-50] Fluorescence spectroscopy has been used to study place-exchange by monitoring the release of molecules with moieties whose fluorescence is quenched while on the surface (such as pyrene-terminated alkanethiols[51] and thiol-terminated Bodipy dye[52]) but that can be detected upon desorption into solution. Gas chromatography has been applied to detect the exchange of one alkylthiol for another of different length, a reaction that is invisible to NMR and fluorescence monitoring techniques.[53] NMR[54] and a more sensitive electron paramagnetic resonance technique[55] have been used to monitor a more complex reaction: the exchange of ligands between differently functionalized NPs in solution.

1.2.5.1 Mechanism of place-exchange

Place-exchange occurs with a 1:1 stoichiometry: one molecule is adsorbed for every molecule desorbed.[46] Furthermore, place-exchange has two regimes, with rapid exchange occurring initially at edges and vertices of the gold core of the NP, followed by

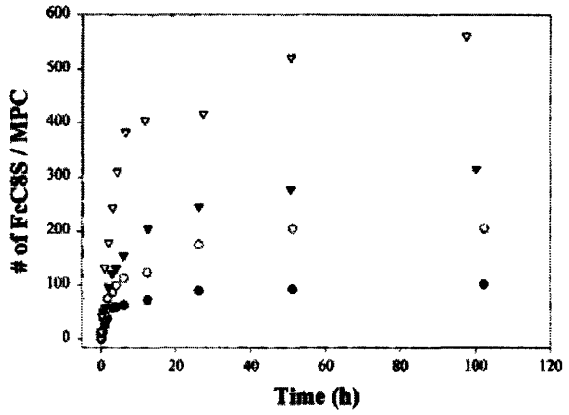

Figure 1.9
Study of the time evolution of place-exchange of ω-ferrocenyloctanethiol (FcC_8SH) onto homoligand Au NPs. An initial regime of rapid exchange and a subsequent slower step are apparent. Symbols represent different concentrations of FcC_8SH. From top to bottom: $1.7 \cdot 10^{-3}$ M (open triangle); $1.2 \cdot 10^{-3}$ M (closed triangle); $4.1 \cdot 10^{-4}$ M (open circle); $1.6 \cdot 10^{-4}$ M (closed circle). (Reproduced from 46)

slower population of terrace sites either by direct exchange from solution or by migration from the initial exchange sites (Figure 1.9).[46,56]

The order of a reaction is determined by its dependence on the concentrations of the reactants. For instance, for a reaction $xA + yB \rightarrow$ Products, the rate of reaction is written $Rate = -\frac{\Delta[A]}{\Delta t} = k[A]^m[B]^n$, where Δt is the time of the reaction and k is the rate constant. If the rate does not depend on the concentration of either ligand, then m and n are both zero, and the reaction is zeroth order. If the reaction depends linearly on the concentration of, for instance, reactant A, then $m = 1$ and $n = 0$ and the reaction is first order in A. Similarly, if both m and n are 1, the reaction is second order. The order of a reaction can be determined by monitoring the reactant concentration with time.

Associative place-exchange is controlled by both ligand adsorption and desorption, and is overall a second order reaction (first order in both nanoparticle concentration and incoming ligand concentration). By contrast, a dissociative mechanism

implies that the process is controlled only by ligand desorption, and is first order in nanoparticle concentration alone. The exact mechanism by which place-exchange occurs on NPs is a subject of substantial debate in the literature.

By focusing on the initial rapid regime, several groups[46,51] have determined a first-order dependence of the rate on the concentration of NPs (e.g. the concentration of existing ligands) and a (non-ideal) first-order dependence on the concentration of the incoming ligands (in this case, ω-Ferrocenyloctanethiol). This dependence on both existing and incoming ligands suggests an associative mechanism for place-exchange on NPS. More accurately, the order of reaction was determined to be 0.33; that is, $Rate = k[A]^{0.33}$.[51] This means that in the rate determining step, the insertion of one incoming molecule weakens the Au-thiol interaction of more than one molecule originally in the ligand shell.

Although most work points to an associative mechanism of place-exchange onto NPs,[46,51] there is some data suggesting either a dissociative mechanism[57,58] or diffusion-limited Langmuir kinetics.[53] Notably, Kassam[53] exchanged 1-dodecanethiol onto Au NPs coated with 1-decanethiol at various ratios of incoming to outgoing ligand. The place-exchange reaction was determined to be zeroth order (no dependence of the rate on the concentration of incoming ligand) with an excellent fit to a second order Langmuir diffusion-limited rate equation (Figure 1.10(a)). Furthermore, the extent of exchange depended on the ratio of incoming to outgoing ligands, and the exchange could be driven further after reaching equilibrium by the addition of excess incoming ligands (Figure 1.10(b)).

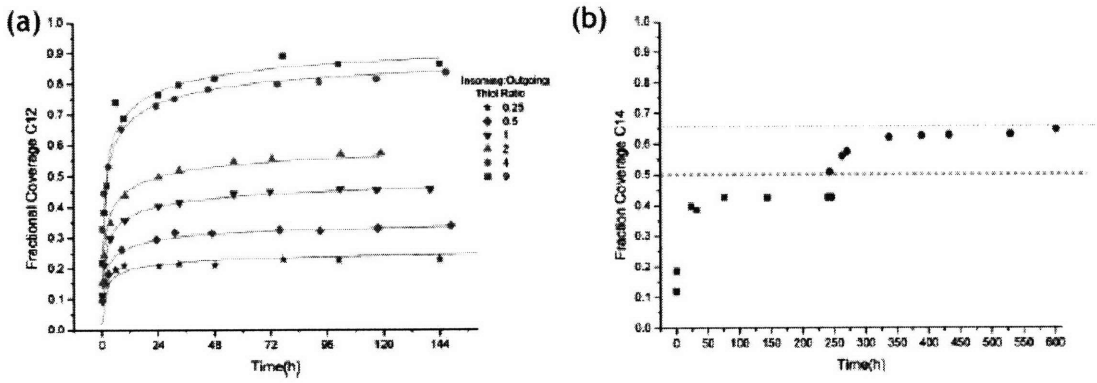

Figure 1.10
(a) Progression of place-exchange of 1-dodecanethiol onto Au NPs coated with 1-decanethiol at different ratios of incoming to outgoing ligands. Points are experimental data; solid lines are fits to a second order diffusion-limited Langmuir model. The extend of exchange depended on the ligand ratio. (b) Place-exchange of $C_{14}SH$ onto 1-decanethiol NPs. The equilibrium can be driven further by adding additional $C_{14}SH$. (Reproduced from 53)

1.2.5.2 Place-exchange kinetics

Further studies of place-exchange in thiolated SAMs on NPs isolated the effects of ligand characteristics. More rapid exchange is observed on NPs protected by monolayers of shorter ligands;[46] this supports the idea of an associative mechanism in which the incoming ligands must penetrate the existing ligand shell. Additionally, ligands that have strong intermolecular interactions (such as the ability to hydrogen bond) resist better the penetration of incoming ligands, slowing the rate of place-exchange.[59] For incoming ligands, the rate of exchange slows for longer or bulkier ligands.[47] Similarly, a primary thiol is more reactive as an incoming molecule than a secondary or tertiary thiol (Figure 1.11).[52] Surprisingly, it was observed that incoming branched molecules react more quickly than linear thiols of the same molecular weight, perhaps because of the enhanced steric stability they provide to the defect sites in the existing SAM (which have a large free volume).[52] The chemistry of the incoming ligands matters as well: for para-

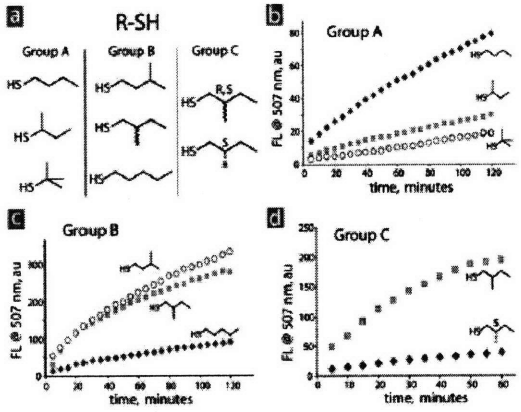

Figure 1.11
(a) Thiolated ligands used to study the effect of incoming ligand structure on the rate of place-exchange onto dye-labeled Au NPs. Dye was liberated as place-exchange proceeded, and the fluorescence intensity at 507 nm was plotted against reaction time. The effects of primary, secondary, and tertiary thiols are shown in (b); (c) shows linear versus branched thiols; and (d) illustrates the effect of thiol chirality. (Reproduced from 52)

substituted arylthiols, the reaction rate is increased for ligands with electron withdrawing substituents, a functionality that favors the polar Au-S bond.[48] Characteristics of the NP core itself also affect the place-exchange kinetics. Faster exchange is observed on more positively charged cores, and the equilibrium exchange percentage on these NPs is also higher.[49] This is again due to the polarity of the Au-S bond; positively charging the Au core enhances the polarity, facilitating bond formation. It has also been found that the initial reactivity of a NP is independent of the core diameter, because (within certain limits) there are the same number of vertices at which initial exchange occurs, regardless of the size of the NP.[50] However, the exchange proceeds to a different equilibrium depending on the NP size, because the ratio of vertex sites to terrace sites is a strong function of core size.

1.2.5.3 Place-exchange equilibrium

Minimal quantitative work has been carried out to investigate the thermodynamics of place-exchange once equilibrium has been reached. It has been determined that equilibrium is reached before the entire original ligand shell is exchanged for incoming ligands.[46] In his experiment exchanging one type of alkanethiol for another, Kassam[53] calculated an equilibrium constant for place-exchange onto Au NPs of approximately 1, suggesting that there is no difference between an incoming ligand binding and an original ligand rebinding to the NP surface.

1.3 One-dimensional assembly of nanoparticles

The assembly of NPs into specific structures is an important aim of nanotechnology, for in order to utilize NPs in devices, their positions relative to each other and to the environment must be precisely controllable. Under the right conditions, NPs can spontaneously assemble into two- and three-dimensional structures,[60,61] and have been made to act as 'artificial atoms' as building blocks of a wide range of crystal structures.[62]

The assembly of one-dimensional (1D) NP structures presents a particular challenge: NPs are inherently isotropic and thus will not spontaneously form into stable 1D assembles without some external driving force to break the symmetry of the inter-NP interactions. In spite of this fundamental barrier, a substantial selection of methods have been developed to guide the assembly of NPs into 1D structures.[63]

1.3.1 Applications of one-dimensional assemblies of nanoparticles

1D arrays of NPs have attracted significant research interest recently because of the immense scientific and technological promise they offer. The ability of 1D NP arrays to guide electromagnetic energy has already been demonstrated,[14,64] raising the possibility that such arrays can be used as sub-diffraction limit waveguides. In a similar vein, 1D assemblies of semiconductor NPs display Förster resonance energy transfer along the direction of the NP chains.[65] Collective magnetic properties[66,67] and nonlinear electrical properties[68] are other intriguing possibilities for application of 1D NP arrays.

1.3.2 Assembly onto a surface

One-dimensional chains of NPs can be formed directly on a surface, either by a patterning technique such as electron beam (e-beam) lithography or by assembly of NPs from solution onto the surface. While assembly directly onto a surface often has the potential to produce longer or more regular one-dimensional assemblies, the applications of such chains are be limited by the fact that they cannot be removed from the surface.

E-beam lithography is perhaps the method of forming 1D NP arrays that affords the most control over both the absolute and the relative positioning of the NPs. However, materials and resolution limitations restrict the scope of this technique. Chen[69] used e-beam lithography to form Au nanowires onto either TiO_2 or SiO_2 substrates; a subsequent anneal converted the wires into linear chains of closely spaced Au NPs (Figure 1.12). Corbierre wrote lines with e-beam lithography into a thin film of Au(I)-thiolate on an SiO_2 surface; pyrolysis of the organometallic line yielded a 1D line of Au NPs.

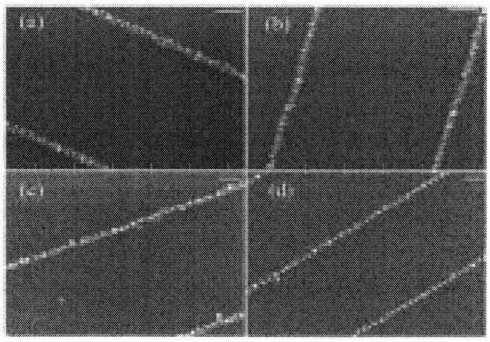

Figure 1.12
SEM images of an Au nanowire with an initial width of about 20 nm. Annealing at (a) 90 °C for 3 h, (b) 135 °C for 2 h, (c) 150 °C for 2 h, and (d) 250 °C for 3 h produces linear arrays of nanoparticles. Scale bars 100 nm. (Reproduced from 69)

Surface features such as grooves or terraces can be used as templates for the assembly or growth of NPs into 1D assemblies. Silica NPs have been assembled into grooves in a blanket SiO_2 film fabricated by interference lithography.[70] Ion-beam sputtering has also been used to fabricate arrays of Ag NPs on faceted alumina surfaces; under certain grazing incidence conditions, only selected facets are exposed to the ion beam, resulting in growth of 1D structures of NPs.[71] Bismuth nanolines have served as a template for the assembly lines of Ag NPs.[72]

NP arrays can also be templated by linear arrangements of molecules pre-assembled onto a surface. Linear supramolecular assemblies of *n*-hexadecyl dihydrogen phosphate and porphyrin derivatives complexed with Ag^+ were formed on a surface through Langmuir-Blodgett assembly.[73] Irradiation then generated 1D arrays of silver oxide NPs that formed along the linear template of the supramolecular surface structure (Figure 1.13). π-conjugated porphyrin polymers deposited onto a surface were used as a molecular template for the 1D assembly of Au NPs functionalized with pyridine-

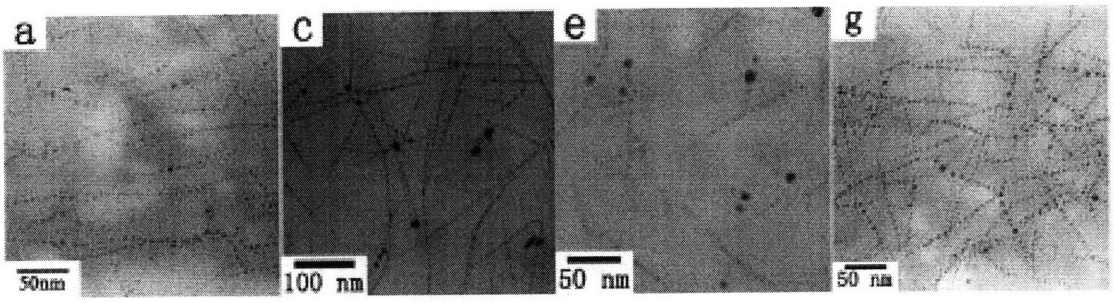

Figure 1.13
One-dimensional arrays of silver oxide NPs templated by linear assemblies of porphyrin derivatives and *n*-hexadecyl dihydrogen. (Reproduced from 73)

terminated ligands.[74] Kim[75] immobilized strands on DNA onto an amine-terminated siloxane monolayer on Si, then conjugated Au NPs coated with amine-terminated molecules onto the DNA via electrostatic interactions between the amines of the NPs and the phosphate groups of the DNA. Pt NPs were assembled onto a graphite surface on which hemicylindrical micellar linear templates had been formed.[76] Pt ions bound electrostatically to the protonated external groups of the surface micelles; the ions were then reduced to generate NPs aligned along the linear micelle templates.

Block copolymers are often used for NP assembly because of the variety of accessible morphologies. Cheng[77] patterned grooves onto a surface using e-beam lithography and then assembled diblock copolymers in the grooves. Because of the confinement, 1D arrays of nanospheres of block copolymer nanospheres were formed (Figure 1.14). Patterned block copolymer structures can also serve as a surface template for the 1D assembly of metal NPs.[78] Specifically, a block copolymer that can undergo a cylinder-to-sphere transition was assembled into a chemically defined linear pattern. Thermolysis of the block copolymer drove the transition to spheres, which were then used to guide NP synthesis (Au, ZnO, and Fe_2O_3), resulting in 1D arrays of NPs.

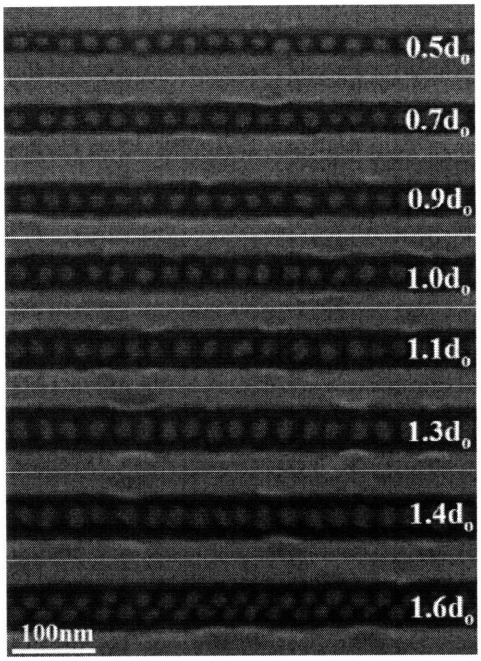

Figure 1.14
A composite image of domains of polyferrocenyldimethylsilane block copolymers within channels of different widths W. Linear arrangements of spheres form for certain ratios of W to d_0, where d_0 is the equilibrium row spacing of the block copolymer. (Reproduced from 77)

1.3.3 Templating on nanotubes

A natural strategy for the 1D assembly of NPs is the use of pre-existing 1D materials, such as nanotubes, as templates onto which NP arrays can be formed. These methods have the advantage that the templates are often microns long, which can translate into equally long 1D structures of NPs. However, there are often electronic interactions between the NPs and their supporting template; thus the use of a template inherently changes the properties of the NP assembly. Furthermore, 1D structures formed on a template do not exist in the absence of the template; that is, once formed, the nanotube template must be considered as an equal part of the NP assembly.

1.3.3.1 Carbon nanotubes

Carbon nanotubes (CNTs) are an obvious choice for templating 1D NP assembly. The highly conjugated electronic structure of CNTs limits the possibilities for covalent functionalization, and thus a variety of noncovalent strategies have also been developed for templated growth of NP arrays. Recent reviews[79,80] have discussed several approaches to assembly of metal and semiconductor NPs onto CNTs; here we highlight a few examples.

Covalent functionalization of the sidewalls of CNTs, although difficult to achieve, is an effective way to precisely control the assembly of NPs. CNTs can be functionalized with molecules terminating in a reactive end group; assembly of NPs then occurs either when the CNT sidewall functionality can directly bind to the NP itself or when the NPs possess a complementary functionality in their ligand shell. Bottini[81] covalently functionalized single-walled CNTs (SWCNTs) with amine- or thiol-terminated molecules, then assembled ZnS-CdSe core-shell NPs along the CNT via bond formation between the CdSe shell and the reactive sidewall groups of the CNTs, forming a 1D array of semiconductor NPs. Ravinandran[82,83] treated both SWCNTs and multi-walled CNTs (MWCNTs) with acid to oxidize the sidewalls and ends, then incubated the oxidized CNTs in a solution of ZnO NPs. The affinity of the Zn atoms for the carboxylic acid groups along the CNTs drove the assembly of ZnO NPs along the CNT templates. Au NPs also were assembled onto sidewall-functionalized CNTs via a click chemistry reaction.[84]

CNTs can also be non-covalently functionalized to template the formation of 1D NP structures. MWCNTs were wrapped in poly(sodium 4-styrenesulfonate), a negatively

charged polyelectrolyte, then coated with a positively charged monolayer of poly(diallyldimethylammonium chloride).[85] Silica-coated Au NPs were then deposited onto this second monolayer via electrostatic and van der Waals interactions (Figure 1.15), coating the CNTs with NPs. A different electrolyte, poly(allylamine hydrochloride), was also used to wrap MWCNTs in order to bind ZnO, CdSe, and CdSe-CdS NPs to the free amine functionalities in the polyelectrolyte layer.[86] Similarly, SWCNTs were wrapped in thiolated DNA molecules, onto which phosphine-stabilized Au NPs were attached through the formation of thiol-Au bonds.[87] SWCNTs were also noncovalently functionalized with 2,2':6',2''-terpyridine (Terpy) molecules.[88] Upon exposure in solution to salts of transition metals, NPs of Ru, Cu, or Sn formed along the CNTs due to electron transfer from the Terpy to the transition metal ions. Instead of functionalization with polyelectrolytes, NPs were also coated with a thin film of Zn.[89] Upon heat treatment to oxidize the film, ZnO NPs were found in 1D arrays along the MWCNTs.

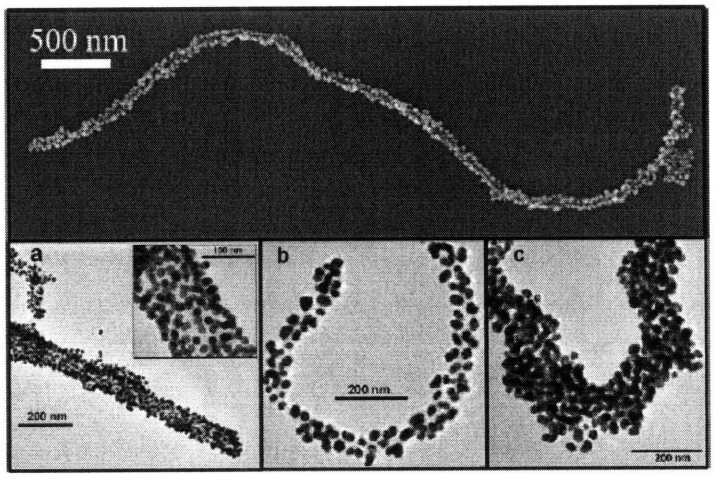

Figure 1.15
SEM (top) and TEM (bottom) images of single or double layers of Au@SiO2 nanoparticles assembled onto multi-walled carbon nanotubes. (Reproduced from 85)

NPs can also be directly assembled via non-specific adsoprtion onto CNT templates. CdSe quantum dots capped with pyridine assembled spontaneously onto bare SWCNTs without any chemical functionalization of the CNTs, due to π-π stacking between the CNT sidewalls and the aromatic pyridine rings on the quantum dots.[90] van der Waals interactions can also be used to bind ligand stabilized NPs to CNTs, as when linear arrays of CdSe and InP quantum dots were assembled using grooves in bundles of SWCNTs as templates.[91] A similar strategy was used to form arrays of noble metal NPs, such as Au, Ag, and Cu (Figure 1.16).[92]

In addition to assembly of NPs from solution, NPs can be synthesized directly at nucleation sites on CNTs. MWCNTs were wrapped with polyetheneimine, a molecule that acts both as a surfactant for the CNTs and as a reducing agent. Upon addition of a gold salt, Au NPs formed in situ along the length of the CNTs.[93,94] Similarly, poly(styrene-alt-maleic acid) can be used both as a surfactant to wrap SWCNTs and as a reducing agent to form Pt or Pd NPs on the CNTs.[95]

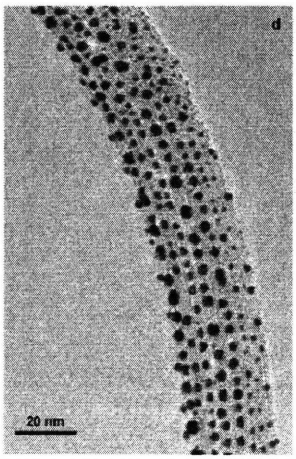

Figure 1.16
TEM image showing multiple linear arrays of Au particles on a curved bundle of nanotubes. (Reproduced from 92)

1.3.3.2 Other types of nanotubes

Inorganic nanotubes are likewise good templates for the growth of 1D NP arrays. For example, TiO_2 nanotubes were functionalized with amine-terminated molecules, then citrate-stabilized Au NPs were assembled along the length of the tubes (Figure 1.17).[96] Nanotubes made of biomolecules can also be used to template 1D NP assembly. Bionanotubes formed of monomers of the FliTrx *E. coli* flagellin protein were formed such that ordered arrays of binding sites for metal ions were located along the surfaces of the tubes.[97] The flagella nanotubes were incubated with solutions of metal ions, including Cu(II), Au(I), Co(II), Cd(II), and Pd(II). Subsequent reduction of the bound ions generated arrays of NPs aligned along the tubes. Peptide nanotubes coated with a synthetic peptide known to mineralize Au ions were also used as templates to grow Au NPs.[98] Prior to mineralization and growth of Au, the nanotubes were separated by size and only nanotubes with a diameter comparable to the desired NP size were selected to ensure 1D arrays of NPs (Figure 1.18).

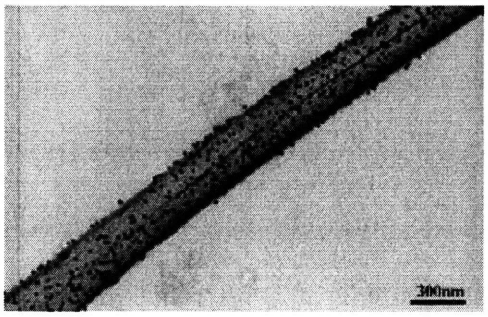

Figure 1.17
TEM image of a single TiO_2 nanotube coated with Au nanoparticles. (Reproduced from 96)

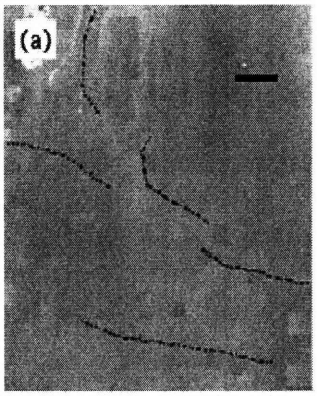

Figure 1.18
One-dimensional chains of Au nanoparticles grown on 10 nm diameter peptide nanotubes. Scale bar 100 nm. (Reproduced from 98)

1.3.4 Molecular templating

Linear molecules, such as polymers and DNA, offer another option for the templated self-assembly of 1D NP arrays. The use of molecules as templates obviates the need for chemical functionalization of the templates, a difficult task for materials such as CNTs. Here we discuss some recent examples of 1D NP arrays synthesized on molecular templates.

1.3.4.1 Templating on biomolecules

DNA has long been used to template the formation of NP arrays because of its ability to specifically bind to given chemical functionalities without modification.[63,99] More recently, the specific binding of DNA sequences has been used to encode self-assembly of Au NPs into linear structures up to 4 μm long.[100] Au NPs were functionalized with a thiol-terminated DNA strand of a given sequence. Rolling-circle polymerization was used to synthesize a template DNA strand with repeat units complementary to the DNA on the NPs. The NPs were then hybridized to the DNA

strand, creating extended arrays of particles. Chains of Ni NPs have also recently been created on DNA strands.[101]

Biomolecules other than DNA can also act as templates for the assembly of NP arrays. Bacteriophage was used to direct the assembly of linear arrays of NPs and also more complex structures. M13 bacteriophage can be engineered to produce specific peptides, such as gold-binding or streptavidin-binding motifs, at specific locations. In this way, the assembly of chains containing Au and/or CdSe NPs was programmed into the genetic code of the bacteriophage (Figure 1.19).[102]

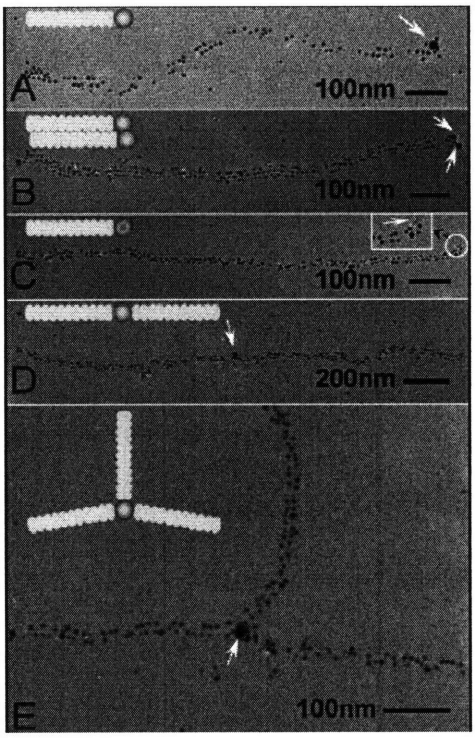

Figure 1.19
TEM images of various nanoparticle structures templated by the virus clone #9s1. 5 nm gold nanoparticles bind to certain proteins along the virus axis, forming one-dimensional arrays, while a motif on another protein binds streptavidin coated CdSe quantum dots and 1.5 nm gold nanoparticles. Arrow point to the streptavidin coated particles. The insets are schematics of the assembly, where yellow dots represent gold NPs, green dots represent CdSe quantum dots, and red dots represent the streptavidin coating around Au NPs or CdSe quantum dots. (Reproduced from 102)

1.3.4.2 Templating on polymers

Polymers are another ideal choice for templating the one-dimensional assembly of NPs because of their length and the regularity of the component repeat units. One strategy for assembly is to simply assemble NPs along the chain of an existing polymer via chemical interactions between the backbone or side groups of the polymer and the ligands or core of the NPs. Au NPs functionalized with carboxylic acid terminated ligands have been assembled along poly(ethylene oxide) (PEO) chains via hydrogen bonding between the regularly spaced oxygens along the PEO backbone and the carboxylic acid groups on the NPs.[104] Similarly, Au NPs were bound to polylysine via amide bond formation between carboxylic acid groups on the NPs and amide groups on the template polymer.[105] Hyaluronic acid was used as a template to assemble citrate stabilized Au NPs upon thiolation of the side chain carboxyl groups.[106]

Non-specific interactions with polymers can also be used to assemble NPs into linear structures. Pyridine- and carboxyl-functionalized dendritic polymers were used as templates for the coordination of Cd^{2+} ions and the subsequent growth of CdS NPs in structures that followed the morphology of the dendritic polymer.[107] Functionalizing Au NPs with thiolated oligo(p-phenylenevinylene) (OPV) and self-assembling them into tapes through π-stacking interactions generated linear hybrids of NPs and OPV.[108] Au NPs functionalized with a pyridyl-terminated porphyrin–oligo(p-phenylene vinylene) (P-OPV-Py) were likewise assembled into 1D and more complex structures through π-π interactions[103] (Figure 1.20).

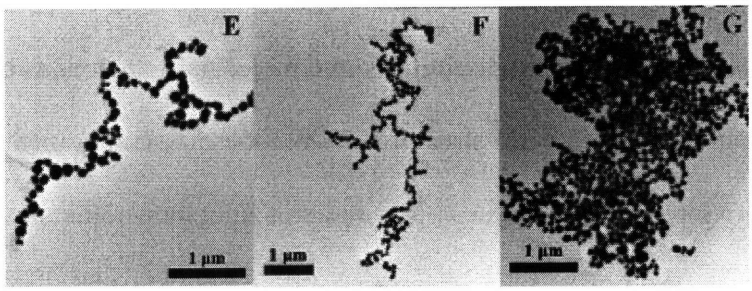

Figure 1.20
TEM images of P–OPV–Py capped Au nanoparticles with increasing ratios of P–OPV–Py to Au NPs. (Reproduced from 103)

Structures that are not technically polymers but are built from repeat building blocks can also be used as templates for NP assembly. For example, amphiphilic nanofibers self-assembled into supramolecular fibers that were designed to carry specific functionalities on the surface. Au NPs were assembled onto surface binding sites on these fibers, generating 1D arrays that extended for microns (Figure 1.21).[109]

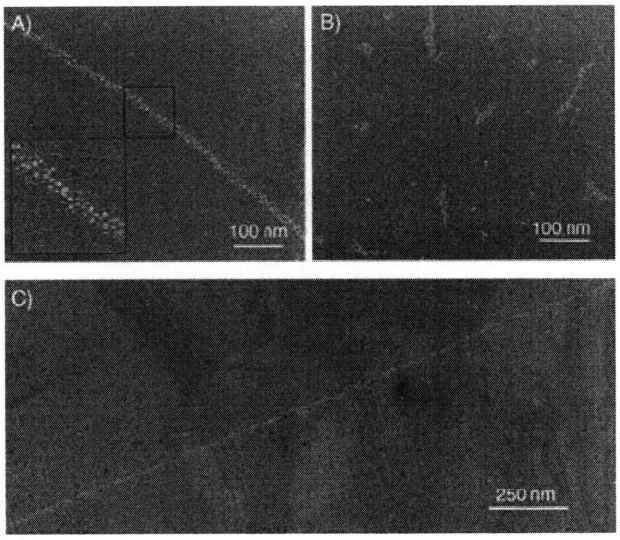

Figure 1.21
(a) and (c) TEM images of linear arrays of gold NPs in the presence of peptide nanofibers. (b) A TEM image of a control sample with unmodified NPs and nanofibers. (Reproduced from 109)

1.3.5 Chemically directed assembly in solution

Chemically directed assembly utilizes intermolecular interactions between NPs to drive the assembly of NPs into 1D structures. While these assembly methods offer more flexibility than templating approaches, there are still limitations: unless a covalent bond forms between NPs in the chain, the arrays may not be stable against changing environmental conditions.

An interfacial polymerization process reacted a gold salt in one phase with aniline in a second phase.[110] Au NPs and polyaniline were formed together, with a directional orientation due to the interfacial reaction. 1D assembly of Au NPs coated with a thiolated liquid crystal (LC) ligand, 4'-(12-mercaptododecyloxy)biphenyl-4-carbonitrile, occurred upon thermal treatment of the NPs.[111] The free LC ligand is nematic but because of the confinement on the NP surface, it behaved as a smectic when attached to the NP, inducing linear assembly.

Solution conditions can also drive interparticle interactions. At certain pH values, Au NPs coated with carboxylate terminated peptide ligands assembled into 1D structures because of intermolecular hydrogen bonding between carboxylic acid groups of adjacent NPs.[112] Tuning the surfactant population and the concentration of NPs in solution affects the interdigitation of the ligand shells of Au NPs;[113] certain situations generated parallel 1D structures of NPs (Figure 1.22).

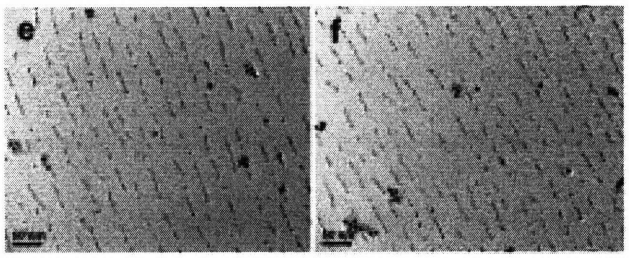

Figure 1.22
TEM images of 1D assemblies of Au nanoparticles formed by adjusting the ligand population and the solution concentration of NPs: (Reproduced from 113)

When Au NPs encapsulated in spherical micellar shells of poly(styrene-*block*-acrylic acid), PAA, were exposed to a solution that induces a transition from spherical to worm-like micelles in PAA, the PAA morphology transition caused the NPs to assemble into 1D chains (Figure 1.23).[114] Covalently bound amphiphilic ligands can also induce one-dimensional assembly: Au or Ag NPs functionalized with polystyrene-*b*-poly(ethylene oxide) spontaneously assembled in water into one-dimensional tubes.[115] This assembly was driven by hydrophobic effects.

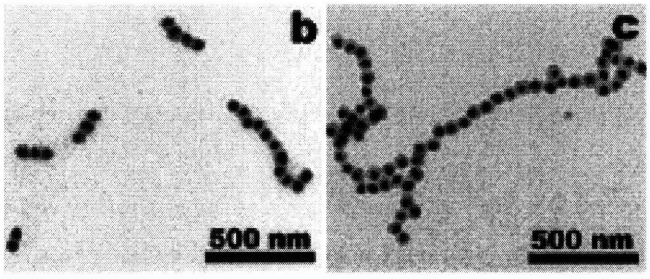

Figure 1.23
TEM images of chains of Au particles coated with poly(styrene-*block*-acrylic acid) formed by the addition of 1-(d-dimethylamino)propyl)-3-ethylcarbodiimide methiodide (EDC), a molecule that induces a transition from spherical to wormlike micelles. The concentration of EDC is 55 μM in (b) and 87 μM in (c). (Reproduced from 114)

1.3.6 Dipole driven assembly

NPs can be assembled into 1D structures based on dipolar interactions between particles. Dipoles arise in NPs because of an anisotropic distribution of surface charge, which can be induced by a change or redistribution of ligands. Lin[116] assembled Au NPs into chains and branched networks by replacing a small amount of surface adsorbed citrate molecules with 2-mercaptoethyl alcohol (Figure 1.24); the mixed ligand coating causes a surface charge separation and stablizes the electric dipole in the NP. Au NPs capped with cinnamic acid were assembled into 1D nanostructures either by changing the concentration of cinnamic acid or by tuning the solution pH, both of which affect the surface charge and thus the interparticle dipolar interactions.[117] Linear assembly of citrate-stabilized Au NPs can also be induced by the addition of cetyltrimethylammonium bromide, which preferentially binds to (100)-type facets, displacing the citrate ligands and causing a redistribution in surface charge.[118] Partial ligand removal resulting in redistribution of surface charge also has led to chain formation via dipolar interactions for Au[119] and CdS[120] NPs.

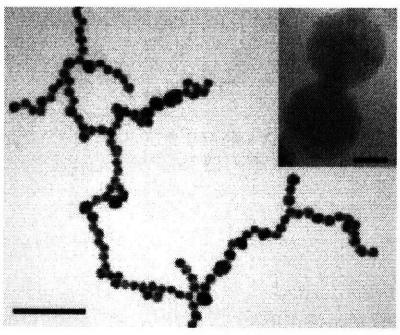

Figure 1.24
TEM image showing a chain network of Au NPs formed upon addition of 2-mercaptoethyl alcohol to citrate-stabilized particles. The inset shows organic material at the contact between two adjacent NPs. Scale bars 100 nm; 5 nm in the inset. (Reproduced from 116)

1.3.7 Field driven assembly

NPs can be assembled by external electric or magnetic fields into one-dimensional structures that align along the field. Zeng[121] described the use of an in situ magnetic field during the synthesis of Co NPs to align the NPs into one-dimensional structures. Poly(vinyl pyrrolidone) present during the NP synthesis was thought to wrap around the chain structure, stabilizing it even after removal of the field. After application of the field, Au^+ ions were added to form Au NPs; the Co was dissolved to leave chains of hollow Au NPs. Similar results were also achieved with Pt and Pd (Figure 1.25). It is believed that the magnetic dipole interactions between Co NPs are too weak to form chains in the absence of an external magnetic field; however, an applied magnetic field can enhance the magnetic dipolar interaction between the NPs. Fang[122] observed chain-like alignment of Fe_3O_4 NPs after application of a magnetic field to a Fe_3O_4 magnetic fluid.

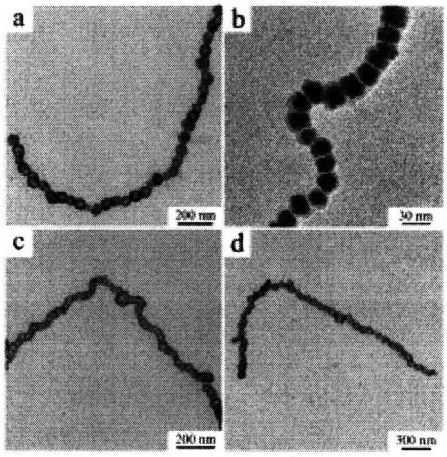

Figure 1.25
TEM images of NP chains assembled under an external magnetic field of 125 mT. Chains are composed of (a) hollow Au NPs, (b) Co NPs, (c) hollow Pt NPs, and (d) hollow Pd NPs. (Reproduced from 121)

An electric field can also be used to align NPs into one-dimensional structures, as demonstrated by Sun,[123] who used a metal probe and a copper TEM grid as two electrodes to induce chaining of Au NPs and organic spheres via the dielectrophoretic force induced by an alternating electric field.

1.3.8 Chemically directed linear assembly of nanorods

A substantial body of work also exists to direct the 1D assembly of nanorods. In general, the strategies presented above for templating 1D structures of NPs are also applicable to nanorod assembly:[124,125] for example, nanorods were bound to CNTs[85,91,126] or assembled onto linear molecular templates on a surface.[73] Here, we focus on a selection of methods to direct the assembly of nanorods based on specific chemical functionalization of the nanorods.

In one method of chemically directed nanorod assembly, the ends of the nanorods are made of a different material than the center; thus, the end can be functionalized by molecules terminated with reactive end groups while the sidewalls of the nanorods remain unreacted. Chen[127,128] formed end-to-end linkages of Ni nanorods capped with Au at the two ends; the gold ends were functionalized with biotin-terminated thiol and the rods were joined into 1D structures via biotin-avidin bonding (Figure 1.26). Similarly, Pt nanorods[129] and CdSe nanorods[130] were synthesized with Au end caps, end functionalized with thiolated biotin, and linked by biotin-avidin coupling.

The other method relies on the crystallographic structure of the nanorods: gold nanorods generally grow with the {110} faces along the length of the rods and the {111} faces at the ends. A number of studies have taken advantage of the fact that the commonly used surfactant, cetyltrimethylammonium bromide (CTAB), preferentially

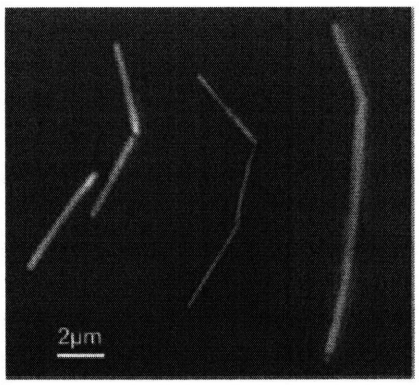

Figure 1.26
Optical images of chains of Au/Ni/Au nanowires formed by selectively functionalizing the Au ends with thiolated biotin and joining with avidin. (Reproduced from 127)

binds to the {110} faces of gold and forms a less ordered monolayer on the {111} faces; simultaneously, thiolated molecules preferentially bind to the {111} faces of gold.[131-137] Various types of inter-rod linkages have been formed by specifically binding thiolated molecules with reactive end groups to the {111} ends of gold nanorods and assembling the rods into 1D structures. Thiolated biotin[131] and thiolated anti-mouse IgG[132] were assembled onto nanorod ends, which were then assembled by linking with streptavidin and mouse IgG (Figure 1.27), respectively. Hydrogen bonding was used to

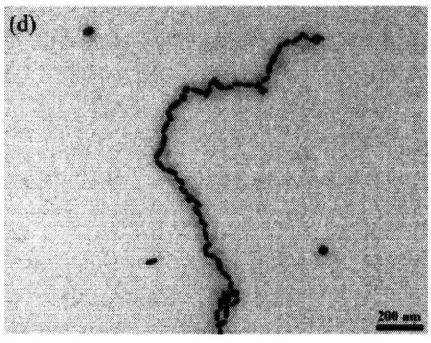

Figure 1.27
TEM image of chains of gold nanorods with anti-mouse IgG at the ends and joined through reaction with mouse IgG. (Reproduced from 132)

assemble nanorods with carboxylic acid terminated alkanethiols[133] or various amino acids[134,135] placed at the ends. Thiolated oligonucleotides enabled specific assembly of nanorods into 1D structures.[136] Placing thiolated crown ethers at nanorod ends and exposing the nanorods to solutions of Na^+ or K^+ ions triggered end-to-end assembly by electrostatic coordination between the crown ethers and the metal ions.[137]

In a similar vein, in TiO_2 nanorods, enediol ligands such as dopamine bind preferentially to undercoordinated Ti atoms at the ends of the rods. This preference was exploited to conjugate biotin to the ends of TiO_2 nanorods; self-assembly into 1D structures can then be triggered by biotin-avidin linkages.[138]

1.4 References

(1) Murray, C. B.; Kagan, C. R.; Bawendi, M. G. *Annual Review of Materials Science* **2000**, *30*, 545-610.

(2) Burns, A.; Ow, H.; Wiesner, U. *Chemical Society Reviews* **2006**, *35*, 1028-1042.

(3) Polleux, J.; Pinna, N.; Antonietti, M.; Niederberger, M. *Advanced Materials* **2004**, *16*, 436-+.

(4) Henglein, A.; Giersig, M. *Journal of Physical Chemistry B* **1999**, *103*, 9533-9539.

(5) Brust, M.; Walker, M.; Bethell, D.; Schiffrin, D. J.; Whyman, R. *Journal of the Chemical Society-Chemical Communications* **1994**, 801-802.

(6) Brust, M.; Fink, J.; Bethell, D.; Schiffrin, D. J.; Kiely, C. *Journal of the Chemical Society-Chemical Communications* **1995**, 1655-1656.

(7) Zanchet, D.; Hall, B. D.; Ugarte, D. *Journal of Physical Chemistry B* **2000**, *104*, 11013-11018.

(8) Stellacci, F.; Bauer, C. A.; Meyer-Friedrichsen, T.; Wenseleers, W.; Marder, S. R.; Perry, J. W. *Journal of the American Chemical Society* **2003**, *125*, 328-329.

(9) Mie, G. *Annalen der Physik* **1908**, *25*, 376-445.

(10) Link, S.; Wang, Z. L.; El-Sayed, M. A. *Journal of Physical Chemistry B* **1999**, *103*, 3529-3533.

(11) Malinsky, M. D.; Kelly, K. L.; Schatz, G. C.; Van Duyne, R. P. *Journal of the American Chemical Society* **2001**, *123*, 1471-1482.

(12) Raschke, G.; Kowarik, S.; Franzl, T.; Sonnichsen, C.; Klar, T. A.; Feldmann, J.; Nichtl, A.; Kurzinger, K. *Nano Letters* **2003**, *3*, 935-938.

(13) McFarland, A. D.; Van Duyne, R. P. *Nano Letters* **2003**, *3*, 1057-1062.

(14) Maier, S. A.; Kik, P. G.; Atwater, H. A.; Meltzer, S.; Harel, E.; Koel, B. E.; Requicha, A. A. G. *Nature Materials* **2003**, *2*, 229-232.

(15) Maier, S. A.; Kik, P. G.; Atwater, H. A. *Applied Physics Letters* **2002**, *81*, 1714-1716.

(16) Wei, Q. H.; Su, K. H.; Durant, S.; Zhang, X. *Nano Letters* **2004**, *4*, 1067-1071.

(17) Averin, D. V.; Likharev, K. K. *Journal of Low Temperature Physics* **1986**, *62*, 345-373.

(18) Andres, R. P.; Bein, T.; Dorogi, M.; Feng, S.; Henderson, J. I.; Kubiak, C. P.; Mahoney, W.; Osifchin, R. G.; Reifenberger, R. *Science* **1996**, *272*, 1323-1325.

(19) Ingram, R. S.; Hostetler, M. J.; Murray, R. W.; Schaaff, T. G.; Khoury, J. T.; Whetten, R. L.; Bigioni, T. P.; Guthrie, D. K.; First, P. N. *Journal of the American Chemical Society* **1997**, *119*, 9279-9280.

(20) Chaki, N. K.; Gopakumar, T. G.; Maddanimath, T.; Aslam, M.; Vijayamohanan, K. *Journal of Applied Physics* **2003**, *94*, 7379-7379.

(21) Brousseau, L. C.; Zhao, Q.; Shultz, D. A.; Feldheim, D. L. *Journal of the American Chemical Society* **1998**, *120*, 7645-7646.

(22) Hicks, J. F.; Templeton, A. C.; Chen, S. W.; Sheran, K. M.; Jasti, R.; Murray, R. W.; Debord, J.; Schaaf, T. G.; Whetten, R. L. *Analytical Chemistry* **1999**, *71*, 3703-3711.

(23) Bain, C. D.; Troughton, E. B.; Tao, Y. T.; Evall, J.; Whitesides, G. M.; Nuzzo, R. G. *Journal of the American Chemical Society* **1989**, *111*, 321-335.

(24) Schreiber, F. *Progress in Surface Science* **2000**, *65*, 151-256.

(25) Love, J. C.; Estroff, L. A.; Kriebel, J. K.; Nuzzo, R. G.; Whitesides, G. M. *Chemical Reviews* **2005**, *105*, 1103-1169.

(26) Ulman, A. *Chemical Reviews* **1996**, *96*, 1533-1554.

(27) Bain, C. D.; Evall, J.; Whitesides, G. M. *Journal of the American Chemical Society* **1989**, *111*, 7155-7164.

(28) Halik, M.; Klauk, H.; Zschieschang, U.; Schmid, G.; Dehm, C.; Schutz, M.; Maisch, S.; Effenberger, F.; Brunnbauer, M.; Stellacci, F. *Nature* **2004**, *431*, 963-966.

(29) Lahann, J.; Mitragotri, S.; Tran, T. N.; Kaido, H.; Sundaram, J.; Choi, I. S.; Hoffer, S.; Somorjai, G. A.; Langer, R. *Science* **2003**, *299*, 371-374.

(30) Barrena, E.; Palacios-Lidon, E.; Munuera, C.; Torrelles, X.; Ferrer, S.; Jonas, U.; Salmeron, M.; Ocal, C. *Journal of the American Chemical Society* **2004**, *126*, 385-395.

(31) Barrena, E.; Ocal, C.; Salmeron, M. *Journal of Chemical Physics* **2001**, *114*, 4210-4214.

(32) Stranick, S. J.; Parikh, A. N.; Tao, Y. T.; Allara, D. L.; Weiss, P. S. *Journal of Physical Chemistry* **1994**, *98*, 7636-7646.

(33) Folkers, J. P.; Laibinis, P. E.; Whitesides, G. M. *Langmuir* **1992**, *8*, 1330-1341.

(34) Smith, R. K.; Reed, S. M.; Lewis, P. A.; Monnell, J. D.; Clegg, R. S.; Kelly, K. F.; Bumm, L. A.; Hutchison, J. E.; Weiss, P. S. *Journal of Physical Chemistry B* **2001**, *105*, 1119-1122.

(35) Singh, C.; Ghorai, P. K.; Horsch, M. A.; Jackson, A. M.; Larson, R. G.; Stellacci, F.; Glotzer, S. C. *submitted* **2007**.

(36) Templeton, A. C.; Wuelfing, M. P.; Murray, R. W. *Accounts of Chemical Research* **2000**, *33*, 27-36.

(37) Jackson, A. M.; Myerson, J. W.; Stellacci, F. *Nature Materials* **2004**, *3*, 330-336.

(38) Boyen, H. G.; Kastle, G.; Weigl, F.; Ziemann, P.; Schmid, G.; Garnier, M. G.; Oelhafen, P. *Physical Review Letters* **2001**, *87*.

(39) Dubois, L. H.; Nuzzo, R. G. *Annual Review of Physical Chemistry* **1992**, *43*, 437-463.

(40) Ulman, A. *An introduction to ultrathin organic films : from Langmuir-Blodgett to self-assembly*; Academic Press: Boston, 1991.

(41) Biebuyck, H. A.; Whitesides, G. M. *Langmuir* **1993**, *9*, 1766-1770.

(42) Biebuyck, H. A.; Bian, C. D.; Whitesides, G. M. *Langmuir* **1994**, *10*, 1825-1831.

(43) Collard, D. M.; Fox, M. A. *Langmuir* **1991**, *7*, 1192-1197.

(44) Lee, L. Y. S.; Lennox, R. B. *Langmuir* **2007**, *23*, 292-296.

(45) Wrzosek, B.; Bukowska, J.; Kudelski, A. *Vibrational Spectroscopy* **2005**, *39*, 257-261.

(46) Hostetler, M. J.; Templeton, A. C.; Murray, R. W. *Langmuir* **1999**, *15*, 3782-3789.

(47) Ingram, R. S.; Hostetler, M. J.; Murray, R. W. *Journal of the American Chemical Society* **1997**, *119*, 9175-9178.

(48) Donkers, R. L.; Song, Y.; Murray, R. W. *Langmuir* **2004**, *20*, 4703-4707.

(49) Song, Y.; Murray, R. W. *Journal of the American Chemical Society* **2002**, *124*, 7096-7102.

(50) Guo, R.; Song, Y.; Wang, G. L.; Murray, R. W. *Journal of the American Chemical Society* **2005**, *127*, 2752-2757.

(51) Montalti, M.; Prodi, L.; Zaccheroni, N.; Baxter, R.; Teobaldi, G.; Zerbetto, F. *Langmuir* **2003**, *19*, 5172-5174.

(52) Hong, R.; Fernandez, J. M.; Nakade, H.; Arvizo, R.; Emrick, T.; Rotello, V. M. *Chemical Communications* **2006**, 2347-2349.

(53) Kassam, A.; Bremner, G.; Clark, B.; Ulibarri, G.; Lennox, R. B. *Journal of the American Chemical Society* **2006**, *128*, 3476-3477.

(54) Song, Y.; Huang, T.; Murray, R. W. *Journal of the American Chemical Society* **2003**, *125*, 11694-11701.

(55) Zachary, M.; Chechik, V. *Angewandte Chemie-International Edition* **2007**, *46*, 3304-3307.

(56) Cygan, M. T.; Dunbar, T. D.; Arnold, J. J.; Bumm, L. A.; Shedlock, N. F.; Burgin, T. P.; Jones, L.; Allara, D. L.; Tour, J. M.; Weiss, P. S. *Journal of the American Chemical Society* **1998**, *120*, 2721-2732.

(57) Ionita, P.; Caragheorgheopol, A.; Gilbert, B. C.; Chechik, V. *Journal of the American Chemical Society* **2002**, *124*, 9048-9049.

(58) Ionita, P.; Caragheorgheopol, A.; Gilbert, B. C.; Chechik, V. *Langmuir* **2004**, *20*, 11536-11544.

(59) Tamchang, S. W.; Biebuyck, H. A.; Whitesides, G. M.; Jeon, N.; Nuzzo, R. G. *Langmuir* **1995**, *11*, 4371-4382.

(60) Ibanez, F. J.; Gowrishetty, U.; Crain, M. M.; Walsh, K. M.; Zamborini, F. P. *Analytical Chemistry* **2006**, *78*, 753-761.

(61) Pileni, M. P. *Accounts of Chemical Research* **2007**, *40*, 685-693.

(62) Shevchenko, E. V.; Talapin, D. V.; Kotov, N. A.; O'Brien, S.; Murray, C. B. *Nature* **2006**, *439*, 55-59.

(63) Tang, Z. Y.; Kotov, N. A. *Advanced Materials* **2005**, *17*, 951-962.

(64) Maier, S. A.; Brongersma, M. L.; Kik, P. G.; Meltzer, S.; Requicha, A. A. G.; Atwater, H. A. *Advanced Materials* **2001**, *13*, 1501-1505.

(65) Tang, Z. Y.; Ozturk, B.; Wang, Y.; Kotov, N. A. *Journal of Physical Chemistry B* **2004**, *108*, 6927-6931.

(66) Petit, C.; Russier, V.; Pileni, M. P. *Journal of Physical Chemistry B* **2003**, *107*, 10333-10336.

(67) Lalatonne, Y.; Richardi, J.; Pileni, M. P. *Nature Materials* **2004**, *3*, 121-125.

(68) Braun, E.; Eichen, Y.; Sivan, U.; Ben-Yoseph, G. *Nature* **1998**, *391*, 775-778.

(69) Chen, Y.; Goldman, A. M. *Applied Physics Letters* **2007**, *91*.

(70) Mertens, K.; Putkaradze, V.; Xia, D. Y.; Brueck, S. R. J. *Journal of Applied Physics* **2005**, *98*.

(71) Camelio, S.; Babonneau, D.; Lantiat, D.; Simonot, L. *Epl* **2007**, *79*.

(72) Owen, J. H. G.; Miki, K. *Surface Science* **2006**, *600*, 2943-2953.

(73) Liu, H. G.; Xiao, F.; Wang, C. W.; Xue, Q. B.; Chen, X.; Lee, Y. I.; Hao, J. C.; Jiang, J. H. *Journal of Colloid and Interface Science* **2007**, *314*, 297-303.

(74) Ozawa, H.; Kawao, M.; Tanaka, H.; Ogawa, T. *Langmuir* **2007**, *23*, 6365-6371.

(75) Kim, H. J.; Roh, Y.; Hong, B. *Journal of Vacuum Science & Technology A* **2006**, *24*, 1327-1331.

(76) Kawasaki, H.; Uota, M.; Yoshimura, T.; Fujikawa, D.; Sakai, G.; Kijima, T. *Journal of Colloid and Interface Science* **2006**, *300*, 149-154.

(77) Cheng, J. Y.; Zhang, F.; Chuang, V. P.; Mayes, A. M.; Ross, C. A. *Nano Letters* **2006**, *6*, 2099-2103.

(78) La, Y. H.; Stoykovich, M. P.; Park, S. M.; Nealey, P. F. *Chemistry of Materials* **2007**, *19*, 4538-4544.

(79) Georgakilas, V.; Gournis, D.; Tzitzios, V.; Pasquato, L.; Guldi, D. M.; Prato, M. *Journal of Materials Chemistry* **2007**, *17*, 2679-2694.

(80) Wildgoose, G. G.; Banks, C. E.; Compton, R. G. *Small* **2006**, *2*, 182-193.

(81) Bottini, M.; Magrini, A.; Dawson, M. I.; Rosato, N.; Bergamaschi, A.; Mustelin, T. *Carbon* **2007**, *45*, 673-676.

(82) Ravindran, S.; Ozkan, C. S. *Nanotechnology* **2005**, *16*, 1130-1136.

(83) Ravindran, S.; Andavan, G. T. S.; Ozkan, C. *Nanotechnology* **2006**, *17*, 723-727.

(84) Voggu, R.; Suguna, P.; Chandrasekaran, S.; Rao, C. N. R. *Chemical Physics Letters* **2007**, *443*, 118-121.

(85) Correa-Duarte, M. A.; Liz-Marzan, L. M. *Journal of Materials Chemistry* **2006**, *16*, 22-25.

(86) Olek, M.; Busgen, T.; Hilgendorff, M.; Giersig, M. *Journal of Physical Chemistry B* **2006**, *110*, 12901-12904.

(87) Han, X. G.; Li, Y. L.; Deng, Z. X. *Advanced Materials* **2007**, *19*, 1518-+.

(88) Lee, Y.; Song, H. J.; Shin, H. S.; Shin, H. J.; Choi, H. C. *Small* **2005**, *1*, 975-979.

(89) Zhu, Y. W.; Elim, H. I.; Foo, Y. L.; Yu, T.; Liu, Y. J.; Ji, W.; Lee, J. Y.; Shen, Z. X.; Wee, A. T. S.; Thong, J. T. L.; Sow, C. H. *Advanced Materials* **2006**, *18*, 587-+.

(90) Li, Q. W.; Sun, B. Q.; Kinloch, I. A.; Zhi, D.; Sirringhaus, H.; Windle, A. H. *Chemistry of Materials* **2006**, *18*, 164-168.

(91) Engtrakul, C.; Kim, Y. H.; Nedeljkovic, J. M.; Ahrenkiel, S. P.; Gilbert, K. E. H.; Alleman, J. L.; Zhang, S. B.; Micic, O. I.; Nozik, A. J.; Heben, M. J. *Journal of Physical Chemistry B* **2006**, *110*, 25153-25157.

(92) Huang, W. J.; Chen, H.; Zuo, J. M. *Small* **2006**, *2*, 1418-1421.

(93) Hu, X. G.; Wang, T.; Qu, X. H.; Dong, S. J. *Journal of Physical Chemistry B* **2006**, *110*, 853-857.

(94) Hu, X. G.; Wang, T.; Wang, L.; Guo, S. J.; Dong, S. J. *Langmuir* **2007**, *23*, 6352-6357.

(95) Wang, D.; Li, Z. C.; Chen, L. W. *Journal of the American Chemical Society* **2006**, *128*, 15078-15079.

(96) Xu, J. Z.; Zhao, W. B.; Zhu, J. J.; Li, G. X.; Chen, H. Y. *Journal of Colloid and Interface Science* **2005**, *290*, 450-454.

(97) Kumara, M. T.; Tripp, B. C.; Muralidharan, S. *Chemistry of Materials* **2007**, *19*, 2056-2064.

(98) Gao, X. Y.; Djalali, R.; Haboosheh, A.; Samson, J.; Nuraje, N.; Matsui, H. *Advanced Materials* **2005**, *17*, 1753-+.

(99) Niemeyer, C. M.; Simon, U. *European Journal of Inorganic Chemistry* **2005**, 3641-3655.

(100) Deng, Z. X.; Tian, Y.; Lee, S. H.; Ribbe, A. E.; Mao, C. D. *Angewandte Chemie-International Edition* **2005**, *44*, 3582-3585.

(101) Gu, Q.; Cheng, C. D.; Suryanarayanan, S.; Dai, K.; Haynie, D. T. *Physica E-Low-Dimensional Systems & Nanostructures* **2006**, *33*, 92-98.

(102) Huang, Y.; Chiang, C. Y.; Lee, S. K.; Gao, Y.; Hu, E. L.; De Yoreo, J.; Belcher, A. M. *Nano Letters* **2005**, *5*, 1429-1434.

(103) Liu, X. F.; He, X. R.; Jiu, T. G.; Yuan, M. J.; Xu, J. L.; Lv, J.; Liu, H. B.; Li, Y. L. *Chemphyschem* **2007**, *8*, 906-912.

(104) Bhattacharjee, R. R.; Mandal, T. K. *Journal of Colloid and Interface Science* **2007**, *307*, 288-295.

(105) Dai, Q.; Worden, J. G.; Trullinger, J.; Huo, Q. *Journal of the American Chemical Society* **2005**, *127*, 8008-8009.

(106) Lee, H.; Choi, S. H.; Park, T. G. *Macromolecules* **2006**, *39*, 23-25.

(107) Zhang, Y. H.; Chen, Y. M.; Niu, H. J.; Gao, M. Y. *Small* **2006**, *2*, 1314-1319.

(108) van Herrikhuyzen, J.; George, S. J.; Vos, M. R. J.; Sommerdijk, N.; Ajayaghosh, A.; Meskers, S. C. J.; Schenning, A. *Angewandte Chemie-International Edition* **2007**, *46*, 1825-1828.

(109) Li, L. S.; Stupp, S. I. *Angewandte Chemie-International Edition* **2005**, *44*, 1833-1836.

(110) Mallick, K.; Witcomb, M. J.; Scurrell, M. S. *Journal of Physics -- Condensed Matter* **2007**, *19*.

(111) In, I.; Jun, Y. W.; Kim, Y. J.; Kim, S. Y. *Chemical Communications* **2005**, 800-801.

(112) Si, S.; Mandal, T. K. *Langmuir* **2007**, *23*, 190-195.

(113) Zhang, Y. X.; Zeng, H. C. *Journal of Physical Chemistry B* **2006**, *110*, 16812-16815.

(114) Kang, Y. J.; Erickson, K. J.; Taton, T. A. *Journal of the American Chemical Society* **2005**, *127*, 13800-13801.

(115) Zubarev, E. R.; Xu, J.; Sayyad, A.; Gibson, J. D. *Journal of the American Chemical Society* **2006**, *128*, 15098-15099.

(116) Lin, S.; Li, M.; Dujardin, E.; Girard, C.; Mann, S. *Advanced Materials* **2005**, *17*, 2553-+.

(117) Wang, L.; Wei, G.; Sun, L. L.; Liu, Z. G.; Song, Y. H.; Yang, T.; Sun, Y. J.; Guo, C. L.; Li, Z. *Nanotechnology* **2006**, *17*, 2907-2912.

(118) Yang, Y.; Matsubara, S.; Nogami, M.; Shi, J. L.; Huang, W. M. *Nanotechnology* **2006**, *17*, 2821-2827.

(119) Si, S.; Kotal, A.; Mandal, T. K. *Journal of Physical Chemistry C* **2007**, *111*, 1248-1255.

(120) Zhang, B.; Mu, J.; Li, X. Q. *Applied Surface Science* **2006**, *252*, 4990-4994.

(121) Zeng, H.; Huang, J. L.; Lu, W.; Wang, X. P.; Wang, B.; Zhang, S. Y.; Hou, J. G. *Advanced Materials* **2007**, *19*, 2172-+.

(122) Fang, W. X.; He, Z. H.; Xu, X. Q.; Mao, Z. Q.; Shen, H. *Epl* **2007**, *77*.

(123) Sun, J. F.; Guo, Z. R.; Wang, C. L.; Gu, N. *Chemphyschem* **2005**, *6*, 2485-2488.

(124) Murphy, C. J.; San, T. K.; Gole, A. M.; Orendorff, C. J.; Gao, J. X.; Gou, L.; Hunyadi, S. E.; Li, T. *Journal of Physical Chemistry B* **2005**, *109*, 13857-13870.

(125) Perez-Juste, J.; Pastoriza-Santos, I.; Liz-Marzan, L. M.; Mulvaney, P. *Coordination Chemistry Reviews* **2005**, *249*, 1870-1901.

(126) Correa-Duarte, M. A.; Perez-Juste, J.; Sanchez-Iglesias, A.; Giersig, M.; Liz-Marzan, L. M. *Angewandte Chemie-International Edition* **2005**, *44*, 4375-4378.

(127) Chen, M.; Guo, L.; Ravi, R.; Searson, P. C. *Journal of Physical Chemistry B* **2006**, *110*, 211-217.

(128) Chen, M.; Searson, P. C. *Advanced Materials* **2005**, *17*, 2765-+.

(129) Salem, A. K.; Chen, M.; Hayden, J.; Leong, K. W.; Searson, P. C. *Nano Letters* **2004**, *4*, 1163-1165.

(130) Salant, A.; Amitay-Sadovsky, E.; Banin, U. *Journal of the American Chemical Society* **2006**, *128*, 10006-10007.

(131) Caswell, K. K.; Wilson, J. N.; Bunz, U. H. F.; Murphy, C. J. *Journal of the American Chemical Society* **2003**, *125*, 13914-13915.

(132) Chang, J. Y.; Wu, H. M.; Chen, H.; Ling, Y. C.; Tan, W. H. *Chemical Communications* **2005**, 1092-1094.

(133) Thomas, K. G.; Barazzouk, S.; Ipe, B. I.; Joseph, S. T. S.; Kamat, P. V. *Journal of Physical Chemistry B* **2004**, *108*, 13066-13068.

(134) Hu, X. G.; Cheng, W. L.; Wang, T.; Wang, E. K.; Dong, S. J. *Nanotechnology* **2005**, *16*, 2164-2169.

(135) Zhang, S. Z.; Kou, X. S.; Yang, Z.; Shi, Q. H.; Stucky, G. D.; Sun, L. D.; Wang, J. F.; Yan, C. H. *Chemical Communications* **2007**, 1816-1818.

(136) Pan, B. F.; Ao, L. M.; Gao, F.; Tian, H. Y.; He, R.; Cui, D. X. *Nanotechnology* **2005**, *16*, 1776-1780.

(137) Nakashima, H.; Furukawa, K.; Kashimura, Y.; Torimitsu, K. *Chemical Communications* **2007**, 1080-1082.

(138) Dimitrijevic, N. M.; Saponjic, Z. V.; Rabatic, B. M.; Rajh, T. *Journal of the American Chemical Society* **2005**, *127*, 1344-1345.

Chapter 2: Ligand arrangement on nanoparticles

2.1 Self-assembled monolayers on nanoparticles: Overview

Thiolated self-assembled monolayers (SAMs) on metal nanoparticles (NPs) share many properties with SAMs on flat surfaces. However, the structure of SAMs on NPs is complicated by the need to arrange what should be a two-dimensional assembly onto a three-dimensional surface. Furthermore, phase separation in mixed ligand SAMs also differs from that on flat surfaces for two reasons: first, because NPs are often of a similar size to the domains that form in phase separated SAMs on flat surfaces; and second, because the spherical nature of a NP imposes boundary conditions on the molecular arrangement.

Here we discuss the structure of homoligand and mixed ligand SAMs on NPs from both a theoretical and an experimental perspective. We then consider a topological approach to understanding the arrangement of ligand molecules.

2.2 Homoligand nanoparticles

Although homoligand NPs are not the focus of this work, knowledge of the ligand arrangement in this simpler system can guide an understanding of the more complex mixed ligand system central to this research.

2.2.1 Models of ligand arrangement

There are two primary models describing the ligand arrangement of SAMs on NPs. In the crystallographic model, the NP core is taken to consist of locally flat {100} and {111} type facets;[1] on each facet, the ligand arrangement resembles that of a SAM

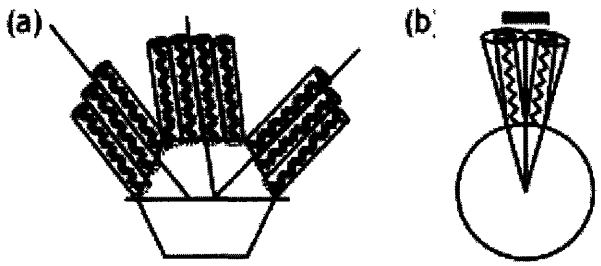

Figure 2.1
Schematics of potential ligand arrangements on nanoparticles. (a) The crystallographic model assumes that the ligands attain their optimal tilt angle on each individual facet of the NP core, generating line defects at facet edges. (b) The continuous model represents NPs as perfect spheres; ligand molecules radiate uniformly outward. (From reference 2)

on a flat surface (Figure 2.1(a)). That is, on each facet the ligands adopt a uniform tilt angle relative to the normal to the facet, thus generating line defects at each facet edge. Alternatively, the continuous model[3] represents NPs as spheres with ligand molecules radiating outward from the core; the thiol groups at the core are closely packed while the extended endgroups of the molecules are only loosely packed (Figure 2.1(b)). Simulations have addressed both of these cases.

Ghorai performed molecular dynamics simulations of the organization of SAMs on Au NPs, considered to be spheres.[4] At high temperatures (and also for short ligands), the ligands do not order but instead point radially away from the surface, as in the continuous model (Figure 2.2). However, at lower temperatures (and for long ligands), long-range ordering of the ligands occurs and the ligand shell divides into various regions, each with a common tilt angle, separated by line defects (Figure 2.2). This low temperature regime surprisingly resembles the crystallographic model, despite the assumption of an underlying spherical NP core. These results are explained thermodynamically: potential energy favors tilted ligands, which can maximize

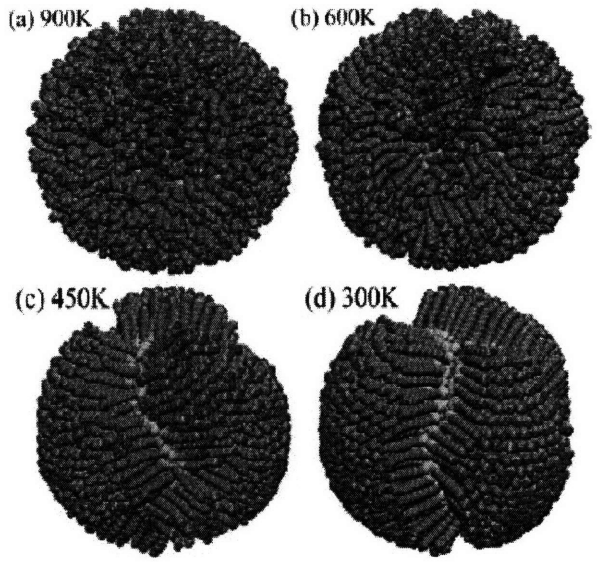

Figure 2.2
Molecular dynamics simulations of ligand arrangements on homoligand NPs show the development of ordering and disinclination lines as the temperature is reduced. (From reference 4)

intermolecular enthalpic interactions, while entropy favors the larger free volume available to molecules oriented perpendicular to the surface. The former contribution dominates at low temperature; the latter at high temperature. Furthermore, it should be noted that the tilt angle is larger on small NPs than on large ones because the curvature of the small NPs intrinsically provides more free space to the ligands.

Luedtke addressed the question of the morphology of the ligand shell SAM on the faceted surface of a gold NP.[5, 6] It was found that ligand molecules conform to one single tilt angle relative to a common particle diameter, rather than assuming their equilibrium tilt angle on each crystallographic facet. Here a temperature effect is observed as well: higher temperatures induce a transformation from the ordered state to a random structure with no preferential orientation (Figure 2.3).

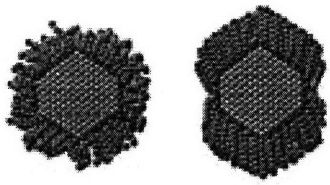

Figure 2.3
Molecular dynamics simulations of Au_{1200} NPs coated with dodecanethiol ligands at 300 K (left) and 250 K (right). At lower temperatures, the ligand molecules adopt a uniform structure. (Reproduced from 5)

2.2.2 Experimental observations

Jackson performed a detailed molecular resolution Scanning Tunneling Microscopy (STM) study of the ligand arrangement on homoligand Au NPs coated with 1-octanethiol (OT).[2] The packing of the ligand headgroups was found to depend on the particle size, while the headgroup spacing (measured as the peak-to-peak spacing between methyl groups visible in STM images) was consistently larger than the spacing of the same molecules on a flat Au substrate.

Both the crystallographic model and the continuous model were applied to correlate the ligand headgroup spacing to the structure of the ligand monolayer (that is, the sulfur-sulfur spacing at the core). In the crystallographic model, since the ligands assemble onto flat terraces, the headgroup spacing should be equivalent to the sulfur-sulfur spacing and should not depend on NP size. In contrast, the continuous model requires that the headgroup spacing is larger than the sulfur-sulfur spacing through a simple geometric relationship, and furthermore that the headgroup spacing should decrease with increasing particle diameter while the sulfur-sulfur spacing should remain constant.

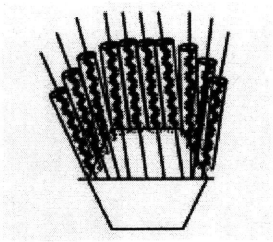

Figure 2.4
The likely configuration of ligand molecules on a facetted nanoparticle is a combination of the crystallographic and continuous models. The ligands roughly conform to an overall tilt angle but splay radially outwards. (From reference 2)

The STM data collected for OT NPs was not fully in agreement with either model; rather, headgroup spacing increased with diameter but was always larger than the value on flat surfaces, and the sulfur-sulfur spacing also depended on the NP size.[2] Thus, it was postulated that a combination of the two models best describes the structure of the homoligand SAM; that is, that the ligands in each hemisphere conform to the same tilt angle but also adopt some radial splay (Figure 2.4).

2.3 Phase separation in mixed ligand nanoparticles

As discussed in Chapter 1, SAMs composed of a binary mixture of immiscible thiolated molecules phase separate either into randomly sized and shaped domains[7-9] or into worm-like structures.[10] Phase separation occurs also on NPs, but is complicated by a variety of factors, including (1) the comparable sizes of the entire NP and the phase separated domains on flat surfaces; (2) the curvature of the NP, which, as discussed above, affects ligand arrangements; and (3) the boundary conditions imposed on the SAM by the spherical NP. The first two issues are discussed below; the third issue is dealt with later in the chapter.

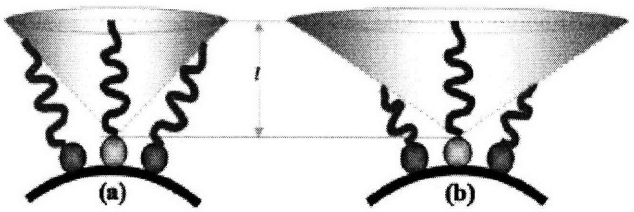

Figure 2.5
Schematic representation of free volume (indicated by the shaded cone) available to ligands on curved surfaces. (a) shows ligands of similar lengths; (b) shows ligands of significantly different lengths. The free volume and thus the configurational entropy for ligands of different lengths is noticeably larger than that for ligands of the same length. (From reference 11)

2.3.1 Models of ligand arrangement

Molecular dynamics simulations of ligand-coated NPs predict nanoscale phase separation into striped domains.[10] As shown in Figure 2.5, phase separation allows for a gain in conformational entropy; the longer molecules can inhabit more space when surrounded by shorter molecules. Striped domains are thus generated when this gain in conformational entropy overcomes the energetic penalty of creating additional interfaces.[10] If the length difference between the two species is not enough, the gain in conformational entropy will not be sufficient and bulk phase separation will occur instead. The morphology of mixed SAMs on NPs depends on the size of the NP (Figure 2.6).[10] On small NPs, a binary mixture of ligands undergoes bulk phase separation and a Janus particle[12] is formed; this is because the high curvature of the core allows the tail groups of the ligands sufficient conformational entropy without requiring the creation of extra interfaces. Increasing the NP radius results in phase separation into ordered ripples as described above. When the radius is further increased, disordered stripes and patchy domains form. Extending the radius to infinity, the worm-like structure of binary SAMs on flat surfaces is obtained.

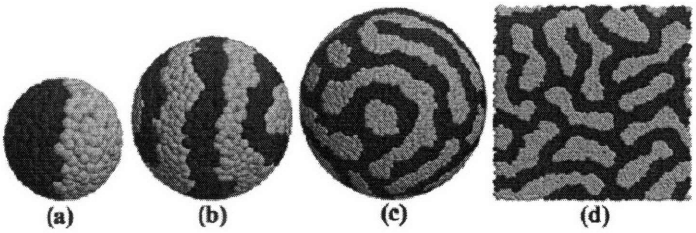

Figure 2.6
Molecular dynamics simulations of equilibrium structures of ligands on nanoparticles with decreasing curvature (i.e. increasing radius). Bulk phase separation is observed for small particles; ripples are seen to form in a middle size range; wormlike phase separation occurs for larger particles and extends to flat surfaces. (From reference 11)

2.3.2 Experimental observations

Jackson et al. first observed spontaneous nanoscale phase separation in mixed monolayer protected gold NPs with STM imaging,[13] as shown in Figure 2.7. This phenomenon of ordered phase separation was observed for a wide variety of binary ligand shell compositions, including molecules of different lengths, molecules with different end groups, and molecules with different backbone structures (e.g. aliphatic versus aromatic), thus suggesting that the formation of these ordered domains, or ripples, is general to nanoparticles rather than specific to certain ligand shell compositions.

Phase separation on NPs has been confirmed using Fourier Transform Infrared Spectroscopy (FTIR);[14] by probing the molecular environment of a given chemical group, it was possible to distinguish between mixed ligand NPs whose ligand shell was homogeneously mixed and those whose ligand shell was phase separated. Specifically, the shift in the CD_2 stretching frequency of deuterated 1-octanethiol (OT-d_{17}) was monitored as a function of the fraction of a second molecule in the ligand shell. In homogeneous mixing (such as between OT-d_{17} and OT), as the fraction of OT increases,

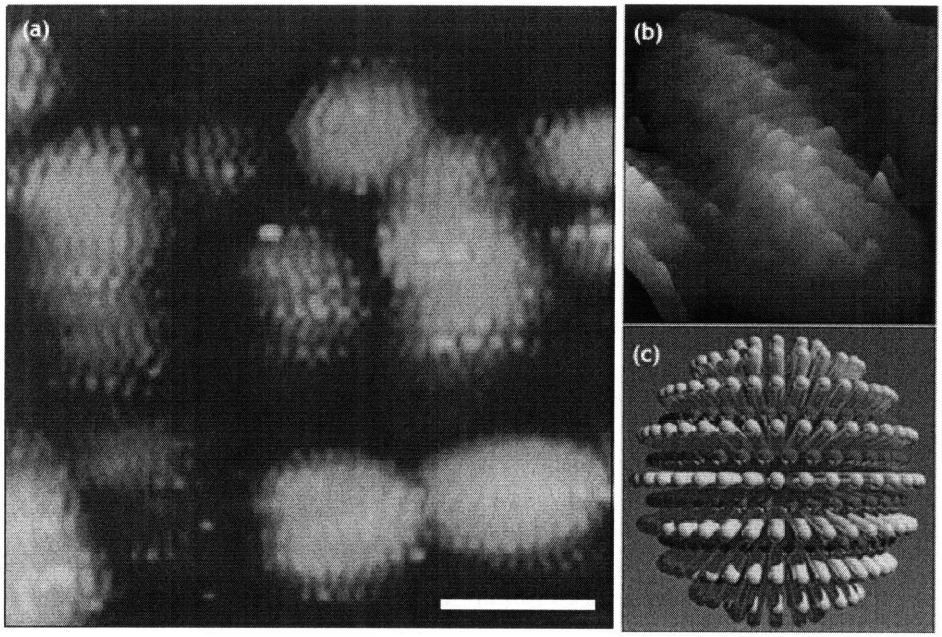

Figure 2.7
(a) Scanning Tunneling Microscopy (STM) image of gold nanoparticles coated with a 2:1 molar ratio of 1-octanethiol and 3-mercaptopropionic acid. Phase-separated ripples are visible in the ligand shell. Scale bar 10 nm. (b) A three-dimensional rendering of an STM image of rippled nanoparticles better shows the morphology of the ligand shell. (c) A cartoon indicates the arrangement of the mixed ligand shell. (From reference 13)

the probability that an OT-d_{17} molecule has as its neighbor another OT-d_{17} molecule decreases linearly, and indeed a linear shift in the CD_2 stretching is seen for this system (Figure 2.8(a)). In contrast, however, a phase separated system such as OT-d_{17} and 3-mercaptopropionic acid (MPA) gives rise to a nonlinear variation in the molecular environment of the OT-d_{17} with increasing MPA composition and thus a nonlinear trend in the frequency shift observed with FTIR (Figure 2.8(b)). It is important to note that, although these results demonstrate that FTIR can be used to detect phase separation on NPs, a complementary method (such as STM) must be used to characterize the precise structure of the phase separated domains.

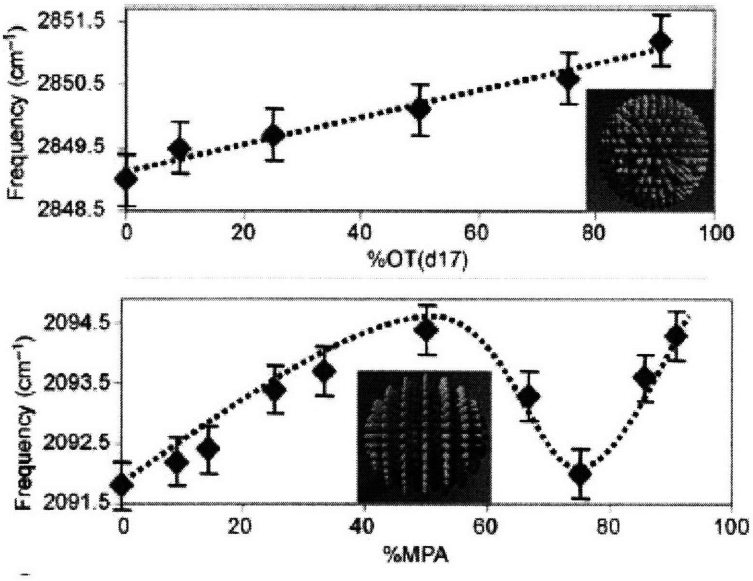

Figure 2.8
(a) Plot of the CH_2 symmetric stretching frequency for NPs coated with 1-octanethiol (OT) and fully deuterated 1-octanethiol (OT(d17)) as a function of OT(d17) composition. The points are experimentally determined by Fourier Transform Infrared Spectroscopy (FTIR); the dotted line is an interpolated linear trend. The data shows homogeneous mixing, as indicated in the cartoon inset. (b) Plot of the CD_2 symmetric stretching frequency for NPs coated with a mixture of OT(d17) and 3-mercaptopropionic acid (MPA) as a function of MPA composition. The dotted line is merely a guide for the eye. The data shows non-homogeneous mixing, indicative of ordering as shown in the cartoon. (From reference 14)

The spacing of the ripples depends on the stoichiometric ratio of the ligand molecules; for example, a 2:1 ratio of OT:MPA gives thicker ripples of OT than does a 3:1 ratio of the same molecules. X-ray diffraction scans of 2:1 OT:MPA NPs revealed temperature-independent peaks in 2θ corresponding to periodic structures with spacings of 0.5 – 2.5 nm, in a reasonable range for ripple spacing.[13] The ripple spacing was also observed to increase discontinuously with NP core diameter.[2] Transitional regions correspond well to previously observed structural transitions in ligand packing on homoligand NPs,[15] suggesting that the packing is dictated at least in part by the shape of the core.

2.3.3 Properties of rippled nanoparticles

Ordered nanoscale molecular structures impart a variety of unique properties to a system.[2, 13, 14] For instance, surfaces composed of NPs coated with a mixture of a hydrophobic- and hydrophilic-terminated species show unusually high resistance to protein nonspecific adsorption.[13] This is believed to occur because the alternation between hydrophobic and hydrophilic regions on the surface is too small to allow the protein to achieve a configuration that would energetically favor adsorption. Rippled NPs with an increasing ratio of hydrophobic to hydrophilic ligands also show anomalous non-monotonic solubility in various solvents,[13] whereas a simple thermodynamic argument assuming homogeneous mixing in the ligand shell would predict a linear relationship between solubility and the composition fraction of the hydrophilic molecule.

Importantly for this work, another implication of this nanoscale phase separation is the generation of two sites, at the north and south pole of a NP, where the alternating rings of ligands collapse into points. We predict that these two points are defects at which the molecule or molecules cannot achieve an optimal tilt angle such that it is stabilized on all sides by intermolecular interactions. In Chapter 3, we demonstrate the existence of these defects by utilizing them to functionalize NPs only at those two points.[16]

2.4 Topological considerations

Interestingly, a topological treatment of ligands on a NP also predicts the existence of two opposing defect points as a natural consequence of the vector nature of the ligand SAM.[17, 18] That is, as in a flat SAM, each ligand can be represented by a vector corresponding to its projection (determined by tilt angle and length) onto the NP core.

The coating of a sphere with a vectorial order is a complex problem; here we briefly discuss the topology of a vector field on a sphere and the nature of the point defects that arise.

2.4.1 Basic topology

In a topological context, a sphere is any object that is homeomorphic with a sphere, where a sphere is defined as the set of all points in three-dimensional space that are at a distance *r* (the radius of the sphere) from a fixed point in space (the center of the sphere).[19] That is, any object that can be transformed (e.g. by stretching) without cutting is considered a topological sphere. A cube is thus homeomorphic with a sphere; a donut is not. A facetted nanoparticle is also considered a topological sphere.

For a topological analysis of the SAM on a NP, it is necessary to consider the assembly of a vectorial order onto a topological sphere. It has been demonstrated that placing an ordered state (such as a vectorial order) onto a topological sphere necessarily requires the generation of defect points;[20-22] a common type of defect is known as a "hedgehog", a radially symmetric point defect.[19] All defects possess a 'charge' and interact via a Coulomb-like potential that is determined in part by that charge and by their spatial separation;[23] thus defects can repel or annihilate each other depending on their interaction. The curvature of the underlying surface has a prominent effect on the position and nature of topological defects.[24]

2.4.2 Defect sites on topological surfaces

2.4.2.1 Flat surfaces

The symmetry of the order parameter that is assembled onto a surface determines the type and number of defects that are created. In general, an order parameter with *p*-fold symmetry will rotate by $2\pi/p$ around a defect site. A vectorial order parameter, for which $p = 1$, represents the projection of tilted molecules such as SAMs and smectic liquid crystals. On a flat surface, a vectorial order will arrange with 2π rotational symmetry around a defect point (Figure 2.9(a)).[25, 26] For a 'headless arrow' order parameter with two-fold symmetry, such as lipids, triblock copolymers, and nanorods, two separate defect points are generated because of the higher symmetry of the order parameter (Figure 2.9(b)).[25, 26]

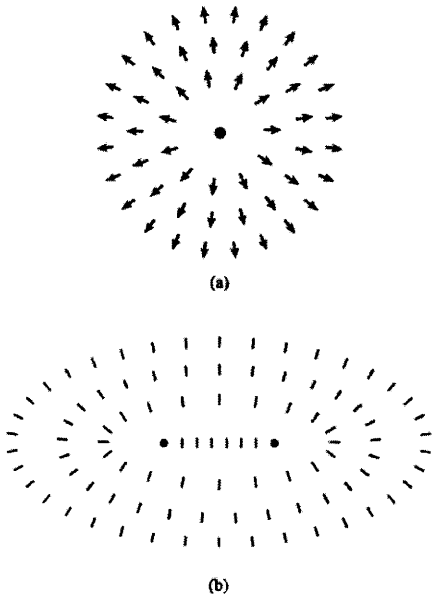

Figure 2.9
(a) A vector order parameter on a plane rotates by 2p around a central defect (marked by a dot). (b) For headless vectors, the configuration in (a) is unstable to two disinclinations; in this case the order parameter rotates by π around each of the defects (marked by dots). (From reference 25)

2.4.2.2 Spheres: The Hairy Ball Theorem

On surfaces with a positive Gaussian curvature, such as topological spheres, the assembly of order parameters is a more complex problem. The Hairy Ball theorem[17, 18, 25] states that there is no nonvanishing continuous tangent vector field on a sphere. That is, it is impossible to arrange a vector field onto a topological sphere without the formation of at least one diametrically opposed singularity. In everyday terms, this theorem can be visualized in an (unsuccessful) attempt to comb a tennis ball: it is impossible to comb the ball such that the hairs all lie down flat without generating at least one defect point where the hairs point in different directions. Incidentally, the Hairy Ball theorem also explains such quotidian phenomena as the whirl in one's hair and the fact that there must always be at least one cyclone in the atmosphere at any given time.

The Poincaré index theorem states that the sum of the defects on a sphere must equal $2p$.[27] Thus, for a vector order parameter ($p = 1$) two point defects, known as boojums,[28] are generated, each with a +1 topological charge (Figure 2.10(a)).[22, 25] For an order parameter with $p = 2$, four +1 disinclinations are created (Figure 2.10(b)).[22, 25]

The defect self-energy, E_d, determines the positions of the defect points. E_d is a long-range repulsive interaction that is proportional to $(n/p)^2$, where n is the defect charge, and diverges logarithmically with the ratio of the sphere radius to the defect separation.[25] This energy explains why the two defect points for the $p = 1$ case reside at diametrically opposed positions on the sphere while the four defects for the $p = 2$ system sit at the four corners of a tetrahedron. Furthermore, E_d provides another means to explain the generation of four defects for the 2-fold symmetric order parameter.[25] For $p = 2$, there could either be two defects of charge +2 or four defects of charge +1. Through the $(n/p)^2$

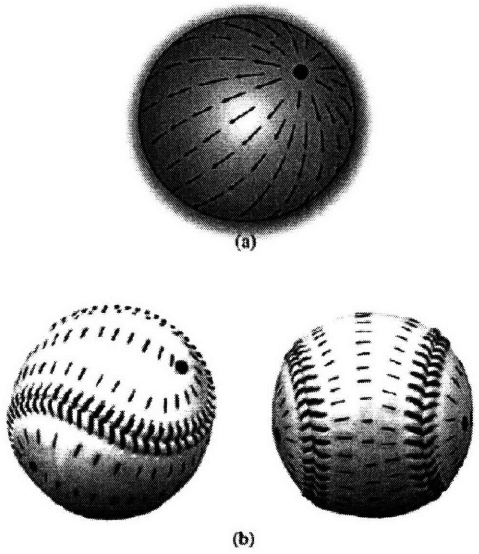

Figure 2.10
(a) The arrangement of a splay vector order parameter on a sphere generates two diametrically opposed +1 defect points. (b) Headless vectors on a sphere generate four disinclinations at the vertices of a tetrahedron; the seams on a baseball are helpful for visualizing this arrangement. (From reference 25)

term, it is evident that the latter is the lower energy configuration. It should also be noted that, because of the long-range nature of the defect self-energy, the positions of the defects are stable against thermal fluctuations.

2.4.3 Implications for nanoparticles

As stated above, a NP, despite its facetted crystallographic nature, is considered a topological sphere. Thus, it is possible to apply the principles of the Hairy Ball theorem for the arrangement of a vector field on a sphere to the case of the structure and organization of a molecular layer on the core of a NP. This implies that two or four defect points can be generated in the molecular coating,[25] depending upon the nature of the ligands coating the NP. Defect points in molecular layers are generally highly reactive; thus it has been suggested that selective functionalization be performed at these points, generating divalent NPs (the nanoscale equivalent of sp hybridization) or tetravalent NPs

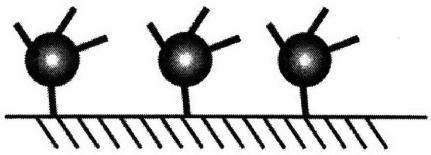

Figure 2.11
The tetravalent nanoparticles proposed by Nelson[25] could be anchored to a surface via functionalization of one defect site, producing an array of trivalent particles on the surface. (From reference 25)

(sp^3 hybridization) that can be used as 'artificial atoms' in the subsequent assembly of complex NP-based structures.[25] Figure 2.11 shows an example application for tetravalent NPs linked to a surface (presumably as part of an array of similar particles), generating periodic localized three-fold binding sites for probing interactions with the NPs.

Numerous groups have studied the defects formed upon assembling various species onto the surface of NPs. Notably, this work characterizes the two diametrically opposed defect points that form when a binary mixed SAM is formed on a gold NP.[16] Several simulations have also been performed. Using self-consistent field theory, the assembly of triblock copolymers has been shown to generated ring- and spiral-like structures of polymer around the NP; the presence of either two or four singularities depends on such factors as the polymer composition and the sphere radius (Figure 2.12).[29, 30] Liquid crystals on spheres have also been shown to give rise to ordering and multivalent defect configurations, both when the liquid crystal is assembled directly onto the sphere[25] and when the sphere is immersed into a liquid crystal bath.[31] More esoterically, the modeling of magnetic vortices (a vector field) on spheres reveals the presence of two diametrically opposed defect points (Figure 2.13).[32] Molecular dynamics simulations specific to the system of gold NPs coated with thiolated ligands also revealed

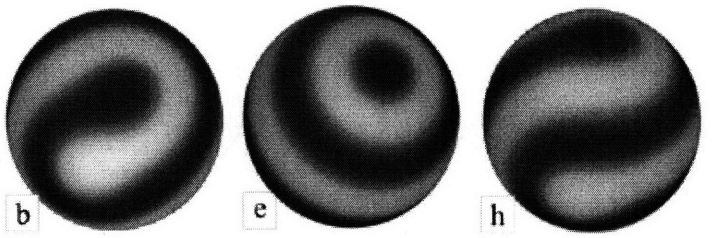

Figure 2.12
Self-consistent field theory simulations of lamellar block copolymer assembly onto spheres shows the appearance of (b) spiral, (e) hedgehog, and (h) quasibaseball phases with either two or four defect points. (From reference 29)

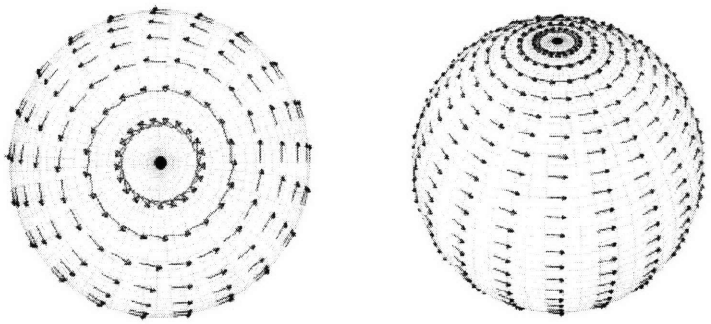

Figure 2.13
Top (left) and side (right) views of spin fields on spheres, showing defect points at the north and south poles. (From reference 32)

the presence of at least one ligand that is more isolated from the others; that is, a ligand that does not achieve an optimal tilt angle.[33]

It is the aim of this work to demonstrate the existence of and characterize the two diametrically opposed singularities in mixed ligand coated gold NPs. In the case of a self-assembled ligand shell, these singularities are defect points, or 'poles', at which the ligands cannot assume their equilibrium tilt angle and thus cannot attain maximal intermolecular stabilization. The ordered domains present in the SAM of mixed ligand NPs further accentuate these poles; in Chapter 3, we demonstrate the existence of two diametrically opposed polar defects and use them to generate divalent NPs.[16]

2.5 References

1. Zanchet, D.; Hall, B. D.; Ugarte, D., Structure population in thiol-passivated gold nanoparticles. *Journal of Physical Chemistry B* **2000,** 104, (47), 11013-11018.
2. Jackson, A. M.; Hu, Y.; Silva, P. J.; Stellacci, F., From homoligand- to mixed-ligand-monolayer-protected metal nanoparticles: A scanning tunneling microscopy investigation. *Journal of the American Chemical Society* **2006,** 128, (34), 11135-11149.
3. Terrill, R. H.; Postlethwaite, T. A.; Chen, C. H.; Poon, C. D.; Terzis, A.; Chen, A. D.; Hutchison, J. E.; Clark, M. R.; Wignall, G.; Londono, J. D.; Superfine, R.; Falvo, M.; Johnson, C. S.; Samulski, E. T.; Murray, R. W., Monolayers in three dimensions: NMR, SAXS, thermal, and electron hopping studies of alkanethiol stabilized gold clusters. *Journal of the American Chemical Society* **1995,** 117, (50), 12537-12548.
4. Ghorai, P. K.; Glotzer, S. C., Molecular dynamics simulation study of self-assembled monolayers of alkanethiol surfactants on spherical gold nanoparticles. *Journal of Physical Chemistry B* **2007,** in press.
5. Luedtke, W. D.; Landman, U., Structure and thermodynamics of self-assembled monolayers on gold nanocrystallites. *Journal of Physical Chemistry B* **1998,** 102, (34), 6566-6572.
6. Luedtke, W. D.; Landman, U., Structure, dynamics, and thermodynamics of passivated gold nanocrystallites and their assemblies. *Journal of Physical Chemistry* **1996,** 100, (32), 13323-13329.
7. Stranick, S. J.; Parikh, A. N.; Tao, Y. T.; Allara, D. L.; Weiss, P. S., Phase-Separation of Mixed-Composition Self-Assembled Monolayers into Nanometer-Scale Molecular Domains. *Journal of Physical Chemistry* **1994,** 98, (31), 7636-7646.
8. Stranick, S. J.; Kamna, M. M.; Krom, K. R.; Parikh, A. N.; Allara, D. L.; Weiss, P. S., Scanning-Tunneling-Microscopy Studies of Self-Assembled Monolayers of Alkanethiols on Gold. *Journal of Vacuum Science & Technology B* **1994,** 12, (3), 2004-2007.
9. Stranick, S. J.; Atre, S. V.; Parikh, A. N.; Wood, M. C.; Allara, D. L.; Winograd, N.; Weiss, P. S., Nanometer-scale phase separation in mixed composition self-assembled monolayers. **1996,** 7, (4), 438-442.
10. Singh, C.; Ghorai, P. K.; Horsch, M. A.; Jackson, A. M.; Larson, R. G.; Stellacci, F.; Glotzer, S. C., *Physical Review Letters, under review* **2007**.
11. Singh, C.; Ghorai, P. K.; Horsch, M. A.; Jackson, A. M.; Larson, R. G.; Stellacci, F.; Glotzer, S. C., Entropy-mediated patterning of surfactant-coated nanoparticles and surfaces. *submitted* **2007**.
12. Casagrande, C.; Veyssie, M., Janus Beads - Realization and 1st Observation of Interfacial Properties. *Comptes Rendus De L Academie Des Sciences Serie Ii* **1988,** 306, (20), 1423-1425.
13. Jackson, A. M.; Myerson, J. W.; Stellacci, F., Spontaneous assembly of subnanometre ordered domains in the ligand shell of monolayer-protected nanoparticles. *Nature Materials* **2004,** 3, (5), 330-336.
14. Centrone, A.; Hu, Y.; Jackson, A. M.; Zerbi, G.; Stellacci, F., Phase Separation on Mixed-Monolayer-Protected Metal Nanoparticles: A Study by Infrared Spectroscopy and Scanning Tunneling Microscopy. *Small* **2007,** 3, (5), 814-817.

15. Hostetler, M. J.; Wingate, J. E.; Zhong, C. J.; Harris, J. E.; Vachet, R. W.; Clark, M. R.; Londono, J. D.; Green, S. J.; Stokes, J. J.; Wignall, G. D.; Glish, G. L.; Porter, M. D.; Evans, N. D.; Murray, R. W., Alkanethiolate gold cluster molecules with core diameters from 1.5 to 5.2 nm: Core and monolayer properties as a function of core size. *Langmuir* **1998,** 14, (1), 17-30.
16. DeVries, G. A.; Brunnbauer, M.; Hu, Y.; Jackson, A. M.; Long, B.; Neltner, B. T.; Uzun, O.; Wunsch, B. H.; Stellacci, F., Divalent metal nanoparticles. *Science* **2007,** 315, (5810), 358-361.
17. Poincare, H., *J Math Pure Appl* **1885,** 1, 167.
18. Eisenberg, M.; Guy, R., Proof of the Hairy Ball Theorem. *American Mathematical Monthly* **1979,** 86, (7), 572-574.
19. Basener, W. F., *Topology and its applications*. Wiley-Interscience: Hoboken, N.J., 2006; p xxxvii, 339.
20. Nelson, D. R., Order, Frustration, and Defects in Liquids and Glasses. *Physical Review B* **1983,** 28, (10), 5515-5535.
21. Mackintosh, F. C.; Lubensky, T. C., Orientational Order, Topology, and Vesicle Shapes. *Physical Review Letters* **1991,** 67, (9), 1169-1172.
22. Lubensky, T. C.; Prost, J., Orientational order and vesicle shape. *Journal de Physique II* **1992,** 2, 371.
23. Vitelli, V.; Turner, A. M., Anomalous coupling between topological defects and curvature. *Physical Review Letters* **2004,** 93, (21).
24. Vitelli, V.; Lucks, J. B.; Nelson, D. R., Crystallography on curved surfaces. *Proceedings of the National Academy of Sciences of the United States of America* **2006,** 103, (33), 12323-12328.
25. Nelson, D. R., Toward a tetravalent chemistry of colloids. *Nano Letters* **2002,** 2, (10), 1125-1129.
26. Mermin, N. D., Topological Theory of Defects in Ordered Media. *Reviews of Modern Physics* **1979,** 51, (3), 591-648.
27. Spivak, M., *A comprehensive introduction to differential geometry*. 2d ed.; Publish or Perish inc.: Berkeley, 1979.
28. Trickey, S. B.; Adams, E. D.; Dufty, J. W., *Quantum fluids and solids : proceedings*. Plenum Press: New York, 1977; p x, 473.
29. Chantawansri, T. L.; Bosse, A. W.; Hexemer, A.; Ceniceros, H. D.; Garcia-Cervera, C. J.; Kramer, E. J.; Fredrickson, G. H., Self-consistent field theory simulations of block copolymer assembly on a sphere. *Physical Review E* **2007,** 75, (3), -.
30. Li, J. F.; Fan, J.; Zhang, H. D.; Qiu, F.; Tang, P.; Yang, Y. L., Self-assembled pattern formation of block copolymers on the surface of the sphere using self-consistent field theory. *European Physical Journal E* **2006,** 20, (4), 449-457.
31. Huber, M.; Stark, H., Tetravalent colloids by nematic wetting. *Europhysics Letters* **2005,** 69, (1), 135-141.
32. Milagre, G. S.; Moura-Melo, W. A., Magnetic vortex-like excitations on a sphere. *Physics Letters A* **2007,** 368, (1-2), 155-163.
33. Rapino, S.; Zerbetto, F., Dynamics of thiolate chains on a gold nanoparticle. *Small* **2007,** 3, (3), 386-388.

Chapter 3: Chains of nanoparticles

3.1 Approach to chaining

On mixed ligand metal nanoparticles (NPs), the ligand shell undergoes spontaneous phase separation into ordered rings, or "ripples," that encircle or spiral around the gold core.[1] As discussed in Chapter 2, this ordering gives rise to two diametrically opposed defect points[2] at which the ligand molecules are not at their optimal tilt angle and thus are not maximally stabilized by intermolecular interactions. Here we explore the consequences of these instabilities and present an approach to functionalize the NPs at those two points. That is, because the ligands located at the two polar defect points, or poles, of each NP are not well stabilized by intermolecular interactions, they are more likely to undergo place-exchange than other sites on the NP. Thus, we can subject the NPs to a controlled place-exchange reaction to place molecules with a reactive end group (such as a carboxylic acid) at the poles, generating divalent NPs. We can then react these NPs with complementary divalent molecules (such as diamine molecules) to form chains.[3]

3.2 Generation of chains of nanoparticles

The generation of NP chains involves two separate reactions: one to place-exchange molecules onto the poles and the other to form chains via reaction with a divalent molecule. The standard process[3] involves placing 11-mercaptoundecanoic acid (MUA) at the poles and linking the NPs into chains with 1,6-diaminohexane (DAH). The chaining reaction is typically a two-phase interfacial polymerization process modeled on the standard synthesis of nylon,[4] although it is also possible to chain the NPs in a one-

phase reaction. Most of the work presented here was performed on small (~3 nm) diameter gold NPs; however, to a lesser extent we also studied silver and platinum NPs of a similar diameter and larger gold and silver NPs. The NPs were generally coated with a mixed ligand shell consisting of a 2:1 molar ratio of 1-nonanethiol (NT) to 4-methylbenzenethiol (MBT). These ligands were chosen because they have a strong driving force toward phase separation and because the methyl endgroups do not interfere with the chemistry of the chaining reaction.

For the standard procedure (see Scheme 3.1), Reaction **1** is a place-exchange reaction, hereafter called pole functionalization:

$$\frac{1}{2}NP + xMUA \xrightarrow{K} \frac{1}{2}NP \cdot MUA + (x-1)MUA\,, \qquad (1)$$

in which MUA is placed at the poles, where x is the molar excess of MUA and $\frac{1}{2}NP$ refers to one pole of a NP. Note that we write Reaction **1** in terms of poles rather than

Scheme 3.1
Reaction **1**, pole functionalization, is a reaction in which rippled NPs are exposed to an excess of MUA (activated with the leaving group NHS, not shown) and stirred for a short time in THF. In the case depicted above, Reaction **1** has occurred twice, once at each pole, to generate a divalent NP. The pole functionalized NPs are separated from any remaining unreacted MUA and transferred into toluene for Reaction **2**, an interfacial polymerization in which the NPs are joined by DAH into chains.

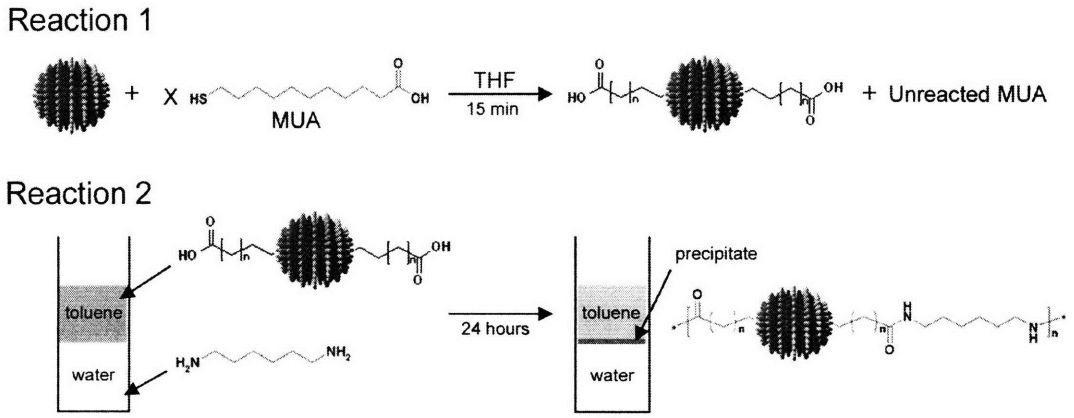

NPs because each pole is functionalized independently; that is, the NP can be either singly or doubly functionalized. The MUA is purchased pre-activated with N-hydroxysuccinimide (NHS), a leaving group. A tetrahydrofuran (THF) solution of NPs and a small excess of MUA (~10-fold molar excess) is stirred for a short amount of time (typically ~15 minutes); the reaction is then rapidly quenched and unreacted MUA is removed from the solution by filtering the reaction solution in a Sephadex™ gel column. The pole functionalized NPs are then transferred into toluene for chaining.

In the two-phase process, Reaction **2**

$$\frac{1}{2}NP \cdot MUA(toluene) + DAH(water) \longrightarrow (\frac{1}{2}NP \cdot MUA \cdot DAH)_n \qquad (2)$$

is an interfacial polymerization process in which the pole functionalized NPs in toluene are placed in contact with a water solution of DAH. A precipitate soon forms at the interface, indicating the formation of insoluble assemblies of NPs. It should be noted that Reaction **2** reaches equilibrium after several hours; that is, no further precipitation is seen. All characterization was performed by sampling the chains after at least 12 hours of Reaction **2**, to ensure that the reaction had gone to completion.

The chaining reaction also can be performed in one phase, where pole functionalized NPs and DAH are dissolved in the same phase (typically THF). This method is less preferable for a number of reasons. First, because there is no interface to control reaction stoichiometry, it is essential that there be exactly the same number of NPs and DAH molecules; otherwise, the polymerization will be artificially terminated by the species in excess. Since it is impossible to know exactly the number of NPs used (the molecular weight used in concentration and MUA excess calculations is an estimate based on a size distribution obtained from Transmission Electron Microscopy (TEM)

imaging), achieving the necessary stoichiometry is almost impossible. Second, a one-phase polymerization reaction is less efficient than a two-phase reaction. Note that hereafter all references to Reaction **2** will refer to the two-phase reaction unless otherwise specified.

3.3 Initial results

3.3.1 Evidence for chains

Soon after the two-phase Reaction **2** is initiated, a black precipitate begins to form at the water-toluene interface (Figure 3.1(a)), and after several hours the toluene phase has lost much of its color and the precipitation has reached an equilibrium.[3] Precipitation indicates the formation of large insoluble aggregates of NPs. The extent of precipitation can be determined by UV-visible spectroscopy: the absorption of the toluene solution can be measured before and after contact with the water solution (Figure 3.1(b)).[a] Since the

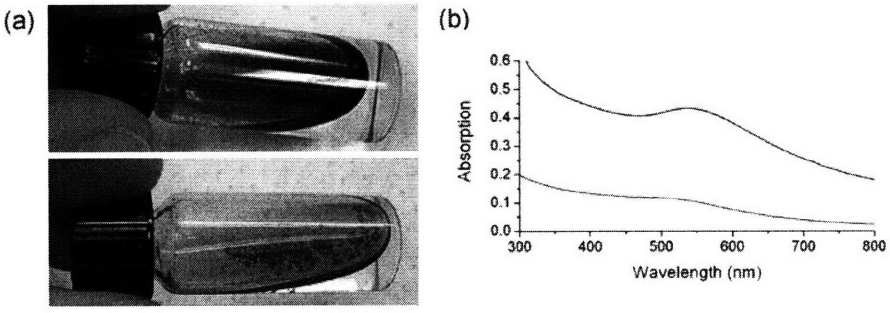

Figure 3.1
(a) Photographs of Reaction 2 initially (top) and after several hours (bottom). The toluene solution loses most of its color and a precipitate forms at the interface. (b) Absorption spectra of the toluene solution shown in (a) initially (blue) and after several hours (red), demonstrating the significant drop in solution concentration.

[a] Note that because of the small quantity of MUA exchanged onto the NPs, it is not possible to directly measure the amount of MUA exchanged during Reaction **1** (e.g. by Nuclear Magnetic Resonance or Fourier Transform Infrared Spectroscopy); instead, the exchange must be inferred from the precipitation from Reaction **2**.

intensity at the peak of the plasmon band is directly proportional to the solution concentration, the value $\frac{A(pre)-A(post)}{A(pre)}$ gives the fraction of NPs precipitated, where *A(pre)* and *A(post)* are the absorption intensities of the toluene solution at the peak of the plasmon band before contact with the water solution and 24 hours thereafter, respectively.

Although the precipitate is insoluble in toluene, it can be dissolved in THF and dropped onto a TEM grid for imaging. TEM images show a large population of linear chains of NPs (Figure 3.2); the low fraction of branched chains and the absence of three-dimensional aggregates in the images strongly supports the idea of selective functionalization at the two opposing polar defect sites.

To further prove that the chains observed in TEM were due to molecular linking of the NPs, we performed Reaction **2** using one of two divalent linking molecules of different lengths: DAH and O,O′-Bis(2 aminoethyl)octadecaethylene glycol (EGDA).[3] We then measured the average interparticle separation along the chain (defined as the distance between the two nearest points or facets of neighbouring NPs). Assuming an all-trans conformation for the molecular linkers (that is, two MUA molecules covalently bonded to either DAH or EGDA), the expected interparticle distance would be 3.6 nm or 9.6 nm, respectively. Analysis of TEM images revealed an average interparticle spacing of 2.2 nm (σ = 0.4 nm) for DAH and 4.2 nm (σ = 0.9 nm) for EGDA (Figure 3.3(a)). The distributions do not overlap at all, proving that the chains are indeed kept together by the molecular linkers. Note that the EGDA distribution has a large spread and its mean is not close to the expected value; this is not surprising, however, because of the greater conformational freedom of this molecule (Figure 3.3(b)).

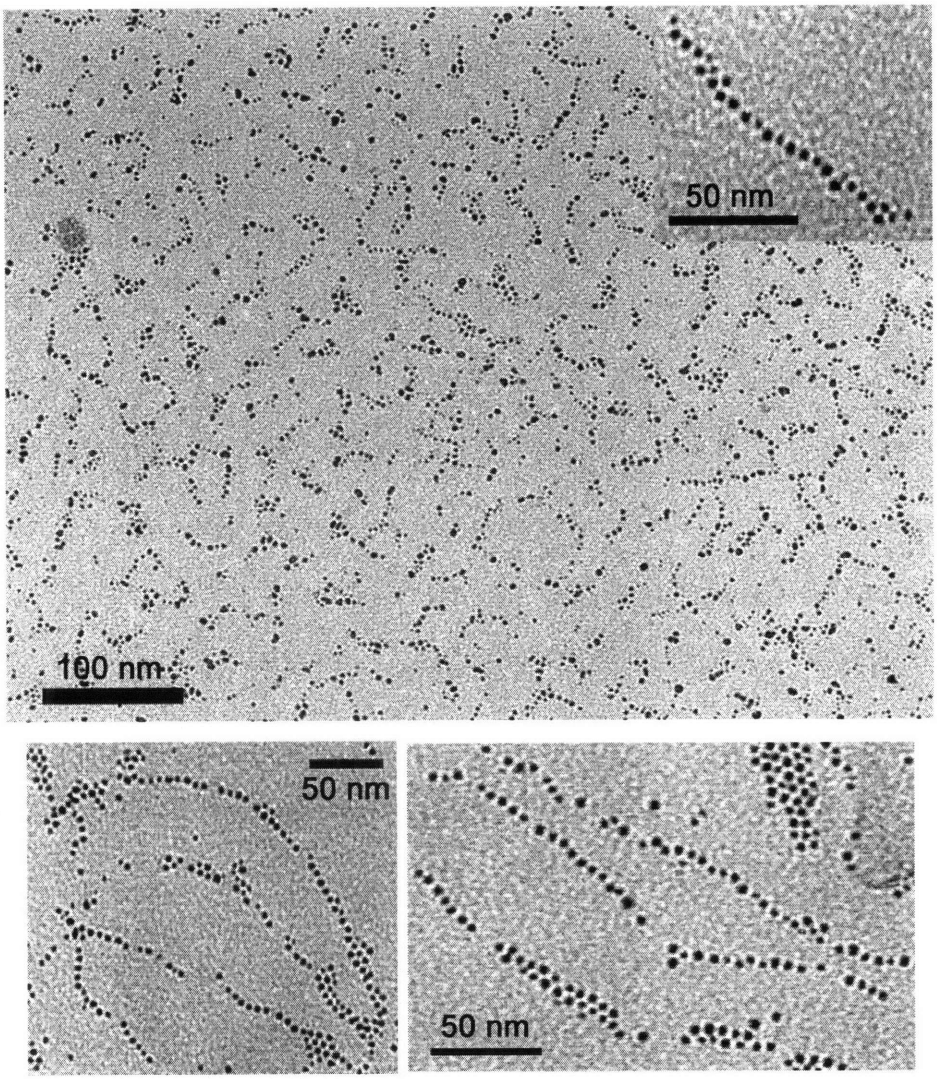

Figure 3.2
TEM images of chains obtained by pole functionalizing rippled NPs with MUA, then performing an interfacial polymerization with DAH. Precipitate at the interface was collected and dispersed for TEM imaging.

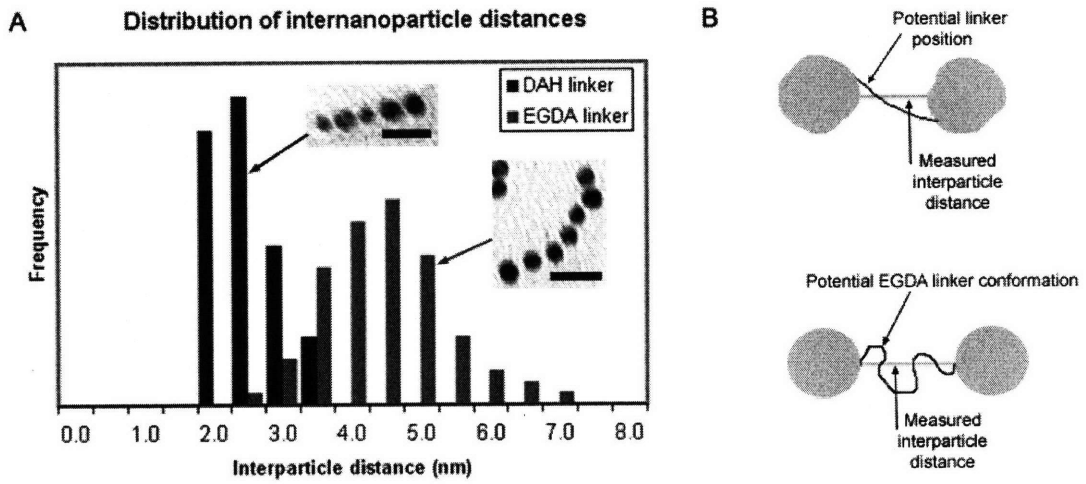

Figure 3.3
Variation in interparticle distance with linker molecule. (a) Distribution of interparticle distances in chains with DAH linkers (blue) and EGDA linkers (red). The average interparticle distance for DAH was 2.2 nm ± 0.4 nm; for EGDA it was 4.2 nm ± 0.9 nm. Note that the measured distributions barely overlap. Insets show TEM images of representative chains of each type. Scale bars 20 nm. (b) Schematics illustrating (left) the potential geometry of faceted NPs that could result in the measured interparticle distances being smaller than the length of the linker; and (right) the conformational freedom of EGDA that could result in the observed wide distribution of interparticle distances for this type of chain.

3.3.2 TEM sample preparation

Preparation of TEM samples is critical for three reasons:

1. If the source solution is too concentrated, the density of NPs on the TEM grid will be too high and it will be difficult to distinguish chains from random structures formed by interparticle interactions upon drying.
2. If the source solution is allowed to sit on the TEM grid for too long, the NPs in solution will have time to arrange into ordered structures, making chains impossible to find (Figure 3.4(a)).
3. The solvent used for casting must be miscible with both toluene and water to avoid artifacts that result from microscale (or smaller) bubbles of phase separation (Figure 3.4(b)).

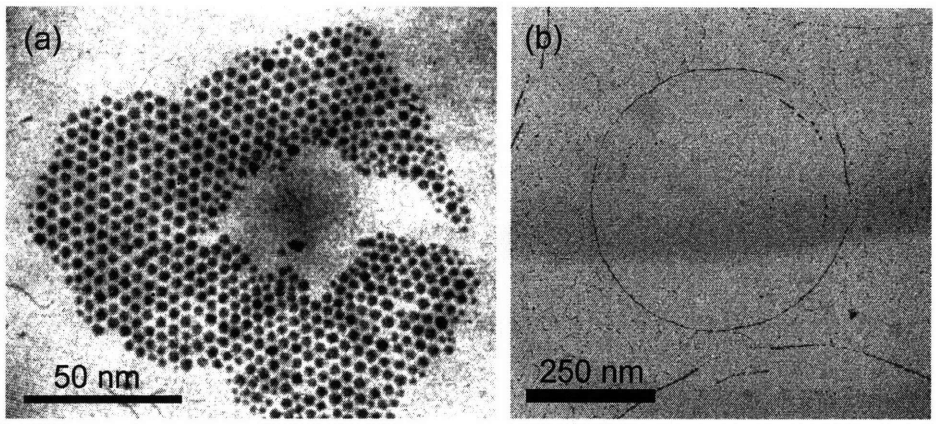

Figure 3.4
TEM images demonstrating (a) an ordered two-dimensional lattice and (b) drying rings.

For these reasons, THF was used as the solvent for TEM sample preparation whenever possible. Precipitate was collected, dissolved in THF, and diluted until the solution was just barely colored. The solution was dropped onto a TEM grid that was placed on several layers of KimWipes™ to rapidly wick away solvent and "freeze" the NPs onto the grid in the same arrangement that they were in solution.

3.3.3 Control experiments

Many control experiments were performed to observe the formation (or lack thereof) of a precipitate and the presence or absence of chains in TEM images of both the precipitate and the toluene phase.[3]

1. Mixed ligand rippled NPs showed precipitate only when pole functionalized with MUA, either activated with NHS or as a bare carboxylic acid. In the latter case, although the poles do not possess strong leaving groups, the nonactivated carboxylic acids can still complex with the amines in solution, generating the equivalent of a nylon salt. These electrostatic bonds could later be heated, converting them to covalent bonds.

2. NPs containing carboxylic acid groups everywhere in the ligand shell (ligand shell composition 1:4 octanethiol : 3-mercaptopropionic acid) were subjected to Reaction **2** to ensure that chains do not form when carboxylic acid is present at points other than the poles. It should be noted that these NPs originally were not soluble in any organic solvent, but dissolved easily in chloroform when a small amount of hydrochloric acid was added to protonate the carboxylic acid groups. Because of this strange solubility, the carboxylic acid groups were not activated prior to the chaining reaction. Upon the addition of the DAH-water solution, phase separation did not occur even though chloroform and water are not ordinarily miscible. This is likely due to the fact that the NPs are slightly water soluble and thus act as phase transfer agents allowing the water and chloroform to mix. Despite the accidental one-phase nature of the system, precipitate formed quickly at the bottom of the vial, indicating the formation of insoluble aggregates. TEM imaging showed large three-dimensional clusters resulting from non-directional interparticle bonding (Figure 3.5).
3. Precipitate was not observed when the NPs were pole functionalized with a molecule not terminated with a carboxylic acid, or when they were not pole functionalized at all.
4. There was no precipitate when DAH was not present in the water phase.

These controls demonstrate conclusively that the precipitate is a product of an amide coupling reaction leading to an amide bond (in the case of activation with NHS) or to a salt. The experiments also suggest that chains observed in TEM are a result of that

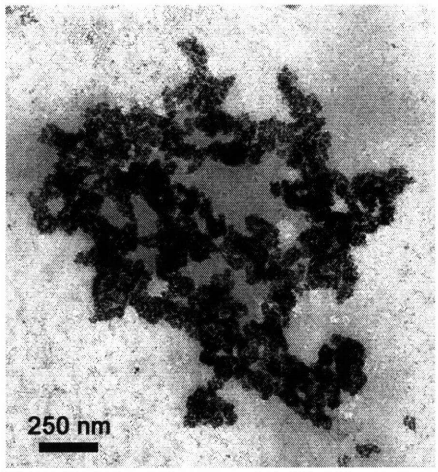

Figure 3.5
TEM images from the precipitate of a control experiment in which NPs containing carboxylic acid terminated molecules uniformly throughout the ligand shell were reacted in Reaction **2** with DAH. A precipitate rapidly formed at the interface; however, the precipitate was not soluble in THF and only large aggregates were seen in TEM, indicating that the NPs had formed bonds in all directions..

amide coupling reaction; however, it does not directly prove that chains are not an artifact of solvent drying during TEM sample preparation. Thus, evidence that chains are present in solution was obtained through light scattering experiments. We found a significant increase in scattering intensity for THF solutions of chains as compared to solutions of identical optical density containing only the starting (isolated) particles (Figure 3.6), proving the presence of aggregates in solution. This observation coupled with the fact that chains are not observed in TEM samples of NPs that were not treated with the chaining procedure proves that chains are indeed composed of chemically coupled NPs that exist in the precipitate, in solution, and on a surface.

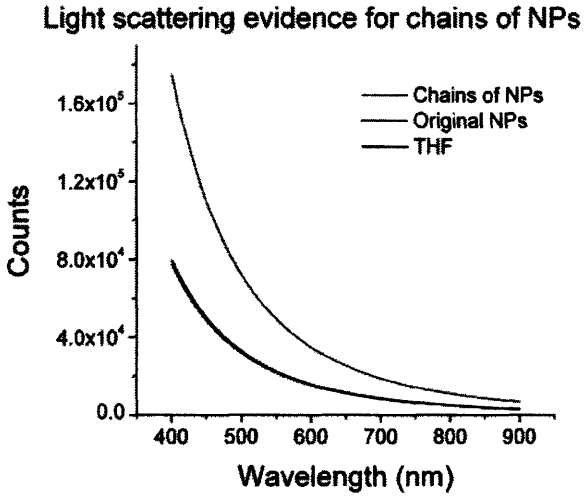

Figure 3.6
90° light scattering plots of THF and THF solutions of NPs and NP chains. These plots are fits to the scans obtained using the synchronous scan option in a fluorometer. Fits are used to eliminate the instrumental response function (R2 = 0.95 for all three curves). The solutions of NPs and NP chains had the same optical density. 4 nm diameter NT:MBT 2:1 rippled NPs were used for the NP sample. The chains were obtained by reacting the same NPs, pole functionalized with activated MUA, with DAH in a two-phase reaction, and collecting the interface precipitate. The increased scattering in the NP chain solution proves that aggregates are present in solution. Given that in TEM images obtained by precipitating such solution the only aggregates present are chains, we may say that chains are present in solution.

A statistical analysis was also performed on chains and controls resulting from the one-phase synthesis.[a] After analyzing more than 40 samples with a total population exceeding 50,000 NPs, it was found that the average fraction of NPs in chains was 20% (σ = 8%), whereas in all control experiments only 3 to 5% of the NPs were found in chain-like structures. Note that the one-phase synthesis has a lower yield than the interfacial two-phase reaction, so it is likely that the yield is even higher for the standard two-phase reaction.

Finally, we designed experiments to prove that the pole functionalization process is fundamentally based on the dynamic equilibrium of a self-assembled monolayer. We

[a] As discussed above, the one-phase synthesis has several drawbacks. However, we chose to perform this analysis with the one-phase method in order to assure an accurate count of isolated NPs and NPs in chains and other structures. Had we used the two-phase reaction, the fact that the precipitate contains most of the chains would have made it virtually impossible to achieve an accurate representation of the fraction of NPs in chains.

dissolved in THF a precipitate that was known to contain chains and added a large excess (~50,000-fold) of NT. At such a high excess, NT is able to place-exchange at the poles, destroying the chains and restoring the sample to isolated NPs. However, chains are stable in solution for at least several days if there are no excess thiols present; this implies that place-exchange at the poles is an associative process[5] that requires an incoming molecule to displace the polar MUA. Both the stability and the possibility of destruction via excess thiols prove that (1) chains are not a drying effect and (2) nanoparticles are molecularly linked within a chain.

3.4 Size selection in chaining

3.4.1 Experimental data

To determine the effect of NP size on chain formation, we pole functionalized and made chains with a polydisperse sample of NPs and then measured the size distribution of the NPs within and outside the chains in both the precipitate and the supernatant.[6] These NPs, synthesized with a one-phase synthesis,[7,8] had an average diameter of 2.9 nm (before the chaining reaction), consistent with those used above for general chaining

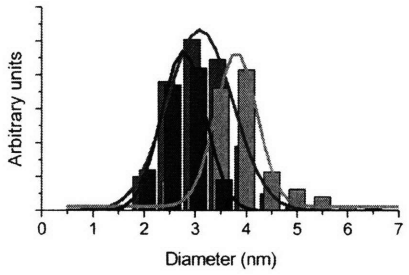

Figure 3.7
NP size distributions before and after chaining as measured from TEM images. Red is the size distribution of the starting NPs, green that of the NPs found in chains, and blue that of unchained NPs. Bars represent the actual distribution; lines are Gaussian fits to the data. The chaining reaction selects for the larger NPs in this case.

studies. We observed a size selection after chaining: the average diameter of the NPs in chains was 3.8 nm and that of isolated NPs was 2.5 nm (Figure 3.7). We repeated this experiment again obtaining the same result.

To strengthen this result, we performed t-tests ($\alpha = 0.05$) on the data. A statistical difference between the sizes of the chained and the unchained NPs was found, but the results from the two experiments were statistically indistinguishable; that is, there was no significant different between the sizes of the NPs in the chains (and outside the chains) from the two experiments. To demonstrate that these results were not influenced by size selective precipitation not linked to chaining, we compared the sizes of chained NPs (and similarly of unchained NPs) in the precipitate to those in the supernatant and found no difference.[a] Similar results were obtained for batches of smaller NPs (2.2 nm diameter).

As explained above, divalent NPs are an effect of the rippled ligand structure. The fact that smaller NPs do not form chains can be explained by postulating either that (1) poles in smaller NPs are less reactive than those in larger ones or (2) that poles in smaller NPs do not exist, and thus that the ripple morphology likewise is not present. To distinguish between these two cases, we focused on three batches of polydisperse NPs with different average diameters (2.2 nm, 4.1 nm, and 6.3 nm). Figure 3.8 shows that, for the smallest set, the NPs in chains were larger than their unchained counterparts (3.2 nm and 1.6 nm, respectively), while for the largest set the reverse was found (5.7 nm in chains versus 7.4 nm out of chains). In both cases the sizes of the chained and unchained NPs were statistically different. For the middle set of NPs, there was no difference between the sizes of the chained and unchained NPs (4.4 nm). These data suggest that

[a] Dimers are often found in the supernatant, and isolated NPs are found in the precipitate. The latter are possibly induced to precipitate via van der Waals interactions with other NPs in chains.

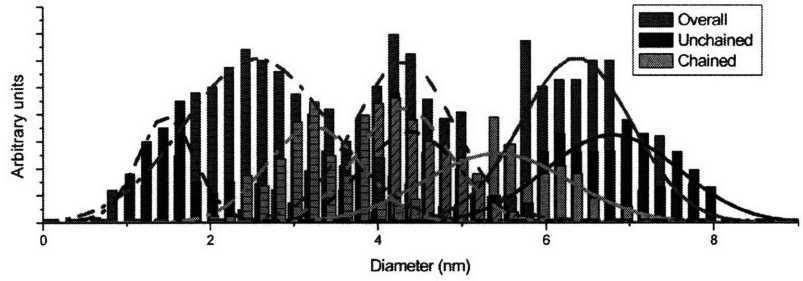

Figure 3.8
Size distributions before and after chaining for three different sets of NPs. It is evident that chains form only for NPs in a certain size range. Bars represent actual data; lines are Gaussian fits. Each type of line (solid, dashed, or dashed-dotted) represents one complete set of NPs (overall, unchained, and chained distributions).

chains form only in a specific size range. For this system (Au NPs; 2:1 NT:MBT ligands), this range is between ~2.5 nm and ~6.5 nm, although it is reasonable to expect that each type of NP will have slightly different behavior.

3.4.2 Interpretation

We believe these results imply that rippled domains form only on NPs in a specific size range. This conclusion is supported by simulations performed by the Glotzer group, as discussed in detail in Chapter 2. Notably, Glotzer finds that ligands on small NPs undergo bulk phase separation, whereas ligands on large NPs phase separate into random worm-like domains (Figure 3.9). Only NPs in a middle size range support a rippled ligand structure.

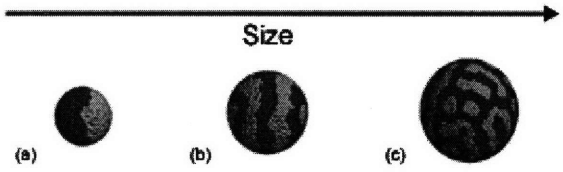

Figure 3.9
Simulation snapshots of phase separation in mixtures of surfactants of unequal length on spheres of increasing diameter. Snapshot (b) shows ripples. (Simulations performed by the Sharon Glotzer group.[9])

This interpretation is supported by our analysis of NPs whose size distribution was entirely below the lower limit for ripple formation. Au_{140} NPs (average diameter 1.74 nm, $\sigma = 0.35$ nm) were imaged in STM,[a] ligand headgroups were clearly visible, but no ordering in the ligand shell was observed. As expected for NPs without ripples, attempts to form chains with such small particles were unsuccessful; only isolated NPs were observed in TEM. It should be noted that the NPs imaged in STM were coated with 1-hexanethiol and 3-mercaptopropionic acid, while those for the chaining reactions were coated with a 3:1 molar ratio of 1-hexanethiol to 2-phenylethanethiol. However, we have no reason to suspect that the ligand organization would be different for the two types of NPs. Furthermore, the difficulty in forming chains of NPs larger than 10 nm as described above was likely due to the absence of ripples on those particles. STM was not performed on the larger NPs to confirm the ligand arrangement.

3.4.3 Equilibrium constant

We have developed a method[10] to calculate the equilibrium constant of pole functionalization by correlating the amount of precipitation from the Reaction **2** with the fraction of pole functionalized NPs (see Chapter 4 for detailed discussion). This method assumes that all NPs are available for pole functionalization and chain formation; that is, that all NPs have a rippled ligand morphology. This is reasonable for some samples, such as that of Figure 3.7, where most of the NPs are within the size range (~2.5 nm to ~6.5 nm) in which chains form. For samples in this size range, we obtained an average equilibrium constant of $1000 \pm 50\ M^{-1}$. However, when we consider the smallest sample of Figure 3.8, for instance, roughly 40% of the NPs fall outside the size range for possible

[a] Au_{140} NPs synthesized by Joe Tracy in the group of Royce W. Murray at the University of North Carolina. STM imaging performed by Cedric Dubois at MIT.

chain formation. When we do not account for the fact that it is impossible for this 40% to form chains, we obtain an equilibrium constant of 400 ± 11 M^{-1}. Accounting for the unavailable NPs, we instead obtain a value of 800 ± 64 M^{-1}, in much better agreement with the value for the sample of larger particles. This result further reinforces the conclusion that only NPs in a certain size range can be 'divalent', i.e. possess two highly reactive point defects arising from the rippled structure of the ligand shell.

3.5 Controlling chain composition

The pole functionalization approach to generating chains of NPs offers the flexibility to control the composition of the chains by substituting another species for the standard Au NPs discussed above. We have explored the possibility of forming chains of larger NPs and NPs of various core compositions via pole functionalization and interfacial polymerization.

It should be noted that many of the experiments described here were performed on NPs of diameter 10 nm or larger. From the above work on the size selection for chaining, we now understand that these experiments were unlikely to have been successful; however, they are included here for completeness.

3.5.1 Chains of large nanoparticles

Efficient plasmon coupling between NPs is not possible for particles of diameter less than approximately 10 nm.[11] For larger NPs, however, the generation of chains of large NPs could be monitored through observation of a red shift in the plasmon resonance wavelength due to plasmon coupling along the chain. Ultimately, the enhanced electric field between NPs in a chain could be applied to single-molecule optical studies such

Surface Enhanced Raman Spectroscopy[12] (for instance, by using a diamine terminated molecule with a Raman-active group as the inter-NP linker).

3.5.1.1 Preparation of large particles

Large NPs are difficult to synthesize so the NPs used for these experiments were purchased from Ted Pella. Both Ag and Au NPs were used, with diameters ranging from 20 nm to 40 nm. The NPs were received in a dilute water solution, electrostatically stabilized by citrate ligands. For chaining, it was necessary to exchange the citrates for thiolated ligands. To do so, the NPs were first transferred into N,N-dimethylformamide (DMF)[a] and a 2:1 molar mixture of NT and 6-mercapto-1-hexanol (MH) was added (the usual composition (2:1 NT:MBT) could not be used because the resulting NPs were not soluble in DMF). Pole functionalization was performed in DMF with only a small excess of MUA (typically a 4-fold molar excess over the number of NPs); a large excess could not be used because the solution was too dilute for Sephadex filtration and thus it was not possible to remove the unreacted MUA. To compensate for the dilute solution (several orders of magnitude more dilute than the standard reaction), the pole functionalization reaction was allowed to proceed for several hours to one day. DAH was then added to the same DMF solution (molar ratio 1:1 DAH : NPs) and the one-phase chaining reaction was stirred for several days. TEM and UV analysis was performed periodically to monitor the evolution of the reaction.

[a] To transfer the NPs from water to a second solvent, the second solvent was added and the water was slowly evaporated on a rotary evaporator. Thus the second solvent was required to be miscible with water and have a boiling point higher than that of water. DMF is not an ideal solvent for the chaining process (primarily because its high boiling point makes it difficult to remove from a reaction), but it is the only solvent that meets these two criteria.

3.5.1.2 Characterization

Chaining 20 nm gold NPs generated a UV spectrum shown in Figure 3.10(a). Unlinked NPs possess a plasmon resonance band around 540 nm. Several days after pole functionalization with MUA and coupling with DAH, a slight red shift to ~570 nm is observed. The slow kinetics of aggregation are likely due to the low solution concentration. TEM images (Figure 3.10(b)) show the presence of some chains; however, there are also a large number of two-dimensional aggregates, suggesting that many NPs have MUA molecules at random sites in the ligand shell. Indeed, it is probable that 20 nm NPs fall outside of the size range that can support ripples in the ligand shell; instead, MUA exchanged onto either crystallographically defined defect sites or vacancies in the ligand shell.

Linking 20 nm silver NPs generated the appearance of a second resonance that can be attributed to interparticle coupling (Figure 3.11(a)). Isolated Ag NPs exhibit a

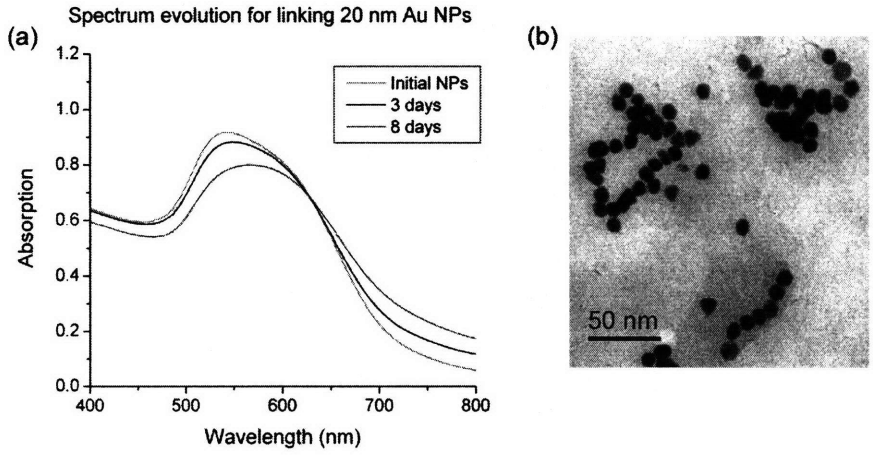

Figure 3.10
(a) UV-visible absorption spectrum of 20 nm Au NPs before linking (green) and at various points during the one-phase chaining reaction (blue and pink). A slight red shift is seen in the plasmon band suggesting interparticle coupling due to aggregation. (b) A representative TEM image of the NPs after 8 days of coupling shows chains but with significant branching and clustering.

plasmon band at ~415 nm. Pole functionalization and coupling reduced the intensity of the original band and gave rise to a new resonance that shifted from ~520 nm to ~560 nm as the chaining reaction progressed. This suggests that isolated NPs were slowly joining aggregates; as the aggregates grew, there was coupling among increasing numbers of NPs. However, TEM images (Figure 3.11(b)) are inconclusive in determining whether this shift is caused by chains or by multi-dimensional aggregates. Two-dimensional structures are seen that appear to have a somewhat 'chain-like' character. Interpreting these images is further complicated by the high interdigitation energy of Ag NPs, in that it is possible the aggregates seen in TEM are in fact composed of covalently bonded one-dimensional chains that are clustered into larger structures by van der Waals interdigitation forces. However, as stated previously, it is unlikely that chaining occurred given the size analysis above; it is more probable that the UV shift is due either to random multidirectional bonding of NPs or to their aggregation due to interdigitation.

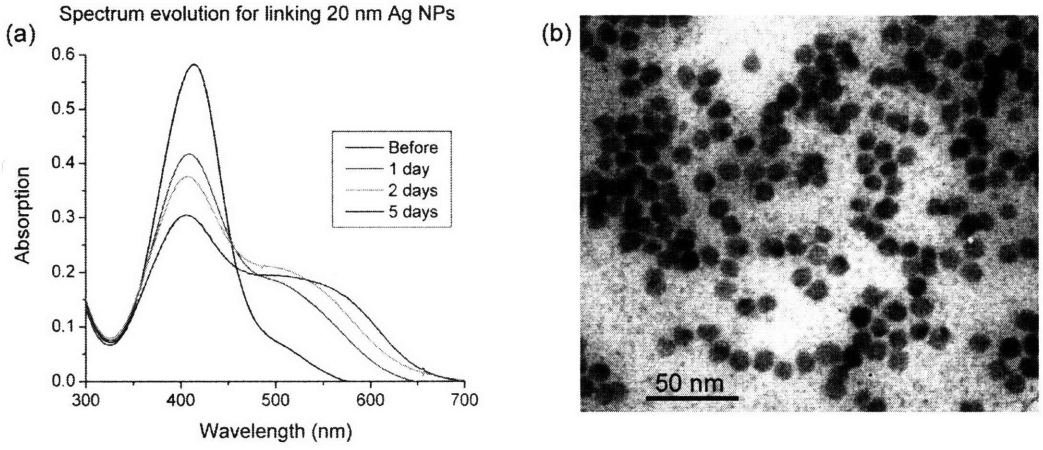

Figure 3.11
(a) UV-visible absorption spectrum for 20 nm Ag NPs before chaining and at several points during the one-phase chaining reaction. The original plasmon band at ~415 nm is reduced in intensity and a second band appears and continually red shifts, suggesting interparticle plasmonic coupling. (b) A representative TEM image primarily shows two-dimensional clusters but with some 'chain-like' character.

3.5.2 Chains of gold and silver nanoparticles

Despite the inconclusive results discussed above for the chaining of large NPs, we also attempted to use large NPs (20 nm diameter) of different core metals to generate chains of alternating composition. The pole functionalization approach to generating chains of NPs offers the ability to dictate precisely the chain composition by pole functionalizing each species of NP with a complementary molecule, something not easily achieved with other methods of chain formation. Chains of Ag and Au NPs in an alternating sequence would be important both as a demonstration of the versatility of the chaining technique and as a way to highlight intriguing optical properties of such chains. To guarantee linking only between Ag and Au NPs (that is, to avoid bonding between like NPs), we pole functionalized the Au NPs with MUA and the Ag NPs with 1-mercaptohexadecyl-16-amine (MHDA).[a] The NPs were pole functionalized separately; a one-phase reaction in DMF was used for chaining.

3.5.2.1 UV analysis

We monitored the optical spectrum of the chaining solution as the reaction progressed; Figure 3.12 shows the spectral evolution of the reaction. Initially, the NPs are completely isolated and the solution has one Ag band at ~420 nm and two Au bands: a dipolar oscillation at ~630 nm and a quadrupolar mode at ~530 nm (due to the large size of the NPs). As the reaction progresses, the Ag plasmon band weakens in intensity but remains fixed at 420 nm; likewise, the Au quadrupolar band weakens and ultimately nearly disappears, but does not shift. The dipolar Au resonance, however, undergoes a red shift of nearly 80 nm.

[a] Synthesized by Markus Brunnbauer and Oktay Uzun

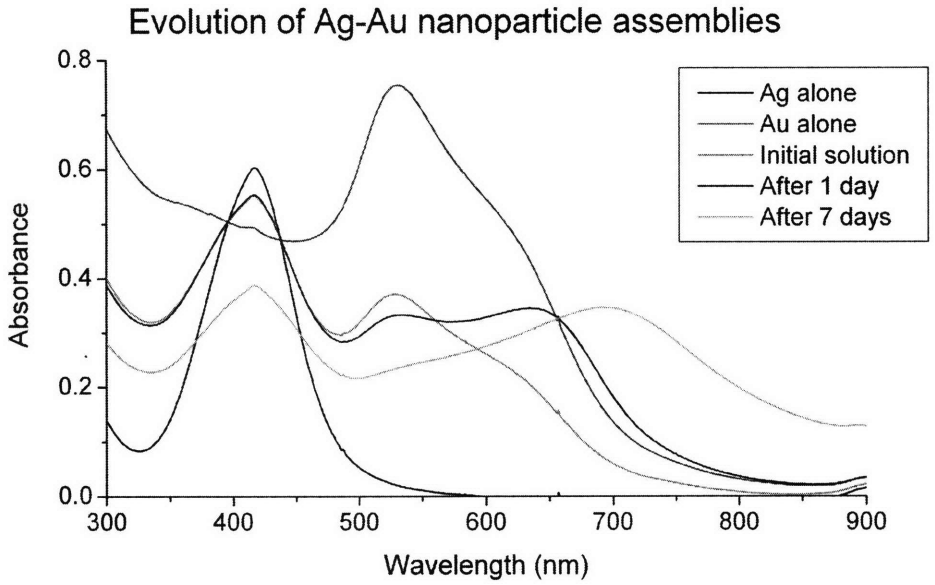

Figure 3.12
UV spectrum of the evolution of alternating Ag-Au NP assemblies. As the reaction proceeds, the Ag plasmon (~ 420 nm) decreases in intensity. The Au plasmon at ~530 nm also weakens, and the band originally at ~630 nm undergoes a significant red shift. This optical behavior can be explained by considering the Ag NPs to be "antennae" assisting in the coupling of neighboring Au NPs.

Assuming chains of alternating composition, this spectral evolution can be explained considering the resonance frequencies of Ag and Au NPs. The free electrons in the Ag NPs are able to oscillate more slowly than their resonance frequency; thus, the Ag particles can act as "antennae" and transfer some of the plasmon energy between next-nearest neighbor Au NPs by oscillating at the Au resonance frequency. This enhances Au-Au plasmonic coupling, generating a strong red shift in the dipolar band and taking energy away from the Au quadrupolar resonance. However, Au free electrons cannot oscillate at the faster Ag resonance frequency and thus cannot similarly contribute to Ag-Ag coupling. The Ag NPs therefore remain plasmonically isolated from each other; the Ag resonance is merely dampened because some Ag electrons instead become involved in the Au system. Note that if the chains were not composed of NPs of alternating composition, some Ag-Ag coupling would have occurred and the Ag band would have

also undergone a red shift; thus, these optical results suggest that chains of alternating composition were indeed formed.

3.5.2.2 TEM analysis

Unfortunately, TEM does not corroborate the spectral results of this experiment. Chains were observed in TEM imaging (Figure 3.13), as were other larger aggregates. High-resolution Scanning Transmission Electron Microscopy (STEM) images were then taken to identify the composition of the NPs in the chains.[a] Here, a bimodal size distribution was observed, with small (~6 nm diameter) NPs of Ag and larger (~20 nm) NPs containing both Ag and Au in the core (Figure 3.14). These images suggest that the Ag NPs partially disappear to alloy with the Au NPs; the metal exchange is likely driven by the difference in electrochemical potential between Ag and Au in solution. Such a phenomenon has previously been observed for smaller thiol-stabilized Ag and Au NPs in

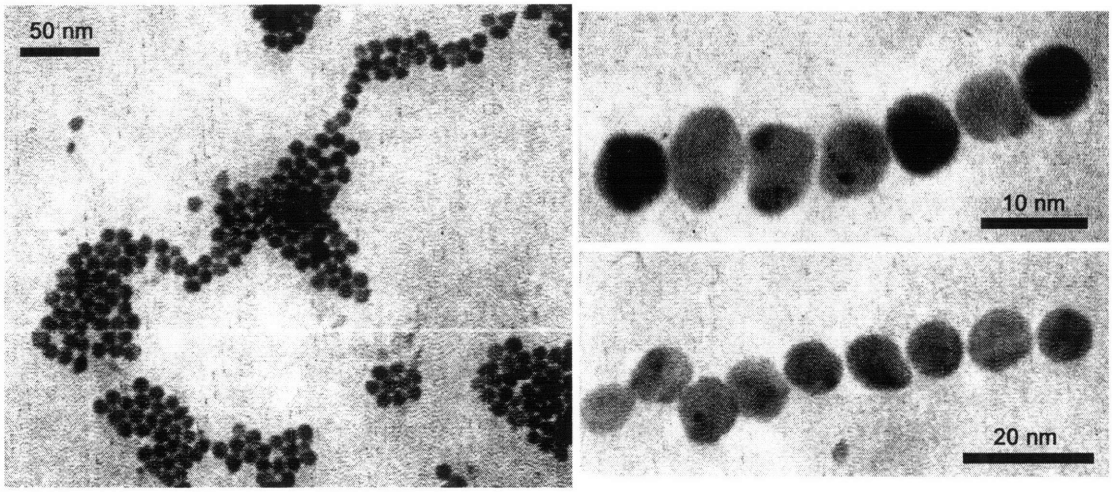

Figure 3.13
TEM images of the Ag-Au NP chaining reaction show fairly significant chains, although two- and three-dimensional assemblies are also present.

[a] STEM imaging performed by Dr. Anthony Garratt-Reed in the Center for Materials Science and Engineering.

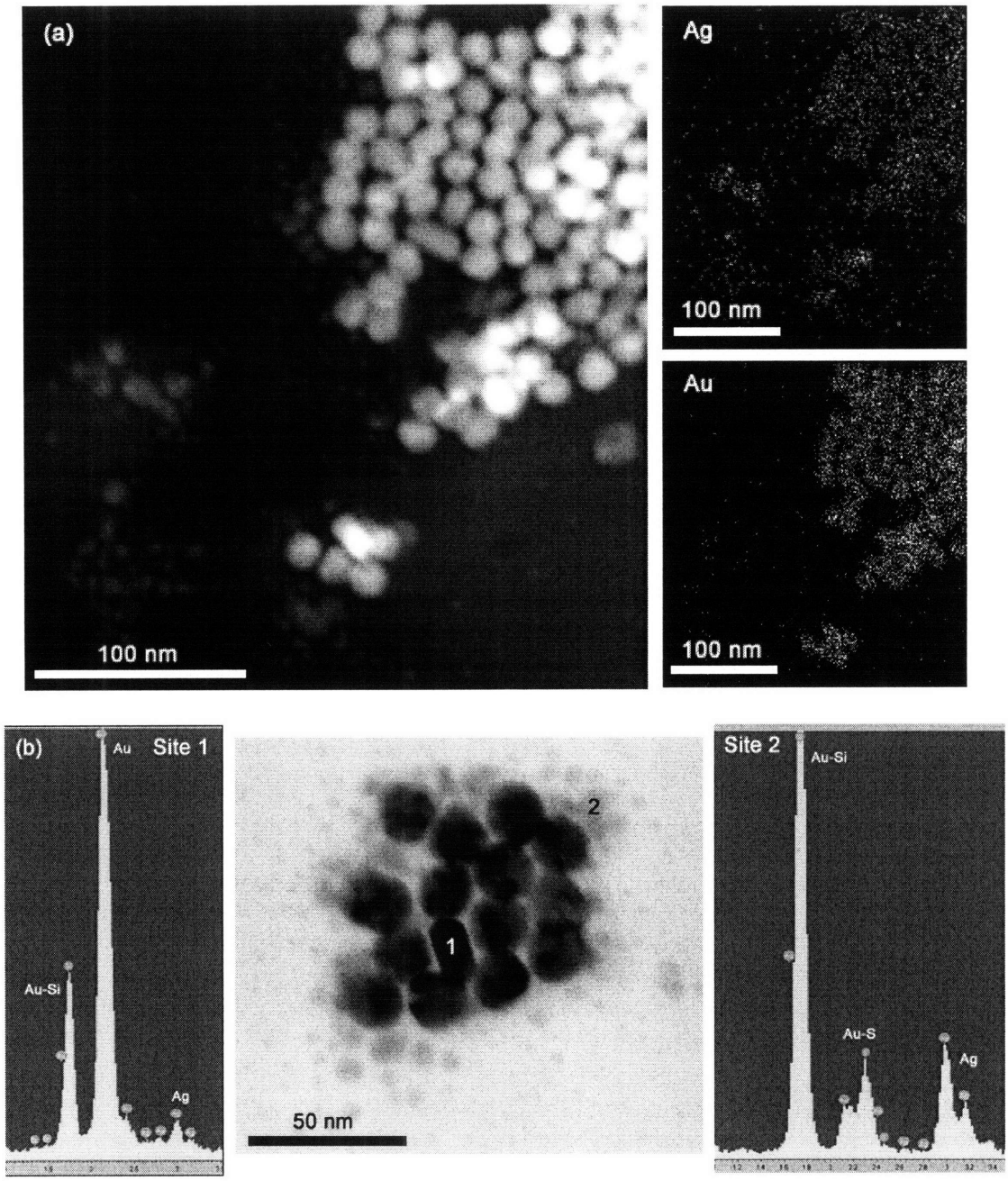

Figure 3.14
STEM images of the Au-Ag chaining reaction. (a) A dark field TEM image at left shows bimodally distributed NPs. Compositional analysis at right shows that the small NPs are Ag, while the large NPs are a mixture of Au and Ag. (b) Further compositional analysis at specific sites suggests that even in the small NPs, there is present a mixture of Au and Ag.

solution.[13] Thus, without a stabilization method such as cross-linking the ligand shell, it seems chemically impossible to generate chains containing both Ag and Au NPs.

In light of the STEM results (and furthermore in light of the size analysis presented above), it is difficult to interpret the spectrum of this experiment. Furthermore, we never succeeded in fully duplicating these results. On one occasion a similar (but not identical) spectral shift was observed (Figure 3.15(a)), but TEM showed few chains and only often aggregates of bimodally distributed NPs (Figure 3.15(b)).

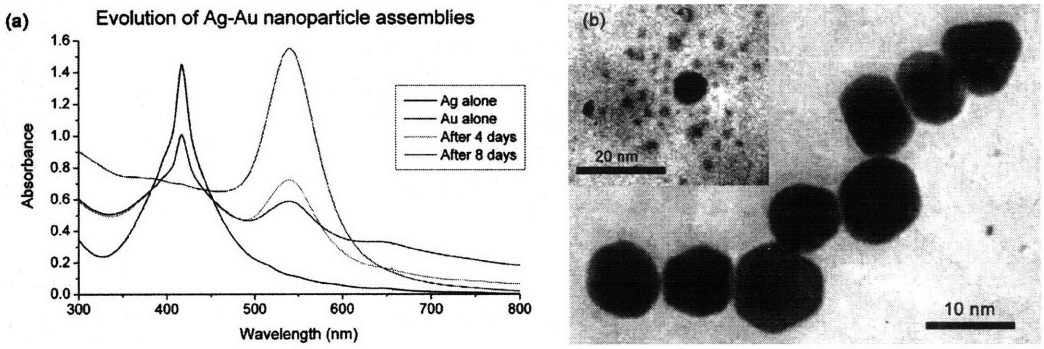

Figure 3.15
A repeat of the Au-Ag chaining reaction. (a) A similar spectral shift was observed, although the plasmon at ~420 nm suggests that there may be a problem with the Ag NPs, and (b) Chains were observed in TEM, but a bimodal size distribution was also seen, as was observed in STEM images of the previous experiment.

3.5.3 Platinum nanoparticles

Given the seeming impossibility of generating chains of Ag and Au NPs, we turned to platinum as another alternative. The electrochemical potential of Pt in solution is approximately the same as that of Au, so it should be possible for the two types of NPs to coexist in solution. Furthermore, as will be discussed at greater length in Chapter 4, we observed a striking difference in the kinetics and thermodynamics of Ag and Au NPs; Pt NPs are the next logical member of this series.

Platinum NPs were synthesized according to a literature procedure[14] in which chloroplatinic acid was reduced by lithium triethylborohydride in the presence of the desired ligands and under a nitrogen atmosphere. TEM images verify that the synthesis was successful. The two-step chaining procedure was performed; however, precipitation from Reaction **2** could not be quantitatively measured because the plasmon wavelength of Pt (λ = ~275 nm and generally very broad[15]) overlapped with the short-wavelength absorption band of toluene.[a]

The results of chaining experiments on the Pt NPs suggest that the standard chaining procedure is not adequate for Pt NPs. Complete precipitation of mixed ligand NPs (ligands 2:1 NT:MBT) was observed under the standard chaining conditions (pole functionalization with MUA followed by interfacial polymerization with DAH). However, significant precipitation of mixed ligand NPs also occurred under a variety of control conditions: when the NPs were pole functionalized but there was no DAH in the water phase, some precipitation occurred; there was complete precipitation when DAH was present, regardless of whether the NPs were pole functionalized. Surprisingly, however, when the above chaining and control experiments were performed on homoligand Pt NPs (coated with 1-octanethiol), no precipitation was observed even after several days. These results are puzzling but seem to suggest (1) that Pt easily reacts with amines and that the presence of diamines may cross-link the mixed ligand NPs into insoluble aggregates; (2) that there is a significant difference in the ligand shell morphology between homoligand and mixed ligand Pt NPs; and (3) that the mixed ligand morphology must somehow allow easier access to bare Pt (perhaps at polar defect sites) than the homoligand morphology,

[a] It is certainly possible to use a different solvent, such as dichloromethane, for Reaction **2**. However, with a different solvent it would be unreasonable to compare the precipitation profile of Pt NPs with that of Au or Ag NPs.

facilitating the diamine cross-linking. STM characterization has not yet been performed to determine the various ligand shell morphologies, and no further investigations were done into Pt NPs.

3.5.4 Chemistries for better control

Pole functionalizing NPs with NHS-activated carboxylic acids and linking with DAH in a two-phase reaction generates satisfactory chains. However, NHS is not a particularly good leaving group, and thus the chaining reaction is inefficient. A more attractive alternative is to replace the carboxylic acid group with an acid chloride, a more active leaving group. There are two options available for carrying out chaining with acid chloride chemistry: (1) place an acid chloride terminated molecule at the poles of the NPs and link with DAH, or (2) pole functionalize the NPs with an amine-terminated molecule and link with sebacoyl chloride, a divalent acid chloride molecule. Both approaches have been explored. The major drawback with this chemistry is that the acid chloride group is quite hygroscopic and thus the reaction is less straightforward to carry out.

3.5.4.1 Acid chloride at the poles

In the first option, the ideal approach would be to pole functionalize the NPs with a thiolated molecule terminated with an acid chloride group. However, such a molecule is not commercially available; instead, a carboxylic acid terminated thiolated molecule (such as MUA) must be converted to an acid chloride through an activation reaction.[16] If MUA were first exchanged onto the poles and then activated, the high temperature of the activation reaction could destabilize the ligand monolayer, potentially destroying the ripple structure and obscuring the poles. If activation were performed before pole

Scheme 3.2
"MUA-disulfide" used to convert the carboxylic acid into acid chloride without interference from the thiol group.

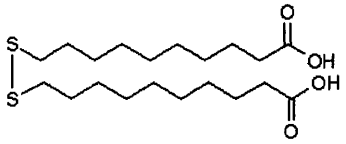

functionalization, the terminal thiol group of the free MUA molecule would likely interfere with the activation reaction. For these reasons, we chose to use an "MUA-disulfide" molecule as shown in Scheme 3.2 to be able to activate before pole functionalization without introducing the complication of the free thiol group. Since place-exchange generally obeys an associative mechanism,[5] the choice of a disulfide as the pole functionalizing molecule leads to at least two acid chloride groups at each pole; however, for the purposes of demonstrating the potential of this linking chemistry we believe that this limitation is not significant.

Using the acid chloride terminated disulfide, we pole functionalized the typical Au NPs (2:1 NT:MBT) for two different times (30 minutes and 3 hours) and performed the standard Reaction **2** to link the NPs with DAH. We collected the precipitate from each sample and imaged it in TEM. Chains do not appear in the 30 minute sample, although the two-dimensional clusters that are present are non-crystalline, implying that the interparticle interactions may be at least partially chemical (e.g. covalent bonding) rather than enthalpic (interdigitation that generally leads to close-packed two-dimensional lattices). The three hour sample (Figure 3.16) shows a large population of chains, although frequently branched or interlinked with other chains. These imperfections in the

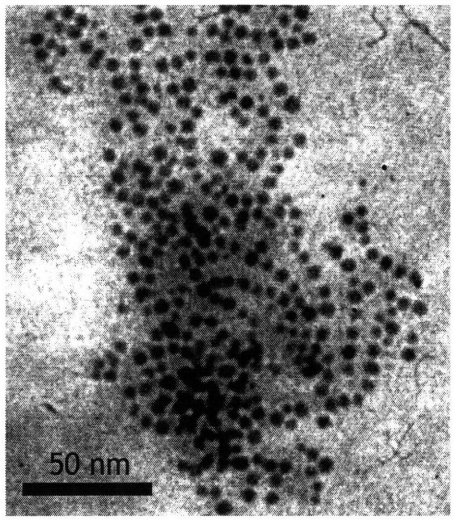

Figure 3.16
TEM image of NP chains formed by pole functionalizing Au NPs with an acid chloride terminated disulfide and linking in a two-phase reaction with DAH. Chains can be seen distinctly, although there appears to be significant branching.

chain structure can be attributed to the disulfide bond not breaking until it was immediately at the gold core, as expected, thus placing at least two acid chloride groups at each pole. If taken far enough, this situation should lead to the generation of fractal aggregates of NPs.

3.5.4.2 Linking with sebacoyl chloride

The second alternative for using acid chloride chemistry, pole functionalization with MHDA (an amine-terminated thiol) and linking with sebacoyl chloride, obviates the need for the acid chloride activation process and does not introduce the complications of the disulfide moiety. However, sebacoyl chloride is not water soluble as is DAH; thus, either the chaining reaction must be performed in one phase (potentially negating any advances in efficiency gained from the acid chloride chemistry), or the NPs must be water soluble to allow a two-phase reaction with the sebacoyl chloride in the organic phase. Accordingly, NPs with a ligand shell composition of 2:1 MH : 3-mercapto-1-

propanesulfonic acid were synthesized and pole functionalized with MHDA; these NPs were highly water soluble and thus enabled an interfacial polymerization reaction. There is no precipitate from this reaction because the NP phase is already on the bottom, but TEM images of NPs collected from the water phase reveal large networks of ball-like assemblies (Figure 3.17). These balls may be a result of interparticle hydrogen bonding between the hydrophilic alcohol termini of the ligands, or may be composed of long chains that find better stability curled upon themselves than extended in an "all-trans" configuration.

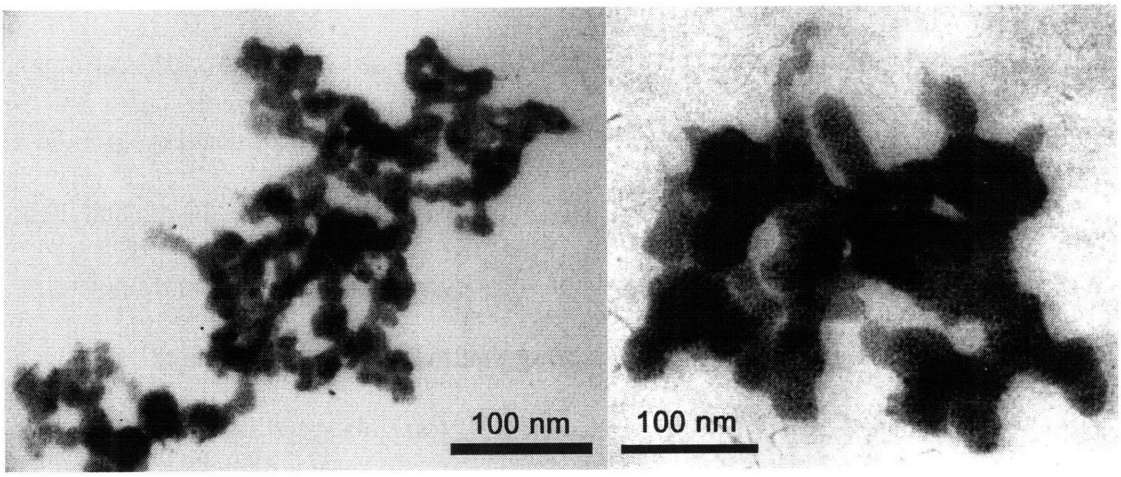

Figure 3.17
TEM images of large ball-like structures formed by performing a two-phase chaining reaction in which water-soluble NPs pole functionalized with MHDA and linked with sebacoyl chloride.

3.5.4.3 Controlling chain composition

As already discussed, a main practical advantage of the pole functionalization approach to chain formation is the ability it offers to control the precise composition of the chains. The attempts at controlling chain composition using carboxylic acid chemistry were not very successful; despite this, we also attempted to form chains of a desired composition by exploiting the more efficient acid chloride chemistry.

We first used 10 nm and 20 nm Au NPs (ligand shell 2:1 NT:MH) to form chains of random composition; both NPs were pole functionalized with MHDA and linked with sebacoyl chloride in a one-phase reaction. Since the reaction solution was so dilute, we hoped that the active acid chloride leaving group would rapidly couple with the amines on the poles of the NPs to generate chains. TEM images in Figure 3.18(a) show randomized chain-like structures. There are a variety of explanations for the presence of networks: (1) secondary bonding occurs between the alcohol groups in the ligand shells of neighboring NPs; (2) the pole functionalization reaction conditions are not optimized for this system and thus place-exchange occurs not only at the poles but also at other defect sites in the ligand shell; or (3) the NPs are too large for the ligands to form good quality ripples, and thus the polar defects are not well-defined, leading to random functionalization. Control experiments easily reject the first conjecture. 10 nm and 20 nm Au NPs with neither amines at the poles nor sebacoyl chloride in solution do not form a networked structure, eliminating the possibility that the structures are due to inter-ligand hydrogen bonding. Similarly, primarily isolated NPs are observed when the same non-pole functionalized NPs are stirred in the presence of sebacoyl chloride (Figure 3.18(b)). Thus, the observed networks are clearly a result of amide bond coupling between the NPs; furthermore, the clear chain-like character suggests that even if these NPs are not perfectly rippled, there is likely some order in the ligand shell that defines "special" defect points.

Chains of specific composition have not yet been achieved using acid chloride chemistry. We attempted to generate chains of alternating large and small NPs by pole functionalizing small (~3 nm diameter) Au NPs (ligand ratio 2:1 NT:MH) with acid

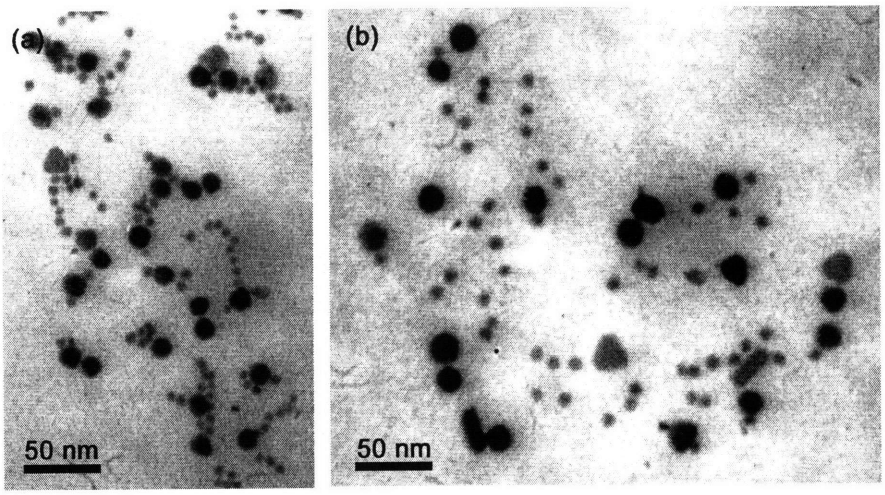

Figure 3.18
(a) TEM image showing randomized chains of 10 nm and 20 nm Au NPs, both pole functionalized with MHDA and linked with sebacoyl chloride in a one-phase reaction. (b) TEM image of a control in which the NPs are not pole functionalized but sebacoyl chloride is present in solution.

chloride activated MUA-disulfide and 10 nm Au NPs (ligand shell 2:1 NT:MH) with MHDA. We then performed a one phase polymerization. Were the acid chloride terminated molecule not a disulfide, this reaction should have generated the desired chains of alternating large and small NPs. However, because of the disulfide, it is likely that two acid chloride groups (at least) reside at each pole. This situation generates spheres containing both sizes of NP (Figure 3.19); the spheres become more dense and interconnected with increasing pole functionalization time. Light scattering of these structures indicates that they are present in solution (Figure 3.20). It is possible that these spheres are a sort of dendritic structure. It would be instructive to investigate that results of short time pole functionalization to observe earlier generation NP dendrites.

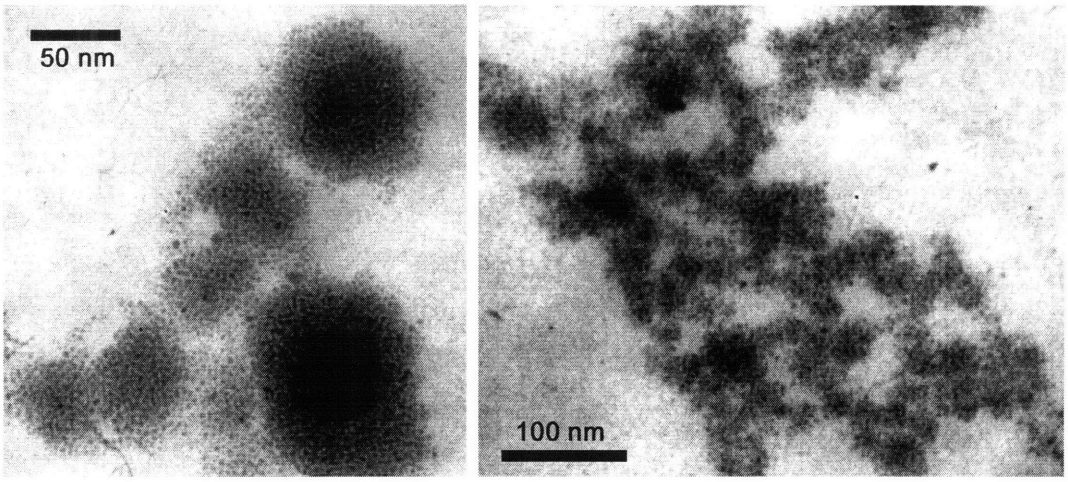

Figure 3.19
TEM images of spheres of NPs generated by pole functionalizing small NPs with acid chloride terminated "MUA-disulfide" and large NPs with MHDA.

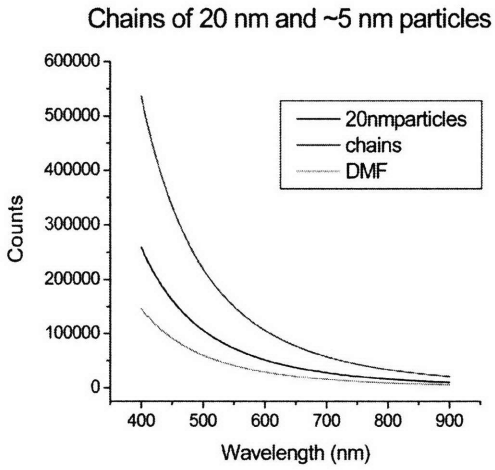

Figure 3.20
λ^{-4} fits to light scattering data of isolated 20 nm NPs and chains formed by pole functionalizing small NPs with acid chloride terminated "MUA-disulfide" and large NPs with MHDA. The assemblies are clearly present in solution, as indicated by the greater scattering intensity of the "chains."

3.6 Films of nanoparticles

During Reaction **2**, a skin forms at the water-toluene interface. This skin can be seen even while there is still toluene in the reaction vial; complete evaporation of the toluene generates a continuous film of NPs that sits on the water surface and can be at least as large as 1 cm^2. Profilometry has indicated that the films can be as thick as 60 μm. The films are self-standing: they can be picked up with a pipette and transferred intact into other non-solvents or spread onto a solid substrate (Figure 3.21). Our preliminary conclusion is that these films must be composed of multiple interwoven chains; the van der Waals interactions between the ligand shells of the NPs together with the interchain morphology likely provide this mechanical strength. In fact, when a film is placed into a good solvent for the NPs and chains (such as THF or dichloromethane), a portion of the film dissolves quickly (likely the isolated NPs) but a significant amount of the film remains intact over a period as long as several days.

One hypothesis about the structure of the films is that they are composed of chains of NPs that are arranged similar to the way polymer chains entangle to give mechanical strength to the bulk polymer. To demonstrate this idea, we performed Differential Scanning Calorimetry (DSC) measurements on the films, hoping to observe a "glass transition temperature." However, the monomer (NPs) has a high molecular weight (~10^6 g/mol); furthermore, the NPs are stabilized by thiol-Au bonds. Thus, in DSC experiments we observed only a sharp peak that we correlate to the desorption of the ligands from the NP core; the untangling of the NP chains (if this is the correct model) must occur at a higher temperature.

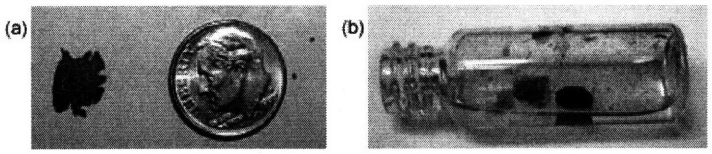

Figure 3.21
Photographs of a film composed of NP chains. (a) A film retrieved from the toluene-water interface was spread onto a glass slide. (b) The film maintains its structure in non-solvents such as ethanol (shown here).

3.6.1 Control experiments

Control experiments show that, in situations where chains are not formed during Reaction **2**, one of two extreme cases happen. (1) When the ligand shell cannot react with diamines (e.g. no pole functionalization has been performed), semi-continuous films form but only after the toluene has completely evaporated; no film is visible while the NPs are still dissolved. Bits of these semi-continuous films can at times be self-standing but always quickly and completely dissolve in any good solvent for NPs. (2) When the entire ligand shell can react with diamine (e.g. there is carboxylic acid present uniformly in the ligand shell), coarse powders that are insoluble in any solvent are formed. These powders are likely large three-dimensional assemblies of NPs covalently bonded together in many directions.

3.6.2 Morphology and mechanical properties

As discussed below, nanoindendation is an ideal method to characterize the mechanical properties of these self-standing NP films. However, nanoindentation requires a homogeneous, flat, and fairly dense material. At this stage, the films meet none of these criteria. Optical microscopy reveals a porous grain-like structure with a typical grain diameter between about 25 μm and 55 μm, but with some as large as almost 400 μm (Figure 3.22). The largest of these grains would be acceptable for nanoindentation in

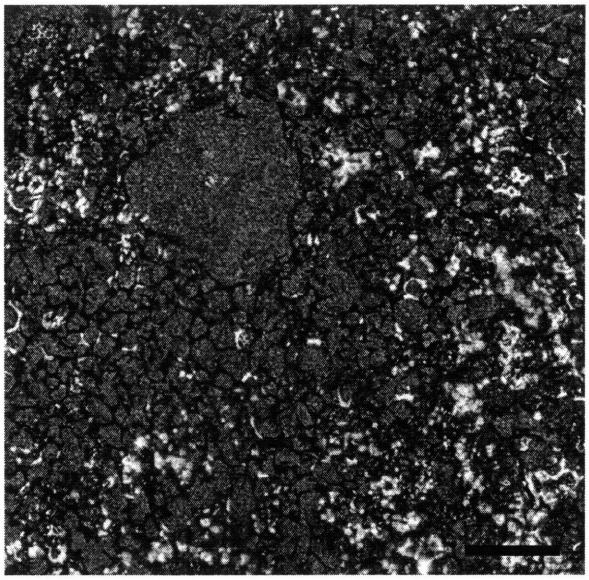

Figure 3.22
An optical microscope image of a film shows a porous grain structure composed of primarily small grains. Only the largest grain is a potential candidate for nanoindentation. Scale bar 200 nm. Image taken by Catherine Tweedie, Van Vliet group.

terms of flatness, but because of the inhomogeneity of the surface such sites are found only infrequently. Furthermore, the high porosity of the films makes nanoindentation difficult. Mechanical properties are determined based on the recovery of the material after the release of a load during nanoindentation. Preliminary indentations[a] on these films have shown that there is rarely a recovery, suggesting that material is pushed aside (probably to fill a void below) rather than returning to its original position.

Although the films are not yet dense enough for thorough mechanical characterization, preliminary studies have demonstrated some interesting properties. As mentioned above, the load-displacement tests do not yield valuable information because the sample does not recover from indentation. The creep behavior yields promising results: films formed of chained NPs have a slightly lower creep compliance than films made only of isolated NPs (Figure 3.23). However, the wide range in behavior of the

[a] Profilometry, AFM, and nanoindentation experiments performed by Catherine Tweedie in the Van Vliet group at MIT.

control samples indicates that the film preparation process is not yet repeatable enough to perform any kind of quantitative comparison.

A number of strategies were employed to address the porosity and inhomogeneity of the samples. Although the morphology is not yet at a quality acceptable for nanoindentation, some improvements have been made by compacting the newly formed film between two glass slides in an attempt to reduce the porosity. Other ideas to reduce porosity and improve homogeneity are to sinter the films or subject them to anneal heat treatments after formation.

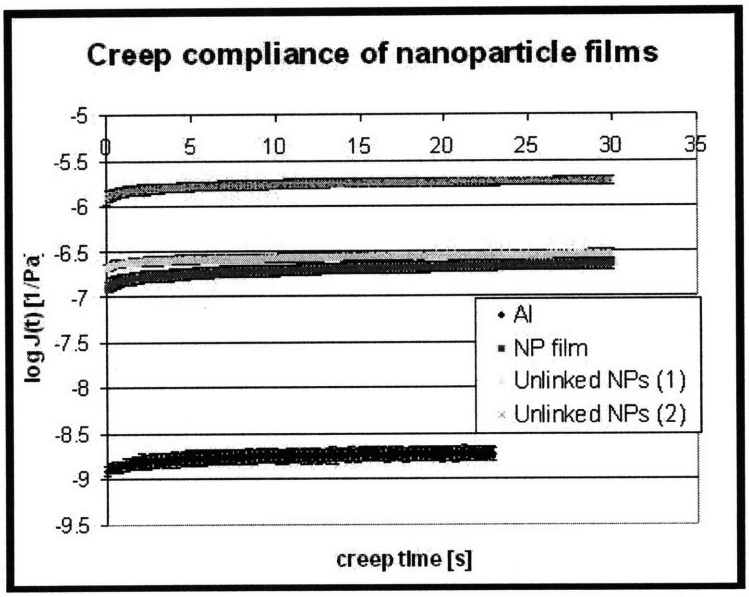

Figure 3.23
Graph showing creep compliance of a film of chained NPs (pink), two control films of unlinked NPs (yellow and turquoise), and bulk aluminum. The creep compliance of all the NP structures is significantly higher than that of the bulk Al. The compliance of the film of chained NPs seems to be slightly lower than that of the control films, but the wide variation in behavior of the control samples does not lend confidence to this result. Experiments performed by Catherine Tweedie, Van Vliet group.

3.6.3 Electrical characterization

A small amount of electrical characterization was performed on the films. Preliminary I(V) characterization indicates a resistivity $\rho = 5\text{-}6 \cdot 10^6\ \Omega\cdot cm$ (conductivity $\sigma = 1.5 \cdot 10^{-7}\ \Omega^{-1}\cdot cm^{-1}$) as shown in Figure 3.24. Data was collected for two different electrode spacings (1.4 μm and 2.2 μm); the calculated resistivity values for each spacing correspond well. An estimated film thickness of 100 μm and film width 1 mm were used in these calculations, as indicated above.

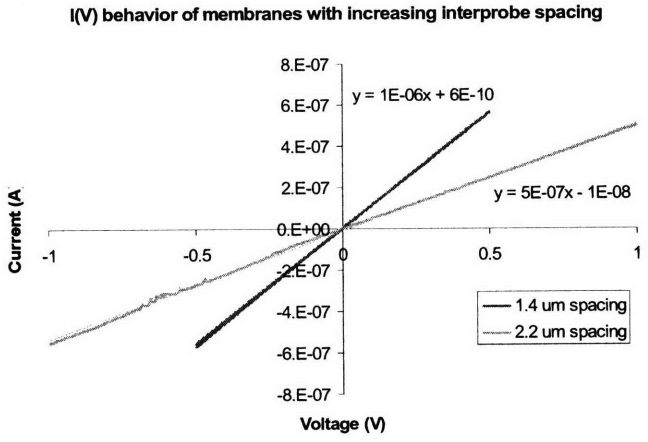

Figure 3.24
Electrical characterization of the NP films gave a resistivity of $\rho = 5\text{-}6 \cdot 10^6\ \Omega\cdot cm$. The two electrode spacings gave similar resistivity values.

3.7 Experimental section

Unless otherwise noted, all chemicals were purchased from Sigma Aldrich and used as received.

3.7.1 Nanoparticle synthesis

Two primary methods were used to prepare NPs: a two phase reduction reaction in toluene and water[17] and a one-phase reduction reaction in ethanol[7,8]. Both reactions were used for gold nanoparticles (NPs), although unless otherwise noted the NPs were synthesized with the one-phase reaction in ethanol; silver NPs were synthesized only with the two-phase reaction.

For both reactions, we used 0.9 mmol of the metal salt (hydrogen tetrachloroaurate trihydrate, $HAuCl_4 \cdot 3H_2O$ from Sigma Aldrich or Alfa Aesar for gold NPs; silver nitrate ($AgNO_3$) for silver NPs) and 0.45 mmol of thiolated ligands, giving a molar ratio of metal : ligand of 2:1. Often two kinds of ligands were used to make mixed ligand NPs; for example, for NPs coated with a 2:1 mixture of 1-nonanethiol (NT) and 4-methylbenzenethiol (MBT), 0.30 mmol of NT and 0.15 mmol of MBT would be used.

For the two-phase reaction, the metal salt was dissolved in 50 mL deionized water. 80 mL toluene containing 4 mmol tetraoctylammonium bromide ($[CH_3(CH_2)_7]_4NBr$), a phase transfer agent, was added and the mixture was stirred for 20 minutes. The ligands were then added and the mixture was again stirred for 20 minutes. A solution of 10 mmol sodium borohydride ($NaBH_4$) in 60 mL deionized water was added dropwise to induce NP formation. The reaction was stirred for two hours. The water was then removed, most of the toluene was evaporated on a rotary evaporator, and roughly 100 mL of pure ethanol was added. The ethanol mixture was stored in the refrigerator overnight to allow

precipitation; the precipitate was then collected by vacuum filtration and washed with ethanol, deionized water, and acetone.

For the one-phase reaction, the gold salt and the ligands were dissolved together in 80 mL of ethanol and stirred for 20 minutes. A solution of 10 mmol $NaBH_4$ in 150 mL ethanol was added dropwise. The reaction was stirred for two hours and then placed in the refrigerator overnight to allow precipitation; the precipitate was then collected by vacuum filtration and washed with ethanol, deionized water, and acetone.

A different method[18] was used to produce larger NPs for the size distribution study. 0.125 mmol chlorotriphenylphosphine gold ($AuPPh_3Cl$) was mixed with 0.0416 mmol NT and 0.0833 mmol MBT in 20 mL of benzene to form a clear solution, to which 1.25 mmol of tert-butylamine borane complex was then added. The mixture was stirred at 55 °C for one hour, then cooled to room temperature. 50 mL of ethanol was then added to precipitate the NPs; the precipitated NPs were collected by vacuum filtration and washed with ethanol, deionized water, and acetone.

3.7.2 Two-phase chaining procedure

For Reaction **1**, pole functionalization of the NPs was performed in tetrahydrofuran (THF) at a concentration of 15 mg/mL (75 μM); the high concentration is necessary for efficient filtration through a Sephadex column in a subsequent step. To the NP solution, a given molar excess (typically 20- to 120-fold over the number of NPs) of 11-mercaptoundecanoic acid (MUA) was added; the MUA was purchased pre-activated with N-hydroxysuccinimide (NHS, Prochimia, Poland), a leaving group. The solution of NPs and MUA was stirred at room temperature for 15 minutes (unless otherwise specified) to place MUA at the poles of the NPs. The unreacted MUA was then removed

from the solution by gel filtration over a size-selective column of LH-20 Sephadex. The purified NPs were then dried with a stream of air.

Reaction **2** is an interfacial polymerization process in which a 40 μM solution (7.5 mg/mL) of NPs in toluene and a 0.1 M solution of 1,6-diaminohexane (DAH) are placed in contact in a vial, briefly shaken, and allowed to sit undisturbed overnight. As the reaction proceeds, precipitation is observed at the water-toluene interface.

3.7.3 One-phase chaining procedure

5 mg of nanoparticles pole functionalized with NHS-activated MUA were treated with an equivalent amount DAH in a 1:1 (by volume) solution of dichloromethane and N,N-dimethylformamide (DCM/DMF). The solution was stirred at room temperature overnight, followed filtration over a LH-20 Sephadex™ column. TEM samples were cast directly from this solution.

3.7.4 Chaining procedure on Au_{140} NPs

For chaining, Au_{140} NPs coated with a 3:1 molar ratio of 1-hexanethiol and 2-phenylethanethiol were used. A solution of 1 mg of NPs in 2 mL THF was formed (this concentration is roughly equivalent to the concentration of the pole functionalization solution for the NPs in Figure 3.1), to which a 40-fold excess of MUA (pre-activated with NHS) was added. The solution was stirred for 15 minutes in a dark environment to ensure stability of the NPs. Subsequently, the solution was filtered over a column of LH-20 Sephadex gel and the NPs were blown dry a stream of air.

After pole functionalization, an interfacial polymerization process was performed in which a solution of 1 mg NPs in 200 μL of toluene and a 0.1 M solution of DAH) are

placed in contact in a vial, briefly shaken, and allowed to sit undisturbed overnight. No precipitate was observed. The supernatant toluene was collected and a TEM sample was prepared as described below.

3.7.5 Acid chloride chemistries

For acid chloride based chemistry, a disulfide-dicarboxylic acid molecule ("MUA-disulfide", Prochimia) was used to avoid interaction with free thiol groups during activation of the carboxylic acid. The activation reaction was performed under nitrogen gas and all liquid reactants and solvents were anhydrous. 0.5 mmol MUA-disulfide was dissolved in 50 mL benzene using heat and sonication. 253 μL pyridine and 3.8 mL thionyl chloride were added and the reaction was heated to reflux (~90° C) for one hour. The reaction was then dried on a rotary evaporator and the product was sealed until use.

Pole functionalization of NPs using the acid chloride activated molecule described above was not performed under anhydrous conditions. Pole functionalization and chaining were performed with the standard procedure, with the exception that one drop of a 1 mM solution of $NaBH_4$in ethanol was added to the pole functionalization solution to facilitate breaking the disulfide bond.

Chaining using sebacoyl chloride also followed standard procedure. Water soluble NPs were pole functionalized with 1-mercaptohexadecyl-16-amine (MHDA) using the standard Reaction **1**, and then dissolved in water at a concentration of 75 μM. A 100 mM solution of sebacoyl chloride in toluene was formed and placed in contact with the NP-water solution for chaining.

3.7.6 Synthesis of MHDA

16-bromohexadecanoic acid was treated with thionyl chloride ($SOCl_2$) to turn the carboxylic acid functionality into the corresponding acid chloride. After the removal of excess $SOCl_2$, the resulting molecules were dissolved in DCM and added to an ice-cooled solution of concentrated ammonia in water, forming a precipitate of 16-bromo-1-hexadecylamide, which was subsequently recrystallized from ethanol to yield the pure product. The bromine functionality was then replaced with the thioacetate group by reacting equimolar amounts of the above intermediate and potassium thioacetate in methanol. In THF, the thioacetate group was reduced by a $BH_3 \cdot THF$ complex and worked up with 6 M hydrochloric acid to yield a hydrochloride of the desired molecule. The free amine was accessed by dissolving the hydrochloride in hot toluene and treating with an aqueous solution of sodium hydrogen carbonate ($NaHCO_3$) in a separation funnel.

3.7.7 Treatment of large citrate-stabilized NPs

Large Au and Ag NPs (10 nm or 20 nm in diameter) were purchased from Ted Pella. These NPs arrive in water, electrostatically stabilized by citrate molecules, and at a concentration of $5.7 \cdot 10^{11}$ mL^{-1} (10 nm NPs) or $7 \cdot 10^{11}$ mL^{-1} (20 nm NPs). A volume equivalent amount of dimethylformamide (DMF) is added to the water solution of NPs and the water is removed by rotary evaporation, thus transferring the NPs into DMF. A 10% excess of thiolated ligands (2:1 molar ratio of NT : MH) relative to the number of surface binding sites on the NPs (see below) is added to the DMF solution and allowed to stir for several hours to several days to place-exchange thiolated ligands for the citrate stablizers.

Chains made from Ted Pella NPs were made with a one-phase procedure because of the low solution concentration (even significant evaporation of DMF would not noticeably increase the concentration). A four-fold excess of the polar molecule (e.g. MUA) was added to the thiol-coated NPs in DMF and allowed to stir for a few hours. A molar equivalent amount of DAH was then added and stirred for a few hours. Note that the unreacted polar molecules were not removed.

3.7.8 TEM sample preparation

A JEOL 200CX Transmission Electron Microscope was used at 200 keV.

To image the starting NPs, a small amount of NPs were dissolved in THF until the solution was slightly colored. The solution was briefly sonicated to break up any clusters of NPs. A few drops of the solution were dropped onto a carbon-coated 200 mesh copper TEM grid (Ladd research) resting on several (3-4) layers of KimWipes™. The tissue causes rapid wicking of the solvent and "freezes" the NPs onto the grid, thus preventing the formation of lattices or other artificial aggregation patterns that might artificially cause size selection and affect the size distribution results.

To image the precipitate of the interfacial polymerization reaction, the water and supernatant toluene were removed from the reaction vial and the precipitate was dissolved in THF until the solution was slightly colored. Brief sonication was used as necessary to break up clusters of NPs. A few drops of the solution were dropped onto a KimWipe™ as described above. In this case aggregates or lattices of NPs are not desirable because they would obscure the observation of chains.

The supernatant toluene was also imaged in much the same fashion to characterize the material that did not precipitate. The toluene was diluted in THF until the solution was slightly colored, then dropped onto a TEM grid as described above.

3.7.9 UV analysis

The concentration of the toluene phase in Reaction **2** was measured by UV-visible spectroscopy using an Agilent 8453 diode array spectrophotometer. A small amount (30 μL for Au NPs, 15 μL for Ag NPs) of the toluene phase was diluted in 2 mL of the same solvent and a spectrum was recorded in the wavelength range 200 nm to 1000 nm. The intensity of the absorption at the plasmon peak (~520 nm for Au NPs, ~480 nm for Ag NPs) was taken as an indicator of the solution concentration. To determine the extent of precipitation during the two-phase chaining reaction, the intensity was read before placing the toluene-NP solution in contact with the water-DAH phase and then again 24 hours afterwards. The quantity $1-\frac{[NP]_{post}}{[NP]_{pre}}$ was taken to be the extent of precipitation.

UV spectra were also collected for one-phase chaining reactions of large NPs to observe any interparticle plasmonic coupling. In these cases, samples were taken directly from the reaction solution without any dilution and spectra were collected from 200 nm to 1000 nm.

3.7.10 Light scattering

Light scattering spectra were collected using a Spex Fluorolog 2 in a synchronous scan mode (emission and excitation wavelength set to be equal). THF was first filtered through a 0.45 μm polypropylene syringe filter. Isolated nanoparticles (collected from the

toluene phase of a control experiment) or chains (collected from the precipitate) were dissolved in THF to an optical density of 0.06 at 520 nm.

3.7.11 Platinum particle synthesis

Platinum NPs were synthesized according to literature.[14] 0.5 mmol $H_2PtCl_6 \cdot 6H_2O$ and 0.5 mmol thiolated ligands (1-octadecanethiol in the original synthesis; NPs were also successfully synthesized with a 2:1 molar ratio of NT:MBT) were stirred vigorously in 10 mL anhydrous THF for 40 minutes at room temperature in a nitrogen environment. 10 mL "Super-Hydride" solution (1.0 M $Li(C_2H_5)_3BH$ in anhydrous THF) was added dropwise to the Pt salt solution to drive a color change from orange to deep brown. The resulting NPs were filtered as usual and stored in the refrigerator.

Another procedure[19] was also tried, but the NP product had poor solubility in most solvents. In this procedure, H_2PtCl_6 in water and a large excess (~25-fold molar excess) of ligands in toluene were stirred vigorously as a water solution of $NaBH_4$ (molar equivalent to the moles of Pt) was added dropwise. After stirring for 15 minutes, the NPs were separated, washed, and dried.

The standard Brust-Schiffrin two-phase method[17] for NP synthesis was also unsuccessful.

3.7.12 Film formation

For the formation of self-standing NP films, a procedure similar to the two-phase chaining process (Reactions **1** and **2**) described above was followed. The toluene solution was made more dilute (6 mg/mL) to hinder the deposition of NPs onto the walls of the reaction vial. A minimum of 10 mg of NPs were used for each film formed in a 5 mL

glass vial. The toluene was allowed to evaporate slowly by partially capping the vial; too rapid evaporation also caused deposition onto the vial walls. When completely dry, the film was gently poured into a beaker contained deionized water, collected onto a glass slide, and rinsed with acetone before any characterization.

3.8 References

(1) Jackson, A. M.; Myerson, J. W.; Stellacci, F. *Nature Materials* **2004**, *3*, 330-336.

(2) Nelson, D. R. *Nano Lett.* **2002**, *2*, 1125-1129.

(3) DeVries, G. A.; Brunnbauer, M.; Hu, Y.; Jackson, A. M.; Long, B.; Neltner, B. T.; Uzun, O.; Wunsch, B. H.; Stellacci, F. *Science* **2007**, *315*, 358-361.

(4) Flory, P. J. *Principles of polymer chemistry*; Cornell University Press: Ithaca,, 1953.

(5) Hostetler, M. J.; Templeton, A. C.; Murray, R. W. *Langmuir* **1999**, *15*, 3782-3789.

(6) Carney, R. P.; DeVries, G. A.; Kim, H.; Kim, J. Y.; Dubois, C.; Singh, C.; Ghorai, P. K.; Tracy, J.; Murray, R. W.; Glotzer, S. C.; Stellacci, F. *Submitted to JACS* **2007**.

(7) Brust, M.; Fink, J.; Bethell, D.; Schiffrin, D. J.; Kiely, C. *Journal of the Chemical Society-Chemical Communications* **1995**, 1655-1656.

(8) Stellacci, F.; Bauer, C. A.; Meyer-Friedrichsen, T.; Wenseleers, W.; Marder, S. R.; Perry, J. W. *Journal of the American Chemical Society* **2003**, *125*, 328-329.

(9) Singh, C.; Ghorai, P. K.; Horsch, M. A.; Jackson, A. M.; Larson, R. G.; Stellacci, F.; Glotzer, S. C. *Physical Review Letters, under review* **2007**.

(10) DeVries, G. A.; Talley, F. R.; Carney, R. P.; Stellacci, F. *Submitted to Advanced Materials* **2007**.

(11) Klabunde, K. J. *Nanoscale materials in chemistry*; Wiley-Interscience: New York, 2001.

(12) Willets, K. A.; Van Duyne, R. P. *Annual Review of Physical Chemistry* **2007**, *58*, 267-297.

(13) Song, Y.; Huang, T.; Murray, R. W. *Journal of the American Chemical Society* **2003**, *125*, 11694-11701.

(14) Yee, C.; Scotti, M.; Ulman, A.; White, H.; Rafailovich, M.; Sokolov, J. *Langmuir* **1999**, *15*, 4314-4316.

(15) Johnson, R. C.; Li, J. T.; Hupp, J. T.; Schatz, G. C. *Chemical Physics Letters* **2002**, *356*, 534-540.

(16) Peter, K.; Vollhardt, C.; Schore, N. E. *Organic Chemistry: Structure and Function*; W.H. Freeman and Company: New York, 1999.

(17) Brust, M.; Walker, M.; Bethell, D.; Schiffrin, D. J.; Whyman, R. *Journal of the Chemical Society-Chemical Communications* **1994**, 801-802.

(18) Zheng, N.; Fan, J.; Stucky, G. D. *Journal of the American Chemical Society* **2006**, *128*, 6550-6551.

(19) Yang, J.; Lee, J. Y.; Deivaraj, T. C.; Too, H. P. *Langmuir* **2003**, *19*, 10361-10365.

Chapter 4: Kinetic and thermodynamic analysis of pole functionalization

4.1 Introduction

As discussed in Chapter 3, mixed ligand metal nanoparticles (NPs) possess two opposing point defects, or poles, at which rapid place-exchange reactions can occur.[1] In this work, we primarily use NPs coated with a 2:1 molar mixture of 1-nonanethiol (NT) and 4-methylbenzenethiol (MBT). Through a controlled place-exchange reaction called pole functionalization (Reaction **1**), molecules with a reactive end group (such as 11-mercaptoundecanoic acid, MUA) can be placed at the poles.[1] The pole functionalized NPs are filtered and transferred to an interfacial polymerization reaction, Reaction **2**, in which they are joined by amide bonds into one-dimensional chains of NPs. Precipitation occurs upon chain formation.

The fact that place-exchange occurs so rapidly at the polar point defects indicates that the poles are unique sites on the NP. This chapter presents a kinetic and thermodynamic characterization of pole functionalization in order to develop a quantitative understanding of the reaction.

4.2 Kinetics of pole functionalization

To determine the optimal duration for the pole functionalization reaction, we allowed Reaction **1** to proceed for different amounts of time and subsequently measured the degree of precipitation and characterized the chains from Reaction **2**. We found that, for a given excess of MUA, the degree of precipitation does not depend on the time of the pole functionalization for times ranging from 5 minutes to 24 hours (longer times were

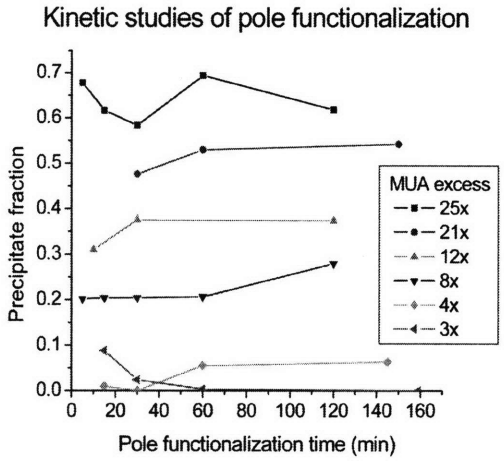

Figure 4.1
Plot of precipitation from Reaction **2** versus time of Reaction **1** shows that pole functionalization rapidly reaches equilibrium. The level of precipitation is affected only by the level of MUA excess, not by the duration of the pole functionalization reaction. This equilibrium allows for the study of the thermodynamics of place-exchange at the polar defect sites. In all cases the Au NPs were coated with a 2:1 molar ratio of NT:MBT.

not studied), as shown in Figure 4.1. That is, when the MUA excess is kept constant but the time of Reaction **1** is varied, we observe no difference in the level of equilibrium precipitation from Reaction **2**.[a] It is clear that equilibrium in Reaction **1** is reached after at most 10 minutes; it is likely that it is reached even more rapidly, but the precision with which the reaction quenching is carried out is not sufficient to characterize shorter reaction times. The level of precipitation was only affected by the amount of MUA used during pole functionalization; see below for a thorough discussion.

4.2.1 Kinetic treatment

Reaction **1** can be written as

$$\frac{1}{2}np + xMUA \longrightarrow \frac{1}{2}np \cdot MUA + (x-1)MUA, \qquad (1)$$

[a] In this and all other experiments in this work, Reaction **2** was allowed to reach equilibrium before any characterization was performed.

where $\frac{1}{2}np$ refers to one pole of a NP and x is the molar excess of MUA (pre-activated with N-hydroxysuccinimide, NHS). The second-order rate constant for pole functionalization (Reaction **1**) can be determined:

$$k_f = \frac{Rate}{[\frac{1}{2}np]_{initial}[MUA]_{initial}} \quad (2)$$

where

$$Rate = \frac{\Delta[\frac{1}{2}np]}{\Delta t}, \quad (3)$$

$\Delta[\frac{1}{2}np]$ is the change in the concentration of unfunctionalized poles, and Δt is the time of Reaction **1**. If we assume that all NPs that have been pole functionalized with MUA will later form chains and precipitate in Reaction **2**, then the quantity $\Delta[\frac{1}{2}np]$ is equivalent to the change in concentration of the toluene solution in Reaction **2**, which can be determined from the change in intensity of the plasmon band in the absorption spectrum. Note that although this treatment requires that two reactions be carried out, it characterizes solely Reaction **1**.

4.2.2 Determination of the rate constant

Making the conservative assumption that every MUA-functionalized NP will react to form an insoluble chain, the number of NPs that contain at least one MUA molecule can thus be experimentally evaluated by UV spectroscopy as described above. The rate constant k_f of pole functionalizing Au NPs (2:1 NT:MBT) with NHS-activated MUA was found to be 0.363 $M^{-1}s^{-1}$, or approximately one order of magnitude larger than

the largest value ($3 \cdot 10^{-2}$ $M^{-1}s^{-1}$) observed for place-exchange onto homoligand NPs.[2] This confirms our assertion that the poles are inherently unstable locations in the ligand shell that are more likely to undergo place-exchange than any other site. Furthermore, if we apply the fastest published second-order rate constant[2] to our system, we determine that only one MUA molecule per one hundred NPs would have reacted at sites other than the poles under our reaction conditions. Importantly, then, the rapid place-exchange at the poles proves that the molecularly defined polar defects are kinetically distinct from crystallographically defined vertices of the core crystal and from ordinary defects in the packing of the ligand shell SAM.

Silver NPs with the same ligand composition (2:1 NT:MBT) and the same average size as the Au NPs described above have also been studied briefly. Ag NPs display a rate constant of 8.2 $M^{-1}s^{-1}$ for pole functionalization, one order of magnitude higher than the rate for pole functionalization on Au NPs.

It should be pointed out that (i) we observe few dimers in TEM images of the precipitate, hence they must still be soluble; and (ii) we assume in our rate constant calculation that only one MUA molecule is located at each pole. Even larger rate constants would be obtained if either of these assumptions were removed.

4.2.3 FTIR studies

We have further confirmed[3] the equilibrium nature of pole functionalization on mixed ligand NPs using Fourier Transform Infrared Spectroscopy (IR).[b] Figure 4.2(a) shows an IR analysis of the efficiency of place-exchange reactions for mixed ligand NPs pole functionalized for different times and then filtered to remove any unreacted MUA. It

[b] IR measurements performed by Andrea Centrone at the Institute for Soldier Nanotechnology.

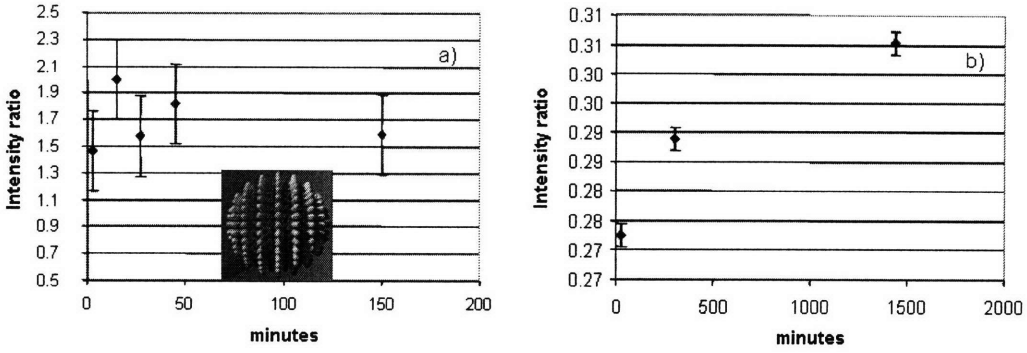

Figure 4.2
Place-exchange of NHS-activated MUA onto Au NPs as monitored by FTIR spectroscopy. **(a)** For NT:MBT NPs (phase separated ligand shell), a plot of the intensity ratio between the carboxylic C-O stretching vibration (~1710 cm^{-1}) and the vibration at 1484 cm^{-1} characteristic of the MBT molecules as a function of pole functionalization time. The intensity ratio stays constant, indicating that the same amount of MUA is exchanged onto the NPs regardless of pole functionalization time. **(b)** For deuterated OT (homoligand) NPs, a plot of the intensity ratio of the CH stretching region (belonging to NHS-MUA) over the CD stretching region (belonging to OT(d17) molecules) as a function of place-exchange time. As in a standard place-exchange reaction,[2] the amount of MUA on the NPs increases with the time of the reaction. The intensity ratios are not corrected for the vibrational cross sections' values and hence should be considered arbitrary units.

is evident that the amount of carboxylic acid exchanged onto the NPs does not vary as a function of the time of Reaction **1**. As a control, we also performed place-exchange reactions with homoligand NPs coated only with deuterated 1-octanethiol (OT); for these NPs the fraction of carboxylic acid containing ligands increases almost linearly with increasing time of place-exchange (Figure 4.2(b)), as would have been expected when comparing this system to literature.[2]

4.3 Thermodynamic model of pole functionalization

Since Reaction **1** is at equilibrium, it is logical to consider the thermodynamic characterization of the reaction in order to determine the equilibrium constant and free energy of pole functionalization. Using the level of precipitation as a proxy for the fraction of NPs that have MUA at one or both poles, we have developed a thermodynamic model to treat pole functionalization.[4]

The equilibrium constant K of pole functionalization (Reaction **1**) can be written as

$$K = \frac{[\frac{1}{2}np \cdot MUA][MUA]^{x-1}}{[\frac{1}{2}np][MUA]^{x}} = \frac{[\frac{1}{2}np \cdot MUA]}{[\frac{1}{2}np][MUA]}. \quad (4)$$

Defining np_0 as the initial concentration of poles in solution (e.g. the starting value of $[\frac{1}{2}np]$), np_{pf} as the instantaneous concentration of poles functionalized with MUA ($[\frac{1}{2}np \cdot MUA]$, and N as the ratio between the concentration of functionalized poles and the starting concentration of poles ($N = \frac{np_{pf}}{np_0}$), the equilibrium constant K can then be rewritten as

$$K = \frac{np_{pf}}{(np_0 - np_{pf})(xnp_0 - np_{pf})} \quad (5)$$

or

$$Knp_0 = \frac{N}{(1-N)(x-N)}. \quad (6)$$

Since x is large compared to N, the approximation $(x-N) \approx x$ can be made. Rearranging under this approximation yields an expression for N, which is the fraction of poles functionalized with MUA:

$$N = \frac{xKnp_0}{1 + xKnp_0}. \quad (7)$$

Chains are present in the precipitate; thus, we can consider that the fraction of poles functionalized in Reaction **1** (N) is directly related to the amount of precipitation from

Reaction **2**. An expression for N in terms of the precipitate fraction will then allow us to develop an expression for K in terms of the MUA excess x (the experimentally controlled variable) and the precipitate fraction (a measurable quantity).

If N represents the fraction of occupied poles in solution, then $1-N$ is the fraction of unoccupied poles. Similarly, N^2 is the fraction of NPs with two poles occupied, $(1-N)^2$ that of NPs with neither pole occupied, and $2N(1-N)$ that of NPs with exactly one pole occupied. Only those NPs that have at least one pole functionalized are relevant for the statistics of polymerization. In this treatment, we assign a singly functionalized NP as the first terminus of each chain and thus remove half of the singly functionalized NPs from subsequent statistics of polymerization. Thus, the total number of pole functionalized NPs available for polymerization is equal to the number of doubly functionalized NPs plus one-half of the singly functionalized ones. Of this set, the fraction that have two poles functionalized is

$$P = \frac{N^2}{N^2 + N(1-N)} = N \qquad (8)$$

and the fraction with exactly one pole functionalized is the quantity $1-P = 1-N$.

To form a chain of length x, we must start with a singly functionalization NP (which was already accounted for above), add $(x-2)$ divalent NPs, and finish with one singly functionalized NP. Thus, the probability of obtaining a chain of length x is

$$p(x) = (1-N)N^{x-2}. \qquad (9)$$

The total population of chains is then given by

$$\sum_{x=2}^{\infty}(1-N)N^{x-2}. \qquad (10)$$

Under the assumption (supported by TEM images of the precipitate) that dimers ($x = 2$) do not precipitate but that chains of all other lengths do, the population of precipitated chains ($x \geq 2$) multiplied by the fraction of pole functionalized NPs gives the overall fraction f of precipitate produced during Reaction **2**:

$$f = N^2(2 - N). \tag{11}$$

Combining Eqs. (7) and (11), an expression emerges that relates the equilibrium constant K to only controllable or measurable quantities of the system (the MUA excess x, the initial concentration np_0 of NPs in solution, and the precipitate fraction f):

$$f = \frac{(xKnp_0)^2(2 + xKnp_0)}{(1 + xKnp_0)^3}. \tag{12}$$

The shape of this function is shown in Figure 4.3. By performing Reaction **1** at different levels of MUA excess and measuring the precipitate fraction from Reaction **2**, Eq. (12) can be applied to extract the value of K for pole functionalization. Once K has been determined, the standard free energy of pole functionalization can be calculated:

$$\Delta G_0 = -RT \ln K. \tag{13}$$

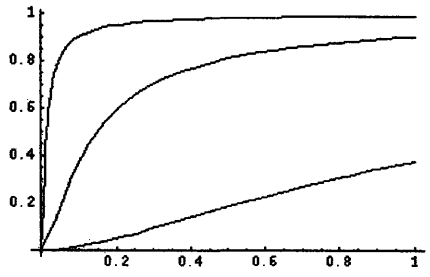

Figure 4.3
Plot of Eq. (11). Increasing the value of K creates a steeper initial slope of the function.

4.4 Thermodynamic characterization

Given the above model for determining the relevant thermodynamic quantities of pole functionalization, we performed a series of chaining experiments, varying the MUA excess in Reaction **1** and measuring the precipitation from Reaction **2**. It is important to note that this analysis would not be valid had we not previously demonstrated that (1) Reaction **2** is at equilibrium after proceeding overnight, because the amount of precipitate remains constant after that point; and (2) Reaction **1** rapidly reaches equilibrium, as shown from the consistent level of precipitation for any duration of the pole functionalization reaction.

4.4.1 Validation of the model

In order to test the above analysis and extract thermodynamic parameters of pole functionalization, it is necessary to relate the amount of precipitate in Reaction **2** to the MUA excess in Reaction **1**. We used standard Au NPs (ligand shell 2:1 NT:MBT) and pole functionalized with a series of MUA excesses, then measured the precipitation from Reaction **2** for each excess. Eq. (12) was applied to the resulting data.[4]

4.4.1.1 Precipitation profiles

Figure 4.4 shows an aggregate precipitation profile obtained by averaging a number of different chaining reactions (using various batches of starting NPs); the line is a fit to Eq. (12). For this type of NP, we determine an average K value of 1000 M^{-1} ± 50. Eq. (12) describes well the evolution of chain formation with increasing MUA excess (R^2 = 0.98). The large value of K indicates that the product of Reaction **1** (pole

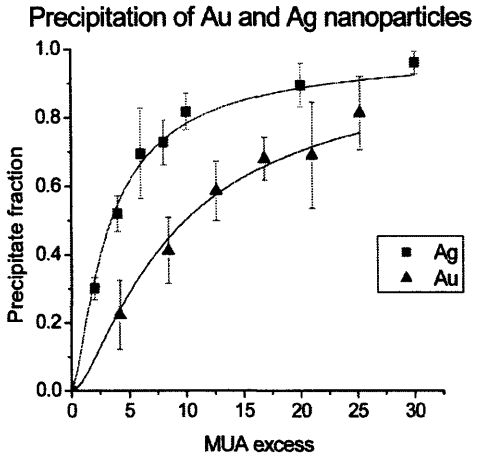

Figure 4.4
Precipitation profiles for Au and Ag nanoparticles of the same size and with the same ligand composition shows that the two have different pole functionalization behaviors. The *K* value for Au is 1000 M^{-1} ± 50; for Ag it is 1400 ± 70 M^{-1}.

functionalized NPs) is strongly favored over the starting material. This value should be compared with the recently determined value for the equilibrium constant of place-exchange onto homoligand Au NPs;[5] for that system, a *K* value of 0.97 ± 0.09 indicates that place-exchange at ordinary defect sites in the ligand shell is evenly balanced between the exchanged and non-exchanged states.

Similar experiments have been performed with Ag NPs of a similar size and with the same ligand shell composition. Ag NPs show more precipitation for a given MUA excess (Figure 4.4) and the *K* value was determined to be 1400 ± 70 M^{-1} (R^2 = 0.99). Recall that the kinetic rate of reaction for Ag NPs is also significantly higher than that of Au (k_f for Ag is 8.2 $M^{-1}s^{-1}$; for Au it is 0.363 $M^{-1}s^{-1}$). The fact that core composition affects both the rate and the final equilibrium of pole functionalization suggests that the interaction between the thiol groups of the ligands and the metal atoms of the core must play a role in regulating the reaction. In particular, it is known that the tilt angle of molecules differs for self-assembled monolayers on Au and Ag:[6] for straight chain

alkanethiols on Au, the angle is 32° and for the same molecules on Ag it is less than 5°. This difference in tilt angle may be an explanation for the differing kinetic and thermodynamic behavior of the two metals.

4.4.1.2 Chain length statistics

To further characterize the pole functionalization reaction, Transmission Electron Microscopy (TEM) samples of the precipitate plus the supernatant were prepared for each MUA excess; the inclusion of the supernatant allowed us to generate a more reliable sample to measure the chain length distribution.[4] From TEM images, we determined the distribution of chain lengths in samples prepared with various levels of MUA excess (Figure 4.5), and fit the chain length distribution data to Eq. (9) to obtain values for N for each sample. We found that both the average chain length and the fraction of occupied poles increase with larger excesses of MUA (Table 1), as expected. To validate the above thermodynamic model, we compared these values of N with the values of N determined using Eq. (7) and hence derived from the measurements of the precipitate fraction. We found remarkable agreement between the two values for each MUA excess: a consistent 20% different between the two values can be attributed to the fact that dimers are not considered when measuring the precipitate fraction but are counted in the chain length distribution statistics. Both cases also bear possible systematic errors: in the former it is reasonable to expect that a small fraction of dimers does indeed precipitate but is too small to be observed consistently in TEM images; in the latter we assume that we are trapping on the TEM grid a representative fraction of dimers from solution, something that could easily not be true.

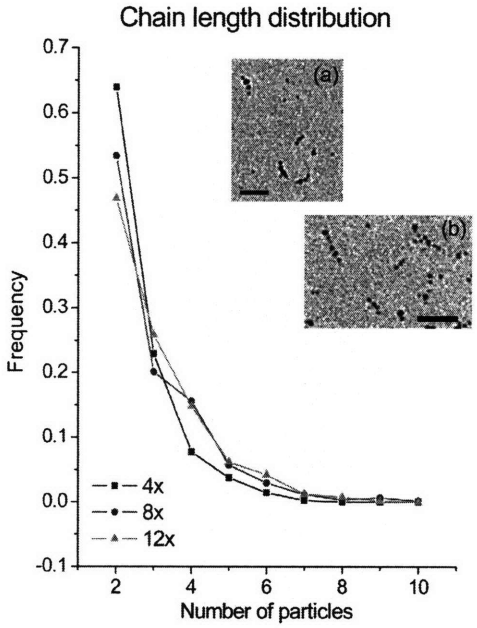

Figure 4.5
Plot of the chain length distribution for various levels of MUA excess. The distribution shifts slightly to longer chains for higher levels of MUA excess, as predicted by the thermodynamic model. Insets are TEM images of selected chains from the (a) 4x and (b) 12x samples; both scale bars are 25 nm.

MUA excess	Average chain length (number of NPs)	N (chain length distribution)	N (precipitation profile)
4.2x	2.6 $\sigma = 0.9$	0.36	0.44
8.4x	2.9 $\sigma = 1.3$	0.47	0.61
12.6x	3.0 $\sigma = 1.3$	0.54	0.70

Table 1
Chain length and N values determined from both chain length measurements and precipitation analyses. A consistent 20% difference between the two values for N can be easily explained by the difference in how the two approaches deal with dimers, as discussed in the text.

As a further verification of the model, we determined the theoretically attainable degree of polymerization for each sample assuming the interfacial polymerization reaction goes to completion (extent of reaction = 1).[7] Under this assumption, the maximum possible degree of polymerization is

$$D.P. = \frac{1+r}{1-r} \qquad (14)$$

where r is the ratio between the two reacting species. In this analysis, the two species were taken to be the population fractions of mono- and bi-functionalized NPs. For the 4.2x, 8.4x, and 12.6x samples, we obtained a degree of polymerization of 1.78, 2.59, and 3.84, respectively, in good agreement with the measured chain lengths. The short chains predicted by this approach thus validate our observation that primarily short chains form due to the low fraction of pole functionalized particles.

4.4.1.3 Implications of the equilibrium constant

The equilibrium constant can be used to determine the standard free energy of pole functionalization via Eq. (13). The values for pole functionalization onto Au and Ag NPs are similar (Table 2) and are approximately one-tenth the strength of a gold-thiol (or a silver-thiol) bond,[6] suggesting that a bond is broken (desorption of an existing polar

	K (M^{-1})	k_f ($M^{-1}s^{-1}$)	k_r (s^{-1})	ΔG (eV)
Au	1000 ± 50	0.36	$3.6 \cdot 10^{-4}$	0.17
Ag	1400 ± 70	8.2	$5.9 \cdot 10^{-4}$	0.18

Table 2

Equilibrium constant (K), forward and reverse rate constants (k_f and k_r, respectively), and reaction free energy (ΔG_0) for gold and silver NPs coated with a 2:1 molar ratio of NT:MBT.

ligand) and reformed (adsorption of the incoming MUA). However, the standard free energies are more than twice what was recently found for place-exchange onto homoligand NPs,[8] indicating that the molecular environment of place-exchange has a significant effect on the reaction.

The forward and reverse rate constants (k_f and k_r, respectively) of Reaction **1** are related to the equilibrium constant by

$$K = \frac{k_f}{k_r}. \qquad (15)$$

The relative values of the two rate constants can provide a better understanding of pole functionalization. The values for all three parameters for pole functionalization on Au and Ag NPs are given in Table 2. The rate constants reveal that, for Ag NPs, the incoming MUA is strongly favored, and once it has exchanged onto the NP it is kinetically disfavored from leaving. While this same trend applies to the Au system as well, the difference in forward and reverse rate constants is less pronounced. We can interpret these results in terms of the ability of the incoming MUA to penetrate the existing ligand monolayer and then its subsequent stability on the surface. A high k_f indicates that the incoming MUA can easily reach the polar site; a lower value suggests that the ligand monolayer hinders penetration and slows the pole functionalization process. Likewise, a low value of k_r suggests that, once the MUA has reached the poles, it is not inclined to leave. In this context, we can interpret the rate constants for Au and Ag as suggesting that the monolayer on Ag NPs is more readily penetrated by the incoming MUA and that the MUA is more stable once positioned at the poles. This leads

to a greater degree of pole functionalization, and explains the high levels of precipitation observed in the Ag system.

4.4.1.4 Control experiments: Reaction 1

A number of experiments were performed to further validate the above model and to prove the equilibrium nature of pole functionalization.

Since pole functionalization is an equilibrium process, it might be expected that the Sephadex filtration step to remove unreacted MUA is unnecessary (since the reaction has reached equilibrium, there should be no further exchange). Indeed, experimental evidence shows the same level of precipitation from Reaction **2** regardless of whether the solution from Reaction **1** is filtered. This result can be considered a second proof of the equilibrium nature of pole functionalization. Furthermore, although no experimental confirmation has yet been obtained, filtration may eventually limit the chain yield. With a filtered solution, once all the pole functionalized NPs have precipitated as members of chains in Reaction **2**, the chaining stops. Without filtration, as pole functionalized NPs precipitate, the equilibrium of a "Reaction **1**" in the toluene phase of Reaction **2** is disturbed. Excess MUA molecules that were not filtered out may then exchange onto formerly empty poles to restore the equilibrium population of functionalized poles, thus facilitating the generation of more chains.

4.4.2 Compositional effects

4.4.2.1 Incoming ligand effects

It is known that the forward place-exchange rate on gold NPs increases with increasing chain length of the incoming molecules.[9] We studied[4] two molecules of differing length but comparable bulkiness (i.e. two straight acid terminated alkanethiols) and observed a similar phenomenon for place-exchange at the poles: the forward rate constant for MUA (with 11 carbons) was 0.36 $M^{-1}s^{-1}$ and that for the 16 carbon molecule 16-mercaptohexadecanoic acid (MHA) was 0.42 $M^{-1}s^{-1}$. However, as shown in Figure 4.6, there is no significant difference in the precipitation profiles of NPs pole functionalized with MUA versus MHA. Fits to Eq. (12) give similar K values: 1028 M^{-1} ± 50 for MUA and 980 M^{-1} ± 41 for MHA. Clearly, the incoming ligand affects solely the rate and not the final equilibrium of the pole functionalization reaction. Note that, while chains have

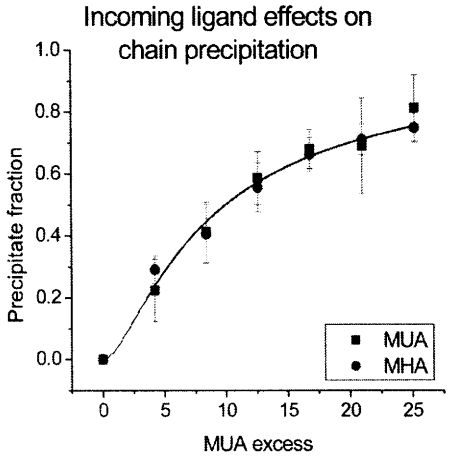

Figure 4.6
The precipitation profiles for Au NPs (ligands 2:1 NT:MBT) pole functionalized with NHS-activated MUA and MHA are similar; the equilibrium constants are 1028 M^{-1} ± 50 for MUA and 980 M^{-1} ± 41 for MHA. Points represent experimental data; lines are fits to Eq. (12).

been observed in TEM for both molecules, a detailed study of the chain length distribution has not been undertaken. As the two K values are similar, however, it is unlikely that different distributions would be observed.

4.4.2.2 Existing ligand effects

The length of the ligands on the NP has a strong effect on the equilibrium of the reaction.[4] We synthesized NPs coated with the following 2:1 mixtures of ligands: 1-butanethiol (BT) : MBT, 1-hexanethiol (HT) : MBT, NT:MBT, and 1-dodecanethiol (DDT) : MBT, at 1-octadecanethiol (ODT) : MBT. The ODT:MBT nanoparticles had poor solubility and were difficult to clean, likely because of either a poor quality ligand monolayer (owing to the inability of ODT to form complete monolayers) or strong interparticle interdigitation (due to the length of the ODT). Thus, this study focused only on the first four compositions. Note that the core sizes of these particles are similar; size distributions are shown in Figure 4.7.

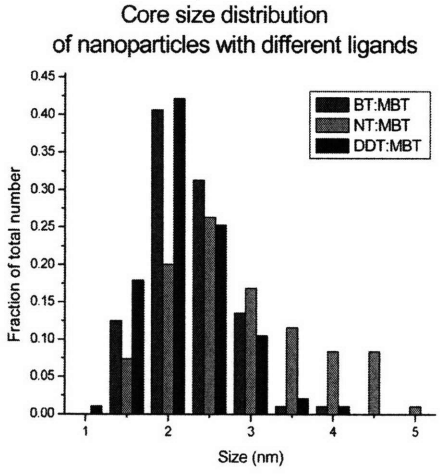

Figure 4.7
The core size distribution for Au NPs with different ligand shell compositions. The sizes are sufficiently similar to justify comparisons of thermodynamic parameters within the set.

Pole functionalizing each sample yields drastically different precipitation profiles (Figure 4.8), with BT:MBT reaching a high level of precipitation (and thus, presumably, also of pole functionalization) at a low level of MUA excess, and DDT:MBT showing extremely low levels of precipitation throughout the series. The equilibrium constant, K, ranged over one order of magnitude for the series of ligands, with the equilibrium favoring further the product as the length of the existing ligands decreases (Table 3). A trend was also observed in the k_f values, with a faster rate constant for shorter existing ligands, as has previously been observed for place-exchange onto homoligand NPs.[2] However, the k_r values are small and similar across all ligand compositions. This suggests that the ability of the MUA to penetrate monolayers of different thickness controls the pole functionalization process, but that once the MUA has exchanged at the poles, it is equally stabilized by any of the ligand compositions. These differences are likely related to the penetrability of the ligand monolayer and the stability it then provides to the MUA at the poles.

We investigated the effect of ligand shell composition on the chain length distribution and thus the values of N. Comparison of N values between samples of different MUA excess was challenging because the region of MUA excess in which chains formed was different for each sample. In general, ligand compositions with larger K values had chains at lower levels of MUA excess. For instance, for the BT:MBT sample at a 4-fold MUA excess, the N value was roughly 30% more than the corresponding value for the NT:MBT sample; however, larger MUA excesses began to generate clusters of NPs and we were unable to obtain credible chain length distributions. Similarly, the DDT:MBT sample did not begin to show chains until a 21-fold MUA

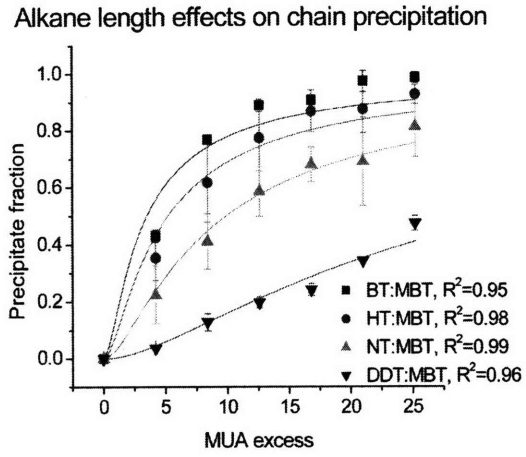

Figure 4.8
Graph of precipitation from Reaction **2** versus MUA excess during Reaction **1**. Points represent experimental data; solid lines represent fits. A pronounced effect of ligand length is seen, indicating that pole functionalization proceeds less efficiently on particles with longer ligands.

	K	k_f ($M^{-1}s^{-1}$)	k_r (s^{-1})	ΔG (eV)	**Diameter** (nm)
BT:MBT (C4)	2800 ± 480	0.68	$2.4 \cdot 10^{-4}$	0.20	2.3 nm $\sigma = 0.5$
HT:MBT (C6)	1900 ± 190	0.54	$2.9 \cdot 10^{-4}$	0.19	
NT:MBT (C9)	1000 ± 50	0.36	$3.6 \cdot 10^{-4}$	0.17	2.9 nm $\sigma = 0.9$
DDT:MBT (C12)	300 ± 20	0.11	$3.8 \cdot 10^{-4}$	0.14	2.2 nm $\sigma = 0.5$

Table 3
Equilibrium constant (K), forward and reverse rate constants (k_f and k_r, respectively), and reaction free energy (ΔG_0) for gold NPs coated with a 2:1 molar ratio of an alkanethiol to MBT. The average size of each set of NPs is comparable.

excess, at which point the other samples all had begun to form clusters. Full results are shown in Table 4. In general, there was roughly a 20% difference between the values of N determined from the chain length distribution and from the precipitation profile, further validating the thermodynamic model. Furthermore, despite the difficulty of comparison, it is clear that the K value affects the chain length distribution and thus the fraction of poles functionalized in a rational and predictable manner.

4.4.3 Reproducibility

A variety of experimental parameters may introduce variability into the data, including: (1) the batch of starting NPs (each batch may have a slightly different core size or ligand shell composition even if synthesized with the same method); (2) the exact concentration of the MUA solution added to the NPs in Reaction **1** (a fresh solution is

		BT:MBT	**NT:MBT**	**DDT:MBT**
	K	2800	1000	300
4.2x	N from length distribution *(N from precipitation data)*	0.5 *(0.6)*	0.4 *(0.4)*	
8.4x			0.5 *(0.6)*	
12.6x			0.5 *(0.7)*	
21x				0.4 *(0.5)*

Table 4
Values of N determined from length distribution data (normal font) and precipitation profiles (*italics*) for NPs of various ligand shell compositions. The given compositions are in a 2:1 molar ratio of the first ligand to MBT. It is evident that the length of the ligands affects the pole functionalization reaction. Many data points could not be obtained either because no precipitate formed or no chains were observed, or because aggregates in the precipitate were too large.

created for each reaction to avoid any potential degradation of the MUA); (3) the exact concentration of the NP solution in Reaction **1** (in addition to measurement errors, the likely variation in core size implies that each batch will have a different molecular weight); (4) the stirring speed; and (5) the accuracy of the dilution for UV absorption measurements during Reaction **2**. We thus performed a number of sets of experiments to study the quantitative reproducibility of chain formation.[3]

Figure 4.9 shows experimental precipitation profiles and thermodynamic fits for various chaining experiments performed with Au NPs coated with a 2:1 molar ratio of NT and MBT and pole functionalized with NHS-activated MUA. Data and trendlines of the same color refer to experiments that were performed with the same starting batch of NPs. Each set of experiments (represented by points of the same shape and color) consisted of several samples of NPs from the same original batch that were pole functionalized with different MUA excesses to generate a precipitation profile; within

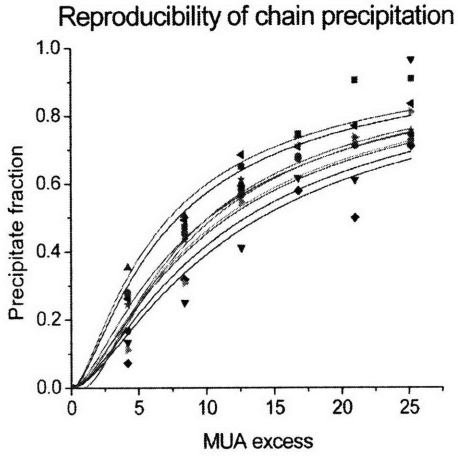

Figure 4.9
Precipitation from Reaction **2** versus MUA excess in Reaction **1** for several sets of experiments. Data points were obtained experimentally; trendlines were fit to Eq. (12). For each set of experiments samples were tested at various levels of MUA excess; each set is represented by one shape. Sets of experiments performed with the same starting batch of NPs are shown in the same color. Given the various potential sources of variability, the data shows good reproducibility across starting batch of NPs, operator, and other experimental parameters.

each set, the same stock MUA solution was used and the same operator performed the experiments at all the MUA excesses. Between sets of experiments, we did not necessarily keep consistent the starting batch of NPs, the stock MUA solution, or the operator.

Given the typical sources of uncertainty mentioned above, the spread in the data is remarkably small. Indeed, the batch of starting NPs, arguably the least controllable of the potential sources of error, affects the outcome of Reaction **2** just as much as (if not less than) the day-to-day variations that enter into the experiments. The range of values of the equilibrium constant for the data shown in Figure 4.9 is between 702 and 1355 M^{-1}; within the red sets of experiments (e.g. those starting from one common batch of NPs) the range is 968 to 1355 M^{-1}, within the blue (a different starting batch) it is 702 to 1243 M^{-1}, for the pink the values are 1015 and 1061 M^{-1}, and for the green the value is 872 M^{-1}. Averaged together, these data generate an aggregate value of 1028 M^{-1} with a standard deviation of 229, or 22%.

It should be noted that, as stated previously, a new MUA solution was generally prepared for each set of experiments, meaning that measurement imprecision could result in slightly different MUA excesses between sets even for the same nominal excess value. Indeed, when the MUA solution is kept the same for two different sets of experiments, thus ensuring an identical level of excess, a standard deviation of approximately 10% is observed in the values of the equilibrium constant. Thus, although the MUA solution is evidently a significant source of error, there is still variation in the data arising from other experimental parameters.

4.4.4 The case of homoligand nanoparticles

Homoligand NPs provide a vehicle for determining the degree to which the rippled ligand structure of mixed ligand NPs accentuates the polar defect sites.[3] We performed the standard chaining procedure on NPs coated only with NT, measured the precipitation from Reaction **2**, and observed the composition of the precipitate in TEM. The resulting precipitation profile had a similar shape as that of mixed ligand NPs (Figure 4.10). However, TEM images of the precipitate showed almost no chains: 12% of the NPs observed were found in dimers and only 4% in chain-like structures; furthermore, these fractions appeared to be independent of the MUA excess levels. This latter observation is in direct contrast to our thermodynamic model of pole functionalization and with experimental observations of chain formation with mixed ligand NPs, where chain length increases with increasing MUA excess. The lack of chains of homoligand NPs implies that they must undergo a place-exchange process that is somehow different than that which occurs at the poles of mixed ligand NPs.

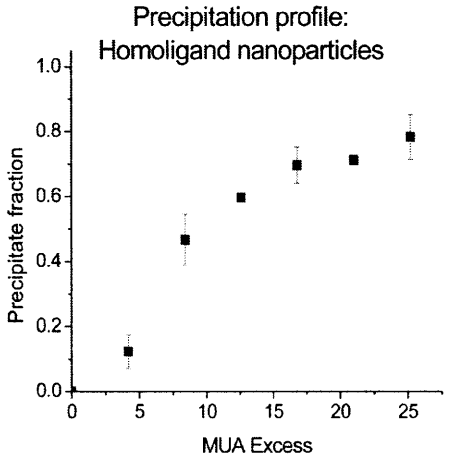

Figure 4.10
Precipitation profile for homoligand (100% NT) NPs shows an increase in precipitation with increasing MUA excess.

4.5 References

1. DeVries, G. A.; Brunnbauer, M.; Hu, Y.; Jackson, A. M.; Long, B.; Neltner, B. T.; Uzun, O.; Wunsch, B. H.; Stellacci, F., Divalent metal nanoparticles. *Science* **2007,** 315, (5810), 358-361.
2. Hostetler, M. J.; Templeton, A. C.; Murray, R. W., Dynamics of place-exchange reactions on monolayer-protected gold cluster molecules. *Langmuir* **1999,** 15, (11), 3782-3789.
3. DeVries, G. A.; Centrone, A.; Stellacci, F., Chains of divalent gold nanoparticles. *Proceedings of SPIE* **2007,** 6768.
4. DeVries, G. A.; Talley, F. R.; Carney, R. P.; Stellacci, F., *Submitted to Advanced Materials* **2007**.
5. Kassam, A.; Bremner, G.; Clark, B.; Ulibarri, G.; Lennox, R. B., Place exchange reactions of alkyl thiols on gold nanoparticles. *Journal of the American Chemical Society* **2006,** 128, (11), 3476-3477.
6. Schreiber, F., Structure and growth of self-assembling monolayers. *Progress in Surface Science* **2000,** 65, (5-8), 151-256.
7. Rempp, P.; Merrill, E. W., *Polymer Synthesis*. 2nd, revised Edition ed.; Huthig & Wepf Verlag: New York, 1991.
8. Kalsin, A. M.; Kowalczyk, B.; Wesson, P.; Paszewski, M.; Grzybowski, B. A., Studying the thermodynamics of surface reactions on nanoparticles by electrostatic titrations. *Journal of the American Chemical Society* **2007,** 129, (21), 6664-6665.
9. Ingram, R. S.; Hostetler, M. J.; Murray, R. W., Poly-hetero-omega-functionalized alkanethiolate-stabilized gold cluster compounds. **1997,** 119, (39), 9175-9178.

Chapter 5: Conclusions

5.1 Future research directions

The work presented here introduced the concept of divalency in metal nanoparticles (NPs) and developed a method to synthesize chains of divalent NPs. Improvements can still be made in the synthesis procedure, and there are several potential directions for this research to proceed. We discuss here a few options.

5.1.1 Chain length

In this work, we have demonstrated a reliable procedure for the synthesis of chains of NPs. However, significantly longer chains are required in order to present any meaningful possibility for technological applications. We have demonstrated that the length can be increased by using larger excesses of 11-mercaptoundecanoic acid (MUA) in the pole functionalization reaction;[1] however, this length increase is minimal and the average chain length is fairly short. Below are presented potential modifications to both the pole functionalization reaction (Reaction **1**) and to the subsequent interfacial polymerization reaction (Reaction **2**) that may result in longer chains.

The short chain lengths achieved in this work are likely due in part to the dynamic equilibrium between adsorbed and desorbed species in self-assembled monolayers (SAMs).[2, 3] That is, the molecules placed onto the poles of mixed ligand NPs are not fixed, and rapid exchange continues to occur at the poles during Reaction **1**. In general, two like molecules will be exchanged due to the large excess of the incoming molecule (e.g. MUA) in solution. However, there is also a small population of molecules from the original ligand shell of the NPs (e.g. 1-nonanethiol and 4-methylbenzenethiol) in

solution, and occasionally these molecules will adsorb onto the poles, generating poles without reactive end groups. By careful choice of the solvent and the incoming molecules, the dynamic equilibrium could be shifted to favor the adsorbed state and this unwanted exchange could be minimized. That is, an incoming molecule that is only slightly soluble in the reaction solvent would exchange onto the poles but feel only a weak driving force to desorb. Subsequent cross-linking of the ligand shell could be performed to ensure stability also during Reaction **2**.

In Reaction **2**, a significant obstacle to growing longer chains is the fact that once a chain has precipitated, it can no longer participate in the reaction. Stirring Reaction **2** would not only encourage the chains to remain soluble in order to grow longer, but would also increase the interfacial surface area and thus improve the reaction efficiency. Choosing a combination of organic solvent and ligand shell composition to maximize NP solubility may also allow the chains to grow longer before precipitating. The available selection of solvents is minimal, as the organic solvent must be immiscible with water and preferably also less dense than water; however, the ligand shell composition could be tuned to provide better solubility in toluene.

5.1.2 Linking chemistry

Alternate linking chemistries should be studied to understand any potential advantages they present over the amide bond coupling used in this work. The explorations of acid chloride chemistries presented in Chapter 3 yielded promising results that should be investigated further. A few other possible chemistries are described here.

Alcohols and carboxylic acids readily form covalent bonds with isocyanates; NPs pole functionalized with MUA or an alcohol-terminated thiol could be reacted with

Scheme 5.1
An alternative chemistry for chaining NPs involves pole functionalization with an alcohol-terminated thiol followed by linking with a diisocyanate.

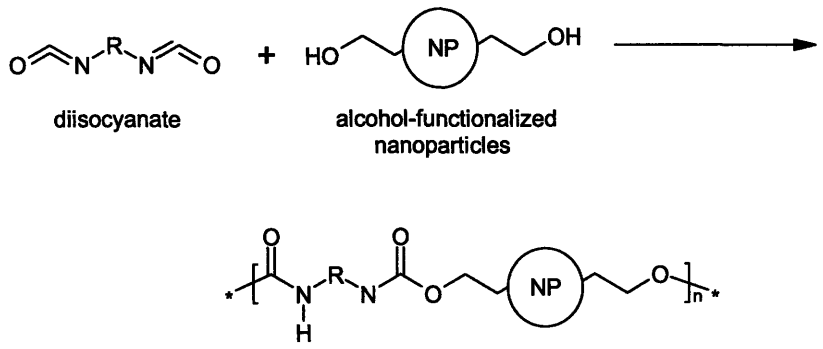

diisocyanates (for instance, phenylene diisocyanate) as shown in Scheme 5.1. Alcohols also react with carboxylic acid and sulfonyl chloride groups, giving rise to a variety of possibilities: pole functionalization with an alcohol-terminated thiol and linking with sebacoyl chloride or a dicarboxylic acid; or pole functionalization with MUA and linking with a diol. The availability of alternative chemistries may enable the synthesis of longer or more stable chains.

Biological molecules are ideal candidates for use as pole functionalization molecules because the specificity of their chemistry would allow precise control over the chain composition. Specific coupling between biotin and either avidin or streptavidin is a strong biological linkage;[4] the biotin-avidin system has been used to successfully couple nanoparticles[5] and nanorods[6] into small structures or short chains. In a similar approach, thiolated biotin could be exchanged onto the poles of NPs, which could be linked by avidin or streptavidin into chains or even more complex structures. Thiolated DNA could be placed at the poles to reversibly generate chains of NPs; furthermore, by designing appropriate complementary DNA sequences for different sets of NPs, the chain composition could be controlled and complex shapes could be engineered.

5.1.3 Core composition

This work has dealt with divalency and chains of primarily gold and, to a lesser extent, silver NPs. However, extension of the concept of divalency to other core compositions may be possible, provided the following requirements are met: (1) the ligand shell is a SAM with a dynamic equilibrium between adsorbed and desorbed species, such that place-exchange can occur at the polar defect sites; and (2) the ligand shell self-organizes into a rippled or other structure that accentuates the polar defects. For instance, this group has developed a chaining procedure for 13 nm iron oxide (Fe_2O_3) NPs using ligands bound by carboxylic acid groups instead of thiols.[7] Compound semiconductor NPs, such as CdSe or ZnS, can be capped with thiolated molecules,[8] raising the possibility that a similar procedure could be developed to produce chains of semiconductor particles.

The ability to form chains of varied composition gives rise to a wide array of possible other structures. The nanoscale equivalent of block copolymers could be synthesized by joining pre-existing chains of one composition with chains of a second composition (Figure 5.1). The chain composition could be tuned to a finer degree as well; chains of alternating metal and semiconductor particles would provide a vehicle to study localized interactions between the two core types.

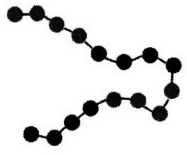

Figure 5.1
A schematic of the nanoscale equivalent of a block copolymer that could be formed by joining chains of different compositions of NPs.

5.1.4 Multivalent nanoparticles

The two diametrically opposed defect sites on mixed ligand protected metal NPs arise due to the constraints imposed by arranging a vectorial order (the projections of the ligand molecules) onto a spherical surface (the NP core). Chapter 2 discussed the possibility for the generation of four tetrahedrally opposed defect sites when a topological sphere is coated with 'double-headed arrows'; that is, molecules that display nematic ordering.[9] Synthesizing such NPs and developing a method to functionalize the four defect sites would generate tetravalent NPs; that is, the nanoscale equivalent of sp^3-hybridized atoms.

We have begun work with the molecule MPAA-1 (Scheme 5.2), that is predicted to behave as a 'double-headed arrow' because of its two degrees of freedom: the tilt angle relative to the NP surface and the rotational angle of the anthracene tail group. This research is still in an early stage; synthesis of soluble NPs of a reasonable size is still a challenge, likely due to the driving force for the anthracene groups to π-stack with a fixed intermolecular distance. Once synthesized, the next challenge in this system is to develop a method to first prove the existence of the four tetrahedrally opposed 'poles' and next to prove that all four poles can be specifically functionalized. Since such functionalization will generate three-dimensional diamond-like aggregates of NPs if allowed to proceed freely, it will be necessary to limit the growth of the aggregates for characterization purposes. One potential strategy to limit the growth is to work with two different groups of NPs: MPAA-1 NPs pole functionalized (at the four tetrahedral sites) with MUA and NPs coated with amine-terminated ligands. A large excess of the amine-terminated

Scheme 5.2
The molecule MPAA-1.

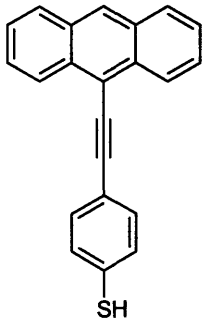

NPs will ensure that each MPAA-1 NP will form amide bonds with only four amine-terminated particles. The resulting clusters of one central tetravalent NP bonded to four amine-terminated NPs should be easily observable in TEM.

5.1.5 Characterization

Chains of nanoparticles likely have interesting optical, electronic, and mechanical properties. Indeed, a significant advantage of the approach to chaining presented here is that it will allow the precise composition and thus the properties of the chains to be designed through the proper choice of linking chemistries. However, challenges exist in the development of adequate characterization techniques. Here we have presented a preliminary set of characterizations; however, besides the Transmission Electron Microscopy (TEM) imaging, all characterization was performed in solution and thus was an ensemble average of all the chains present. In order to characterize properties of individual chains, the chains must be isolated from one another.

Chains dispersed on a surface are ideal for scanning probe microscopy characterization. To achieve a population of separated chains on a surface, we have already demonstrated the importance of a sufficiently dilute solution in a solvent that

dries rapidly. A filtration or selective precipitation step prior to deposition may result in samples that contain primarily chains with no isolated NPs or large aggregates. During deposition, the application of a flow or an external field could induce chain alignment (for instance, the alignment of chains of iron oxide NPs with an external magnetic field). A second approach to obtain chains dispersed on a surface is to first anchor single pole functionalized NPs to a SAM that contains a small amount of a group that will bind the terminal group at the poles; for example, in the chemistry presented in this work, a dilute dispersion of MUA in a background matrix of 1-octanethiol would, in the presence of 1,6-diaminohexane capture NPs pole functionalized with MUA (Figure 5.2). Chains could then be grown from the free pole of the surface-bound particles. A variety of properties of surface-bound chains could be studied. For example, plasmonic energy transfer along chains of Ag NPs has previously been reported,[10, 11] and Förster energy transfer has been observed between semiconductor quantum dots.[12] Further study of

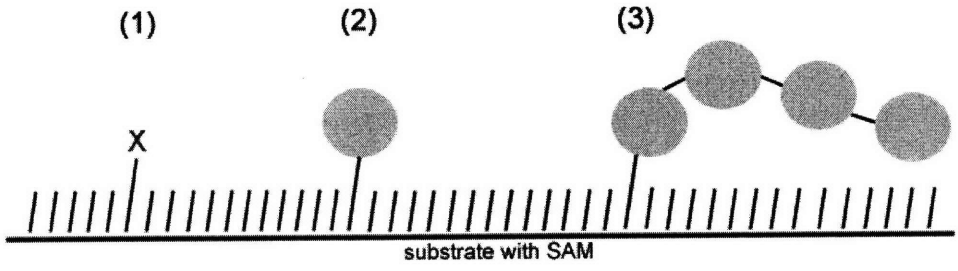

Figure 5.2
Cartoon of a proposed method for obtaining chains of NPs isolated on a surface. (1) A mixed SAM is formed with a small amount of a molecule with a reactive end group (X) in a matrix of methyl-terminated molecules. (2) NPs pole functionalized with the complement to X are assembled onto the surface. (3) Chains are grown starting from the unbound pole of the first NP.

energy transfer, particularly along chains of mixed composition, could be performed with Near-Field Scanning Optical Microscopy. A microprobe setup could be used to study electronic properties of the chains.

An alternative approach to generating isolated chains of NPs is to grow a single chain off of the end of an Atomic Force Microscopy (AFM) tip that had been functionalized with a molecule complementary to the pole functionalization of the NPs (Figure 5.3). Electronic properties could then be probed by operating the microscope in conductive AFM mode, applying a voltage between the tip and a substrate and monitoring the current flow through the NP chain. Similarly, mechanical properties of the chains could be studied by measuring the force between the tip (i.e. the chain) and a substrate as a function of tip-substrate distance.

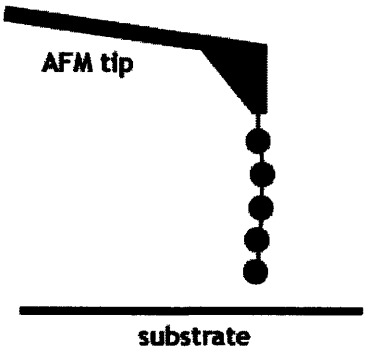

Figure 5.3
A schematic of a chain of NPs grown on the end of an AFM tip for electrical or mechanical characterization.

5.2 Conclusion

We have here demonstrated the existence of two diametrically opposed point defects in the ligand shell of mixed ligand protected metal nanoparticles. Through a brief selective place-exchange process at the poles, we have first introduced a novel method to generate one-dimensional assemblies of NPs, and second characterized the defect points as highly reactive and thermodynamically unique. In particular, by taking advantage of the fast rates of reaction at the poles, this work has presented a thorough study of the kinetics and thermodynamics of place-exchange at specific sites in the ligand shell of nanoparticles.

More importantly, the development of a method to generate valency in nanoparticles may introduce new ways to handle and assemble the particles. Indeed, a library of 'artificial atoms' can be created, bringing about the possibility of fabricating anisotropic NP-based structures assembled via controlled and directional chemical interactions. By synthesizing and characterizing divalent metal nanoparticles, we hope to have made the first step toward the capability to construct, characterize, and apply complex structures at the nanoscale.

5.3 References

1. DeVries, G. A.; Talley, F. R.; Carney, R. P.; Stellacci, F., *Submitted to Advanced Materials* **2007**.
2. Biebuyck, H. A.; Bian, C. D.; Whitesides, G. M., Comparison of Organic Monolayers on Polycrystalline Gold Spontaneously Assembled from Solutions Containing Dialkyl Disulfides or Alkenethiols. *Langmuir* **1994,** 10, (6), 1825-1831.
3. Biebuyck, H. A.; Whitesides, G. M., Interchange between Monolayers on Gold Formed from Unsymmetrical Disulfides and Solutions of Thiols - Evidence for Sulfur Sulfur Bond-Cleavage by Gold Metal. *Langmuir* **1993,** 9, (7), 1766-1770.
4. Diamandis, E. P.; Christopoulos, T. K., The Biotin (Strept)Avidin System - Principles and Applications in Biotechnology. *Clinical Chemistry* **1991,** 37, (5), 625-636.
5. Mann, S.; Shenton, W.; Li, M.; Connolly, S.; Fitzmaurice, D., Biologically programmed nanoparticle assembly. *Advanced Materials* **2000,** 12, (2), 147-150.
6. Salem, A. K.; Chen, M.; Hayden, J.; Leong, K. W.; Searson, P. C., Directed assembly of multisegment Au/Pt/Au nanowires. *Nano Letters* **2004,** 4, (6), 1163-1165.
7. Nakata, K.; Hu, Y.; Bakr, O.; Stellacci, F., Self-Assembled Nanostructured Chains from Superparamagnetic Nanoparticles. *submitted to Advanced Materials* **2007**.
8. Rogach, A. L.; Kornowski, A.; Gao, M. Y.; Eychmuller, A.; Weller, H., Synthesis and characterization of a size series of extremely small thiol-stabilized CdSe nanocrystals. *Journal of Physical Chemistry B* **1999,** 103, (16), 3065-3069.
9. Nelson, D. R., Toward a tetravalent chemistry of colloids. *Nano Letters* **2002,** 2, (10), 1125-1129.
10. Maier, S. A.; Kik, P. G.; Atwater, H. A.; Meltzer, S.; Harel, E.; Koel, B. E.; Requicha, A. A. G., Local detection of electromagnetic energy transport below the diffraction limit in metal nanoparticle plasmon waveguides. *Nature Materials* **2003,** 2, (4), 229-232.
11. Maier, S. A.; Brongersma, M. L.; Kik, P. G.; Meltzer, S.; Requicha, A. A. G.; Atwater, H. A., Plasmonics-A Route to Nanopscale Optical Devices. *Advanced Materials* **2001,** 13, (19), 1501-1505.
12. Tang, Z. Y.; Ozturk, B.; Wang, Y.; Kotov, N. A., Simple preparation strategy and one-dimensional energy transfer in CdTe nanoparticle chains. *Journal of Physical Chemistry B* **2004,** 108, (22), 6927-6931.

Appendix A: Abbreviations

1D: one-dimensional

BT: 1-butanethiol

CNT: carbon nanotube

DAH: 1,6-diaminohexane

DCM: dichloromethane

DDT: 1-dodecanethiol

DMF: N,N-dimethylformamide

DSC: Differential Scanning Calorimetry

EGDA: O,O'-Bis(2-aminoethyl)octadecaethylene glycol

FTIR: Fourier Transform Infrared Spectroscopy

HT: 1-hexanethiol

MBT: 4-methylbenzenethiol

MH: 6-mercapto-1-hexanol

MHA: 16-mercaptohexadecanoic acid

MHDA: 16-mercapto-1-hexadecylamine

MPA: 3-mercaptopropionic acid

MUA: 11-mercaptoundecanoic acid

MWCNT: multi-walled carbon nanotube

NHS: N-hydroxysuccinimide

NMR: nuclear magnetic resonance

NP: nanoparticle

NT: 1-nonanethiol

ODT: 1-octadecanethiol

OT: 1-octanethiol

OT-d_{17}: fully deuterated 1-octanethiol

SAM: self-assembled monolayer

STEM: Scanning Transmission Electron Microscopy

STM: Scanning Tunneling Microscopy

SWCNT: single-walled carbon nanotube

TEM: Transmission Electron Microscopy

THF: tetrahydrofuran